Titre: Title:	Smart Textiles for Tactile Sensing and Energy Storage
Auteur: Author:	Stepan Gorgutsa
Date:	2012
Type:	Mémoire ou thèse / Dissertation or Thesis
Référence: Citation:	Gorgutsa, S. (2012). Smart Textiles for Tactile Sensing and Energy Storage [Mémoire de maîtrise, École Polytechnique de Montréal]. PolyPublie. https://publications.polymtl.ca/926/

URL de PolyPublie: PolyPublie URL:	https://publications.polymtl.ca/926/
Directeurs de recherche: Advisors:	Maksim A. Skorobogatiy
Programme: Program:	Génie physique

UNIVERSITÉ DE MONTRÉAL

SMART TEXTILES FOR TACTILE SENSING AND ENERGY STORAGE

STEPAN GORGUTSA

DÉPARTEMENT DE GÉNIE PHYSIQUE

ÉCOLE POLYTECHNIQUE DE MONTRÉAL

MÉMOIRE PRÉSENTÉ EN VUE DE L'OBTENTION DU DIPLÔME DE

MAITRÎSE ÈS SCIENCES APPLIQUÉES

(GÉNIE PHYSIQUE)

AOÛT 2012

UNIVERSITÉ DE MONTRÉAL

ÉCOLE POLYTECHNIQUE DE MONTRÉAL

Ce mémoire intitulé:

SMART TEXTILES FOR TACTILE SENSING AND ENERGY STORAGE

présenté par : GORGUTSA Stepan

en vue de l'obtention du diplôme de : Maîtrise ès sciences appliquées

a été dûment accepté par le jury d'examen constitué de :

M. FRANCOEUR Sébastien, Ph.D., président

M. SKOROBOGATIY Maksim A., Ph.D., membre et directeur de recherche

Mme. BERZOWSKA Joanna, Ph.D., membre

ACKNOWLEDGMENTS

It would be very hard to acknowledge all the people that have contributed to or supported me during my Master's studies. First of all, I would like to express my gratitude to my supervisor and research director Prof. Maksim Skorobogatiy for his constant support, assistance and guidance during my Master's studies.

Also during the last several years, I had a pleasure to work with Dr. Jian Feng Gu and Dr. Yang Liu whom I would like to thank for their expertise in chemistry and help with fiber design and fabrication. All the time I was surrounded by wonderful colleagues: Anna Mazhorova, Andrey Markov, Hang Qu, Bora Ung. Mathieu Rozé, Alexandre Dupuis. I would like to thank them all for the helpful discussions, advices and mutual support.

Besides, I would like to give a special acknowledgement to our ex-technician Francis Boismenu and current technician Yves Leblanc. They not only provided excellent technical assistance in any situation but also were fun to work with.

Finally, I would also like to thank all those professors, employers and stuff members of Genie Physique who taught me, answered my numerous questions and helped with paperwork.

RÉSUMÉ

Durant ma maîtrise, j'ai surtout travaillé sur 2 sujets dans le domaine des textiles intelligents électroactifs.

Mon premier projet portait sur la fabrication d'un pad textile sensible au toucher utilisant des fibres capacitives en polymères. Les fibres capacitives, présentent une grande capacité et résistance, ont été fabriquées utilisant des techniques de fibrage. Pour permettre une connectivité facile, un mince fil de cuivre a été intégré dans le cœur de la fibre durant l'extrusion. Ces fibres (soft-capacitor) ont des une capacité par unité de longueur typiques de 69 nF/m, et des résistances de 5 kΩ•m. Nos mesures et nos modèles théoriques montrent que la capacité est un paramètre très stable déterminé par la géométrie utilisée, qui ne dépend pas du diamètre de la fibre ni de ses paramètres de fabriquation. La resistivité de la fibre, quant à elle, a un important coefficient thermique (positif), est très sensible aux contraintes de tension et dépend grandement des paramètre d'extrusion.

Il a aussi été démontré qu'une fibre capacitive individuelle peut servir de capteur de glissement qui permet de déterminer, sur sa longueur, la position du contact tactile en mesurant la réponse AC de la fibre à un point donné sur sa surface. La réponse électrique d'un senseur de ce type est décrite par le modèle de réseau RC, qui est en accord avec les résultats expérimentaux.

Les fibres capacitives développées sont souples, de faible diamètre, légères et n'utilisent pas d'électrolyte liquide, donc elles sont idéales pour l'intégration dans les produits textiles. À la fin du chapitre, nous avons démontré qu'en tissant un ensemble de fibres capacitives en 1 dimension (fibres parallèles), il est possible de tisser un senseur tactile en 2 dimensions. Les performances de ce senseur ont été caractérisées et une bonne isolation entre les canaux a été démontrée. Un tel senseur possède aussi des fonctionnalités multi-touch.

Mon deuxième projet portait sur l'assemblage de cellules Li-ion flexibles et étirables, leur intégration dans un textile et leur caractérisation électrique dans un contexte de «textiles intelligents». L'aspect chimique de ces cellules a été développé par mon collègue Y.Liu, qui a réussi à intégrer la cathode ($LiFePO_4$), l'anode ($Li_4Ti_5O_{12}$) et l'électrolyte solide (PEO) dans un système de cellule électrochimique souple. J'ai démontré de façon expérimentale que des batteries de cellules flexibles peuvent être fabriqués en grande feuilles, puis coupées en fines

lanières et tissées dans les textiles. Les performances électrochimiques des cellules ont été caractérisées de façon rigoureuse et elles se sont avérés être inférieures aux cellules basées sur des électrodes en poudre et des électrolytes liquides. Cependant leur performances cycliques, leur souplesse et leur texture s'apparentant à du cuir les rendent bien adaptées à des applications de «textiles intelligents». Même si leur tension électrique de fonctionnement est relativement basse (~0.3V), lorsque plusieurs d'elles sont connectées en série, le voltage net peut être suffisamment grand pour des applications pratiques. Finalement, comme démonstrateur de technologie, j'ai testé une batterie textile faite de 8 cellules en bande flexibles tissées ensemble et connectées en série pour alimenter une DEL de 3 volts pendant plusieurs heures.

ABSTRACT

During my master's I have mainly worked on two subjects in the research area of electroactive smart textiles.

My first project involved building a touch sensitive textile pad using original home-made all-polymer soft capacitor fibers. The capacitor fibers featuring relatively high capacitance and resistance were fabricated using fiber drawing technique. For the ease of connectorization, a thin copper wire was integrated into the fiber core during drawing procedure. Soft-capacitor fibers have a typical capacitance per unit length of 69 nF/m, and a typical resistivity parameter of 5 kΩ•m. Our measurements and theoretical modeling show that the fiber capacitance is a very stable, geometry defined parameter independent of the fiber diameter, and fiber fabrication parameters. In contrast, fiber resistivity has a very strong positive temperature coefficient, it is highly sensitive to stretching, and it is strongly dependent on the fiber drawing parameters.

Next, an individual capacitor fiber was demonstrated to act as a slide sensor that allows determining the touch position along its length by measuring the fiber AC response at a single point at the fiber surface. Electrical response of such a sensor was described by the RC ladder model, with the modelling data in excellent agreement with experimental observations.

Developed capacitor fibers are soft, small diameter, lightweight and do not use liquid electrolytes, thus they are ideally suited for the integration into textile products. At the end of the chapter, we have demonstrated that by weaving a one dimensional array of capacitor fibers (in parallel to each other) a fully woven 2D touchpad sensor could be build. Performance of a touchpad sensor was then characterised and the absence of the inter-channel crosstalk was confirmed. We also note that a 2D touchpad has a partial multi-touch functionality.

My second project involved assembly of flexible and stretchable Li-ion batteries, their integration into a textile, and their electric characterization in a view of smart textile applications. The chemistry for the battery was developed by my colleague Y. Liu who has combined the relatively conventional Li battery materials including $LiFePO_4$ cathode, $Li_4Ti_5O_{12}$ anode and PEO solid electrolyte into a non-conventional soft electrochemical battery system. I have experimentally demonstrated that flexible batteries can be first cast as sheets, and then cut into thin strips, and finally integrated into textile using conventional weaving techniques. The

electrochemical performance of the film batteries was extensively characterized and found to be poorer compared to the performance of batteries based on the powder electrodes and liquid electrolytes. At the same time, cycling performance of the solid film batteries was stable, and together with their soft leather-like feel and appearance, this makes such batteries well suitable for smart textile applications. Although operating voltage of a single flexible battery is relatively low (~0.3V), nevertheless, when several of them are connected in series, the net voltage can be large enough for practical applications. Finally, as a demonstrator of the technology I have tested a textile battery comprising 8 flexible battery strips woven together and connectorized in series to power up a 3V LED over several hours.

TABLE OF CONTENTS

LIST OF FIGURES

LIST OF ABBREVIATIONS AND SYMBOLS

PCE	Power conversion efficiency
OPV	Organic photovoltaic cell
T_g	Glass transition temperature
PE	Polyethylene
PVDF	Polyvinylidene fluoride
PC	Polycarbonate
PET	Polyethylene terephthalate
PMMA	Polymethyl methacrylate
LDPE	Low density polyethylene
HDPE	High density polyethylene
CB	Carbon black
ADC	Analog-to-Digital Convertor
1D	One dimensional
2D	Two dimensional
PEG	Polyethylene glycol
PEO	Poly Ethylene Oxide
WAXD	Wide-angle X-ray scattering
KVL	Kirchhoff's Voltage Law
KCL	Kirchhoff's Current Law
R_{ref}	Reference resistance
ω	Current frequency
R_t	Transverse resistance of the fiber
R_l	Longitudinal resistance of the fiber

ρ_v	Volume resistivity
L	Length of the fiber,
W	Width of the conductive electrodes
d_c	Thickness of the conductive electrodes
d_i	Thickness of the rolled isolating films
N	Number of turns of the conductive electrode
C	Fiber capacitance
ε	Dielectric constant of the isolating films
ε_0	Permeability of the vacuum
x_b	Position of the finger touch on the fiber surface
x_p	Position of the probe attachment on the fiber surface
R_b	Effective resistance of the finger
C_b	Effective capacitance of the finger
R_p	Effective resistance of the probe and oscilloscope
C_p	Effective capacitance of the probe and oscilloscope
$\tilde{L}$	Characteristic length of the current decay
C_e	Capacitance of the anode/electrolyte or cathode/electrolyte double layer
R_e	Charge transfer resistance
R_s	Bulk electrolyte resistance

INTRODUCTION

Smart textiles that can sense and respond to environmental stimuli of different nature (mechanical, thermal, chemical, electrical, magnetic, etc.) currently attract considerable attention due to a multitude of commercial opportunities and advanced applications in sport and wellness industries, work ware and military. In this work, I address two narrow topics related to the development of smart electroactive textiles.

The first research topic discussed in this work concerns the fabrication of tactile sensors based on recently developed soft capacitor fibers. In their crossection, the fibers feature a periodic sequence of hundreds of conductive and isolating plastic layers positioned around metallic electrodes. The fibers are fabricated using a fiber drawing method, where a multi-material macroscopic preform is drawn into a sub-millimeter capacitor fiber in a single fabrication step. I start with an overview of the different tactile sensors developed to the present moment, then I continue with a discussion of fabrication of soft capacitor fibers, then I introduce a theoretical model to describe the electrical response of a single capacitor fiber using an electrical ladder network model, and, finally, I show that such fibers can be used as touch-based slide sensors. The effects of different parameters on the sensing performance of a soft capacitor fiber are also studied. Softness of the fiber materials, absence of liquid electrolyte in the fiber structure, and high capacitance of such fibers make them ideally suited for integration into textiles. As a proof of concept, the prototype of a woven touchpad sensor featuring a one dimensional array of capacitor fibers is presented in the final section and its performance is characterized.

The second research direction described in this thesis is the fabrication and the characterisation of a flexible and stretchable battery composed of a strain free $LiFePO_4$ cathode, a $Li_4Ti_5O_{12}$ anode and a solid polyethylene oxide (PEO) electrolyte as a separator layer. Featuring a solid thermoplastic electrolyte as a key enabling element, this battery is potentially extrudable or drawable into fibers, which are directly compatible with the weaving process used in smart textile fabrication. As a proof of principle, a large battery sample made of several long battery strips woven into a textile and connectorized with conductive threads was demonstrated to light up an LED.

Finally, I conclude with a discussion of future research perspectives.

SCIENTIFIC OUTCOMES OF MY MASTER'S RESEARCH

Publications, conference proceedings and presentations resulting from my work during the master's studies:

Journal Publications

1. Y. Liu, **S. Gorgutsa**, C. Santato, and M. Skorobogatiy "Flexible, Solid Electrolyte-Based Lithium Battery Composed of $LiFePO_4$ Cathode and $Li_4Ti_5O_{12}$ Anode for Applications in Smart Textiles", Journal of The Electrochemical Society, vol. 159 (4), pp. A349-A356 (2012)
2. **S. Gorgutsa**, J.F. Gu and M. Skorobogatiy "A woven 2D touchpad sensor and a 1D slide sensor using soft capacitor fibers", Smart Mater. Struct., vol. 21, 015010 (2012)
3. J.F. Gu, **S. Gorgutsa**, and M. Skorobogatiy "Soft capacitor fibers using conductive polymers for electronic textiles," Smart Mater. Struct., vol. 19, 115006 (2010)
4. J.F. Gu, **S. Gorgutsa**, and M. Skorobogatiy "Soft capacitor fibers for electronic textiles," Appl. Phys. Lett., vol. 97, 133305 (2010)

Conference Proceedings

1. A. Mazhorova, J.F. Gu, **S. Gorgutsa**, M. Peccianti, R. Morandotti, T. Ozaki, M. Tang, H. Minamide, H. Ito, M. Skorobogatiy, "THz metamaterials using aligned metallic or semiconductor nanowires," We-P.31, The 35th International Conference on Infrared, Millimeter, and Terahertz Waves, IRMMW-THz 2010.

Book chapters (to be published)

1. **S.Gorgutsa** and M. Skorobogatiy,"Tactile sensing textiles using soft capacitance fibers" in Multi-disciplinary know-how for smart textile developers, Tünde Kirstein ed. (Woodhead Publishing Ltd, 2012), Ch.5.
2. **S.Gorgutsa**, J. Berzowska and M. Skorobogatiy, "Photonic Textiles using optical fibers" in Multi-disciplinary know-how for smart textile developers, Tünde Kirstein ed.(Woodhead Publishing Ltd, 2012), Ch.3.

CHAPTER 1
LITERATURE REVIEW

1.1 Smart textiles

Fuelled by the rapid development of micro and nanotechnologies, and driven by the need to increase the value of conventional textile products, fundamental and applied research into smart textiles (or high-tech textiles) has recently flourished.

Generally speaking, textiles are defined as "smart" if they can sense and respond to environmental stimuli that can be of mechanical, thermal, chemical, electrical or magnetic nature. Some of the first uses of smart textiles were in military and medical applications. For example, with the support of US Naval Department in 1996 Georgia Tech has developed a garment called Wearable Motherboard (with the commercial name of Smart shirt).[22], [23] The Wearable Motherboard is a fabric featuring woven electric wires and/or optical fibers that serve as a flexible information bus. To integrate electronics directly into textiles leads to the so called technique of "wearable computing" or "E-textiles" [24]-[26]. Another application of smart textiles is in harnessing (and recently in storage) of the energy of human motion or the energy of various ambient fields, such as electromagnetic fields. Electric energy generation from human motion, for example, has been recently demonstrated using piezoelectric fibers made of ceramic materials like PZT (lead zirconate-titanate) as well as polymers such as PVDF (polyvinylidene fluoride) [27] , [28]. Smart textiles can also be found their usage in heat-storage and thermo-regulated clothing [29], [30] and various wearable sensors including those for biomedical monitoring [31]. For example, conventional fabrics coated with a thin conducting polymer layer possess remarkable properties of strain and temperature sensing [11]. A multi-layer structure consisting of two conductive fabrics separated by a meshed non-conductive one can be used as a pressure sensor [10]. Sensing garments for monitoring physiological and biomechanical signals of human body have already been invented for healthcare [33] and sports training [34]

Applications of smart textiles have been demonstrated from responsive seats in automobiles [35] where textiles can indicate the level of comfort of an individual passenger, to apparel with tuneable or adjustable color and appearance in fashion and design [36]. Recently various textile

based displays became especially popular. One of the most commonly used inks for this new type of displays is thermochromic ink that change color based on temperature. Typically such inks are deposited on textile [16], [17] or on paper [18] and then are actuated by either electrically conductive yarn that is woven into the fabric or by incorporated wires. When powered up, the conductive yarn heats up and in turn actuates the thermochromic inks to change the color. In 'Mosaic Textiles' [18], authors use liquid crystal inks which work on the same principle as thermochromic inks, actuated by conductive yarn. However most of such displays have several major limitations. First, they can only demonstrate images that are pre-selected during the manufacturing. Second, resolution of the thermochromic displays is limited by the size of the electrically conductive heaters, and by the lateral and diffusion of heat emanating from the heaters. Finally, the displays that use only heating source such as body heat or conductive yarn without any cooling method, lack controllability as it may take from 10 seconds to several minutes for such a display too go back to idle state. Those thermochromic ink displays that have a cooling system typically require high-cost and complex standard "rigid" electronics.

Another popular concept is electrochromic textiles [20] the idea is similar to thermochromic textiles but color changes is achieved as a result of the oxidation or the reduction of the material by electrochemical means [21].

As it was already mentioned in this work two research directions in smart textile domain are studied: touch sensitive textiles and flexible energy storage textiles.

1.2 Touch sensitive technologies

Touch sensing as a human interface device (HID) technology is becoming increasingly popular and ubiquitous finding its applications in smart phones, computers and responsive garments to name a few. Various touch sensing systems have been developed based on the different physical principles including resistive, capacitive, infrared, surface acoustic wave, electromagnetic, near field imaging, etc. Resistive [22] and capacitive [23] methods have been widely used in conventional touch screens of the commercial products such as mobile phones, PDAs, and consumer electronics devices. Resistive touch screens are composed of two material sheets that are coated with a resistive material, commonly indium tin oxide (ITO), and separated by an air gap or microdots. When a finger presses the screen, the two sheets are connected at the

touch position which changes the current flow in the screen. A sensing circuit then detects changes and locates the touch position. A capacitive touch sensor is based on the capacitive coupling effect. A typical design involves coating the screen with a thin, transparent metallic layer, in order to form a collection of capacitors on the surface. When a user touches the surface, the disturbance caused by the finger changes the capacitance and current that flows on the display.

A significant limitation for most of these technologies is that they are only capable of detecting a single touch. Multi-touch techniques allow touch screens to recognize touches of multiple fingers or inputs of multiple persons simultaneously. The multi-touch detection mechanisms can be classified into three categories: sensor array, capacitive sensing, and vision and optical based ones. A sensor array touch surface consists of a grid of touch sensors that work independently. When a user exerts multiple touches on the surface, the system can indentify activated sensors and determine these touch positions simultaneously. An example, originally proposed by Lee *et al.* [24], is FMTSID (Fast Multiple-Touch-Sensitive Input Device) - one of the first multi-point touch sensor-based devices. The system consists of a sensor matrix panel, rows of the sensors, A/D converter and a control CPU. The design of the sensor matrix is based on the technique of capacitance measurement between a fingertip and a metal plate. A capacitive touch method uses the capacitive coupling between two conductors to sense a touch. Typically, the touch surface contains a mesh of horizontal and vertical antennas which function as either a transmitter or a receiver of electric signals. Examples based on this technology include Rekimoto's SmartSkin [25], and DiamondTouch developed by Dietz and Leigh [26].

In addition to touchscreens, touch sensors with force sensing ability has been studied as tactile sensors for many years [27]. Such sensors have found their applications in artificial skin for robot applications [28], minimally invasive surgery [29], wearable computers [30], and mobile or desktop haptic devices [31]. Up to date tactile sensors have mainly focused on silicon-based sensors that use piezoresistive [32], [33] or capacitive sensing mechanism [34], [35], [36]. The silicon tactile sensors have limitations of mechanical brittleness, and hence are not capable of sustaining large deformations. Polymer-based tactile sensing approaches that use piezoelectric polymer films [37], [38], [39], pressure-conductive rubber [40], carbon fiber based polymer composite [41] and conductive polymers [42], have been reported as well. These sensors provide

good spatial resolution but the applied force range is low due to the limited thickness of a membrane.

So far, capacitive sensing is probably the most promising technique for the textile based touch sensors as it does not depend on the applied mechanical force (including bends and stretching) and also enables multi-touch and gesture recognition functionality.

1.3 Smart Fibers

With the constant improvement of the technology, there is no doubt that smart textiles will soon become an integral part of our daily life [43]-[45]. However nowadays most of the "smart" functionalities in the currently existing smart apparel are typically enabled by various point devices attached to a textile matrix. Such point devices (electronic chip-sets, for example) are typically not compatible with the weaving process and, thus, have to be introduced onto a textile surface in a post-processing step. This, in turn, makes fabrication of smart apparel labour intensive and therefore expensive. Additionally, most of the point devices such as sensors and batteries are not flexible, and therefore wearability of such garments is usually problematic. Limitations introduced by the rigid point devices motivated recent effort into the development of flexible electronic components. For example, a flexible energy storage devices based on nanocomposite paper was reported [46]. The device, engineered to function as both a lithium-ion battery and a supercapacitor, can provide the long and steady power output.

Ideally, if all the electronic functionalities could be implemented in a fiber itself, such fibers would provide a perfect building material for smart apparel as they could be naturally integrated into textiles during weaving process. Because of the technical complexity of integration of advanced electronic functionalities into a textile fiber, currently there are only few examples of such fibers. Thus, a conductive fibre prepared from ultra-high molecular weight polyaniline by continuous wet spinning techniques was recently commercialized [47]. The researcher group of Wang [48] has developed a microfiber nanogenerator composed of a pair of entangled fibers which can generate electrical current using the piezoelectric effect. It has been demonstrated that commodity cotton threads can be transformed into smart electronic yarns and wearable fabrics for human biomonitoring using a polyelectrolyte-based coating with carbon nanotubes (CNTs) [49]. A stretchable, porous, and conductive textiles have recently been invented by a simple

“dipping and drying” process using a single-walled carbon nanotube (SWNT) ink [50]. The loading of pseudocapacitor materials into these conductive textiles can lead to a 24-fold increase of the areal capacitance of the device. Finally, several groups [51]-[53] have recently demonstrated organic all-fiber transistors which can potentially allow creation of electronic logic circuits by weaving.

To integrate tactile sensors in the smart-textiles applications one could, for example, use arrays of conventional rigid electric devices embedded into a textile matrix, as it was done in early prototypes of the “smart apparel”. But as it was already mentioned this approach does not provide acceptable wearing comfort or good mechanical properties. This motivated recent efforts into the development of truly wearable smart textiles.

Recently there have been several reports on the capacitor fibers compatible with a textile weaving process. By adding an external inductance such fibers make a resonant LC circuit, thus allowing the use of many highly sensitive resonant detection techniques which are able to detect small changes in the capacitor structure. Among several proposals for a capacitor fiber we note a multicore fiber capacitor in the form of a bundle of ~50μm-sized coaxial cables connected in parallel on a micro-level [54]. However, such capacitors were never actually fabricated.

One important note should be made regarding various smart textiles discussed above, typically all prototypes are powered by conventional external power supply or small batteries. However, truly wearable smart textiles will also require wearable, flexible and environmentally friendly power sources.

1.4 Energy storage textiles

Broadly speaking, the advancements in flexible batteries have been in the following categories: (a) flexible organic conducting polymers [55]-[58], (b) bendable fuel cells [59], (c) polymer solar cells [60]-[62] and (d) flexible lithium polymer batteries [48], [63], [64].

Conducting polymers are particularly interesting materials to fabricated energy storage devices as they possess inherent fast redox switching, high conductivity, mechanical flexibility, low weight and could be integrated into existing production processes [65]. Plus conductive polymers are more environmentally friendly and cost-efficient than most metal containing electrode materials, however insufficient cycle stabilities and the high self-discharge rates often

limit their applicability in commercial battery systems. One approach to improve the performance of nonmetal-based energy storage devices would be to use composite electrode materials of conductive polymers deposited as thin layers on a suitable large surface area substrate.

Flexible components, especially current collectors, are crucial parts of bendable fuel cells and could be implemented, for example, by preparing flexible membrane electrode assemblies [66]. Swedish company «myFC» developed flexible fuel cells (called FuelCellSticker) that convert hydrogen into electricity via proton exchange membrane. Except these quite complex solutions there are bendable on-chip fuel cells which were fabricated on flexible COP films. Such fuel cells fabricated on a flexible polymeric substrate were reported for the first time by Ito et al. [67]

Polymer solar cells have certain attractive features as a power source for the smart textile solutions. First of all, active materials used for fabrication devices are soluble in most of common organic solvents. Second, polymer solar cells have potentials to be flexible and to be manufactured in a continuous printing process. Various printing and coating technologies have been proven their compatibility with semiconducting polymer processing. Still, power conversion efficiency (PCE) of such solar cells is low (PCE about 6% [68], [69] was recently reported). Also stability of organic photovoltaic cells (OPVs) without encapsulation have very short lifetime, ranging from a few minutes to a few days [70]. The mechanism of the degradation of OPVs through difference pathways was investigated by Jørgensen et al. [71]. The organic materials and metal used as the electrodes react with oxygen and water which are diffused from both electrodes or lateral of the device are believed the major reason causing short lifetime of OPVs.

Recently, a rechargeable textile battery was created by Bhattacharya et al [51]. It was fabricated on a textile substrate by applying a conductive polymeric coating directly over interwoven conductive yarns. Approaches to produce stretchable and foldable integrated circuits have also been reported. This includes integrating inorganic electronic materials with ultrathin plastic and elastomeric substrates [52] and printing high viscous conductive inks onto nonwoven fabrics [53]. Among those flexible batteries, the lithium polymer battery has taken much attention for its potential in electric vehicle applications. It employs a solid polymer electrolyte,

which can act both as the electrolyte and the separator, with the aim of improving battery design, reliability, safety, and flexibility.

There are two features shared by the majority of existing flexible batteries that make them ill-suited for applications in smart textiles. The first one is that conventional polymer electrolytes and binders used in lithium batteries to blend anode, cathode and conducting materials are processed with organic solvents, which are poisonous and caustic and, thus, do not fit well with wearables. The second one is the fact that, at present, flexible film batteries are not extrudable or drawable to form fibers or strips, which are the necessary building block for smart textile fabrication.

CHAPTER 2

TACTILE SENSING TEXTILES USING SOFT CAPACITANCE FIBERS

In this section fabrication and characterization of the touch sensitive textile prototype is discussed. This prototype is based on the novel all-polymer soft capacitor fibers recently developed in our research group.

2.1 Soft capacitor fibers for electronic textiles

Another novel type of electronic fiber was recently developed in our laboratory - high capacitance, soft fiber from conductive polymer composites. One key advantage of our fibers is that they do not require the use of electrolytes for their operation, which is especially desirable for wearable applications. Another key advantage is that the fibers can be made fully polymeric (no metallic electrodes) and very soft for applications in wearable sensing. Because of the relatively high capacitance of the fiber (60-100nF/m) it can be also used for energy storage applications. In terms of capacitance our fibers take an intermediate position between the coaxial cables and supercapacitors. Thus, capacitance of a coaxial cable with comparable parameters is typically 1000 times smaller than that of our fibers.

2.1.1 Fiber materials and fiber fabrication

The soft capacitor fibers are fabricated by the fiber drawing technique which consists of three steps. The first step involves rolling or stacking conductive and dielectric films into a multilayer preform structure. During the second step the preform is consolidated by heating it to temperatures somewhat above the polymer glass transition temperature (T_g). Consolidation is needed as the diffusion of the polymer molecules through interfaces of adjacent layers fuses these layers together thus reduces the effect of property mismatch of different materials in the drawing process. Finally, at the third step consolidated preform is drawn into fibers using fiber drawing tower. Drawing is typically performed at temperatures higher than the polymer T_g. During successful drawing the resultant fibers generally preserve the structured profile of a preform, thus, fibers with very complex microstructure can be fabricated via homologous reduction (during drawing) of a macrostructure of the preform. Described drawing technique is

directly analogous to the one used in manufacturing of microstructured polymer optical fibers [72].

Flexible multilayer capacitors presented in this Chapter generally consist of two conducting polymer layers serving as two electrodes of a capacitor, and two isolating polymer separator layers. To result in a successful drawing the preform materials should be compatible with each other in terms of their rheological and thermo-mechanical properties. In the first tests an attempt to draw thin continuous layer of low-melting temperature metal sandwiched between the two isolating polymer layers was made. As a metal Bi_{58}/Sn_{42} alloy with a melting point of 138℃ was used. Various polymers were tested as isolating layers. However, it was found that in all cases it was difficult to preserve the laminated structure with a thin metal foil during drawing process. Particularly, when melted, metal foil would break into wires during drawing, thus destroying the continuous electrode structure. This observation have been rationalized by noting that the visco-elasticity ductility and interfacial tension of alloy and the surrounding polymer cannot match well at drawing temperatures. For example, at the temperature for the polymer to be drawn into fibers the viscosity of melted metal becomes very low, thus it is easy for a thin sheet of melted metal to develop a flow instability and form several larger wires to minimise surface energy associated with a polymer/metal interface. Another potential problem during drawing of metal sheets is that when the polymer surrounding the molten metal becomes too soft it can no longer hold the melt; as a consequence a large drop of metal would form at the preform end even before drawing starts, thus draining the rest of a preform from metal. From these initial experiments it was concluded that drawing of a thin metallic sheet sandwiched between two plastic sheets is in general problematic due to strong mismatch of the material properties during drawing process.

After realizing the challenge of drawing metallic electrods in the form of thin sheets, a natural option to remedy this problem was to substitute metals with thermoplastic conductive polymers as electrodes. Unfortunately, thermoplastic intrinsic conductive polymers suitable for drawing are not available commercially. The only thermoplastic conductive polymers which are currently available commercially are either carbon black filled or most recently carbon nanotube filled films. In this research polyethylene (PE)-based carbon black filled films (BPQ series) provided by Bystat International Inc. were used. The film, with a thickness of 91 μm, has a surface resistivity of 17 KΩ/sq. The messured volume resistivity is around 2.2 Ω·m in the

directions along the surface. To find the isolating materials that can be co-drawn with this conductive film, various polymer films such as polyvinylidene fluoride (PVDF), polycarbonate (PC), polyethylene terephthalate (PET), polymethyl methacrylate (PMMA), and others were tested. Among all the attempted polymers the two best materials for the isolating layer were found, which appeared to be low density polyethylene (LDPE) film or a polycarbonate film.

2.1.2 Capacitor fiber designs

Originally, three distinct fiber capacitor geometries that were developed. They all share the same concept but each of them poses its own features. The first fiber type has a cylindrical geometry with two plastic electrodes in the form of a spiralling multilayer (see Fig. 2-1(a)). Central part of a fiber was either left empty with the inner plastic electrode lining up the hollow core, or a metallic electrode was introduced into the hollow core during drawing, or the core was collapsed completely thus forming a plastic central electrode. In all these fibers, the second electrode was wrapped around the fiber.

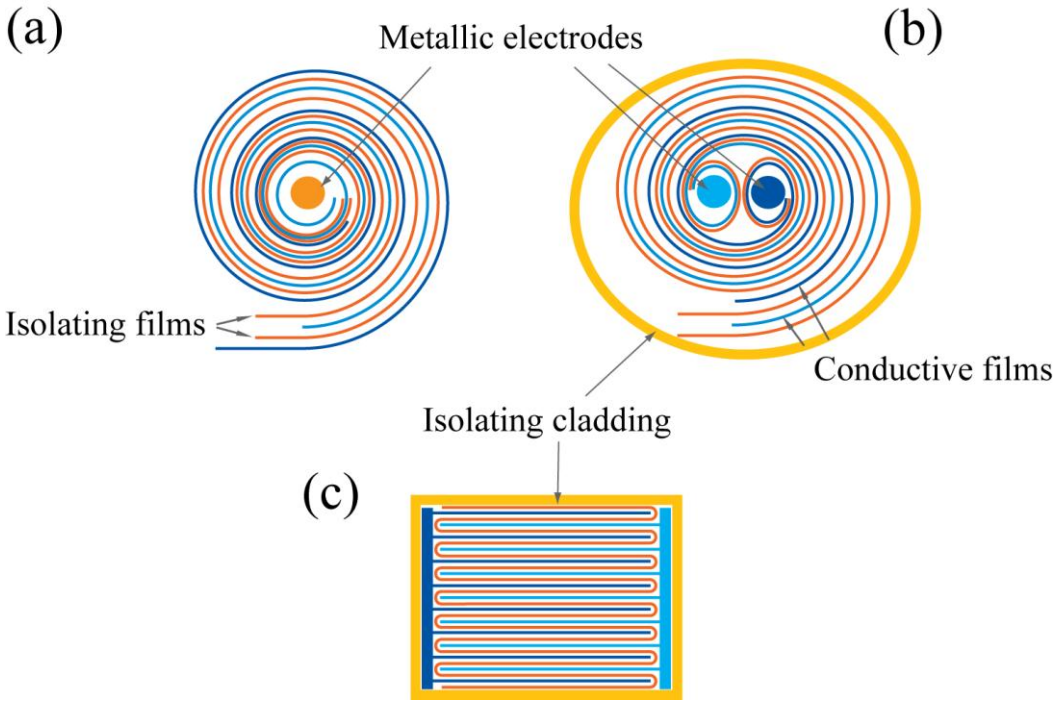

Fig. 2-1 (a) Schematic of a cylindrical capacitor fiber preform featuring a spiralling multilayer comprising two conductive and two isolating films. (b) Schematic of a cylindrical capacitor fiber with two electrodes in the center. (c) Schematic of a rectangular preform prepared by encapsulating a zigzaging stack of two conductive and an isolating layer inside a rectangular PMMA tube.

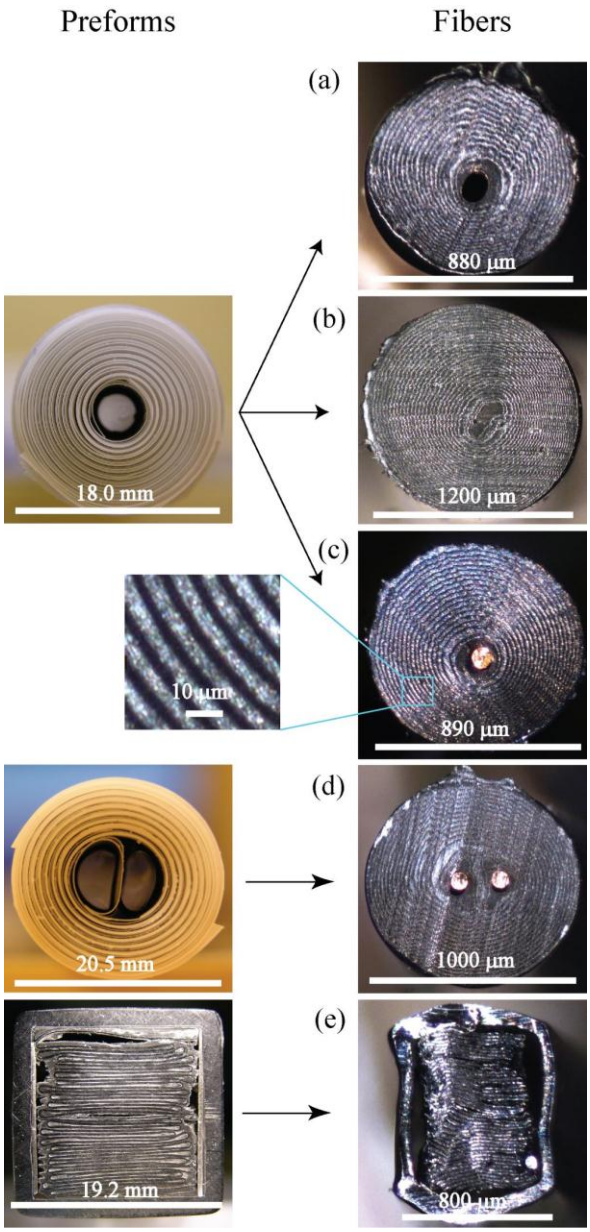

Fig. 2-2 Design I: hollow core fiber with the first electrode lining the inside of a holow core, and the second plastic electrode wrapping the fiber from outside. During drawing fiber hollow core can be left open (a) or collapsed (b) depending on the application requirement. Design II: Hollow core fiber can be drawn with a metallic electrode in the center. Such an electrode can be a copper wire (c) in contact with the plastic electrode lining the hollow core. Design III: fiber containing two hollow cores. The cores are lined with two plastic electrodes electrically separated from each other. Fiber is drawn with two copper wires threaded through the hollow cores in the preform (d). Design IV: square fiber capacitor. Fiber features a zigzaging stack of two plastic electrodes separated with an electrically isolating PC layer (e). Furthermore, two metallic electrodes are placed in contact with plastic electrodes, and the whole multilayer is encapsulated inside a square PMMA tube.

The second fiber type (see Fig. 2-1(b)) is also of cylindrical multilayer geometry, however it features two hollow cores lined with two plastic electrodes. The fiber is wrapped into an isolating material so there is no direct contact with environment. During drawing two metallic electrodes were introduced into the fiber cores. Finally, the third fiber type features a square electrically isolating tube comprising a zigzagging stack of the plastic electrodes (see Fig. 2-1(c)) separated by a zigzagging dielectric layer. The metallic electrodes were integrated on the left and right sides of a tube for the ease of connectorization.

Fibers of the first type Fig. 2-1(a)) were fabricated by co-rolling of the two conductive polymer films which were physically and electrically separated with the two isolating LDPE films. In the resultant fiber the inner conductive film forms one electrode inside the hollow fiber core, while another electrode is created by the other conductive film at the fiber surface. Similar fabrication strategy was used in the fabrication of the second fiber type (Fig. 2-1(b)), with the only exception of positioning two isolated fiber cores in the fiber center, while encapsulating the fiber into an isolating HDPE plastic wrap. Finally, fibers of the third type (Fig. 2-1(c)) were created by encapsulating a zigzagging stack of the electrodes and isolating layers inside a rectangular PMMA tube.

2.1.3 Capacitor fiber connection, and potential applications

An important issue when designing any smart fiber concerns connection of such fibers either to each other or with the external electrical probes. In a view of various potential applications of a capacitor fiber we have explored several connection geometries. In Fig. 2-2(a)-(e) we show four complete designs for a capacitor fiber. In each figure we present both the structure of a preform before drawing, as well as the structure of a resultant fiber.

Design one is presented in Fig. 2-2(a) and (b) where we show a circular hollow core fiber with the first electrode formed by the conductive layer lining the hollow fiber core (see also Fig. 2-1(a)), and the second electrode formed by the other conductive layer wrapping the fiber from outside. The outside electrode is exposed for the ease of access. Hollow core can be either collapsed (Fig. 2-2(b)) or left open during drawing (Fig. 2-2(a)). In general, to access the electrode inside the fiber core one has to use a needle-like electrical probe; in fact, we have used

50 μm-100 μm diameter hypodermic needles to perform electrical characterization of this fiber. One of the advantages of the hollow core fibers is that they are very soft due to the lack of metallic components in their structure, and, therefore, are most suitable for the integration into wearable textiles. Moreover, hollow fiber core can be filled with functional liquids which will be in direct contact with one of the electrodes. This can be useful for various sensing applications, where physical or chemical properties of a liquid could be interrogated electrically.

Design two is presented in Fig. 2-2(c) where we show a circular hollow core fiber with one of the electrodes formed by a small 100 μm diameter copper wire which is integrated into the fiber core directly during drawing. With a tension-adjustable reel installed on the top of a preform, copper wire can be passed through the preform core, pulled down and embedded into the fiber center during drawing by collapsing plastic cladding around it. The second electrode is formed by the other conductive layer wrapping the fiber from outside, similarly to the first design. Main advantage of this design is the ease of connection to the inner electrode as plastic capacitor multilayer can be easily stripped from the copper wire. This fiber has lower effective resistivity compared to the hollow core fiber as one of the electrodes is made of a highly conductive metal. Despite of the copper electrode in its structure the fiber is still highly flexible. As outside electrode is exposed, this fiber can be used for the detection of electromagnetic influence or as a proximity sensor.

Design three is presented in Fig. 2-2(d), where we show a circular fiber containing two hollow cores positioned in the middle of the fiber. Each core is lined with a distinct conductive layer which are forming electrode one and two. The cores with electrodes are electrically isolated from each other. Moreover, the whole preform is then wrapped into several layers of pure LDPE plastic to isolate the capacitor layers from the environment. The preform is then drawn with two copper wires threaded through its holes. Resultant fiber features two copper electrodes and a fully encapsulated capacitor multilayer. Such fibers can be interesting for energy storage applications due to ease of connection and electrical isolation from the environment.

Finally, design four is presented in Fig. 2-2(e) where we show a thin PMMA tube of square crossection comprising a zigzagging multilayer of the two conductive layers separated by a single electrically isolating PC layer. The first plastic electrode is located to the left and the second plastic electrode is located to the right of the isolating PC layer. At the left and right inner

sides of the square tube we place foils of Bi_{58}/Sn_{42} alloy in contact with the plastic conductive layers. During fiber drawing wire-like metallic electrodes are created from the foils. Finally, the structure of the resultant fiber is similar to the one of an encapsulated fiber with two copper electrodes.

In comparison with standard capacitors, we notice that a 10nF ceramic capacitor measures about 600μm x 300μm and 10 μF components measure 2.0mm x 1.25 mm. The fiber capacitor does not possess advantages over the standard capacitors in terms of size, but the flexibility and softness it featured are essential for applications in wearable smart textiles. Encapsulation of RC series in a single fiber makes the circuit in wearable e-textiles more compact and reliable because it may reduce the number of connection joints. Although the equivalent resistance of the capacitor is very high for a short fiber, which is limited by the properties of available conductive films, it can be reduced simply by increase the length of the fiber as demonstrated in the following paragraphs.

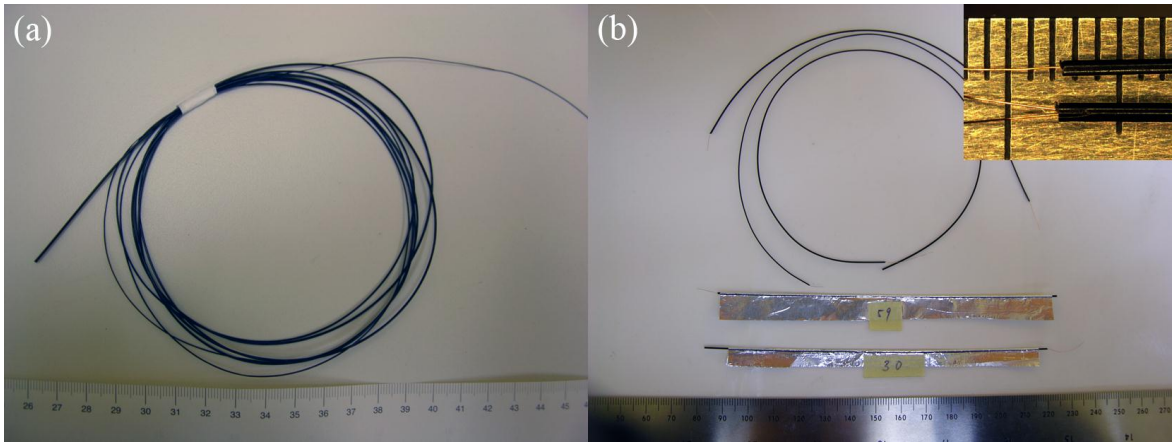

Fig. 2-3 (a) Capacitor fiber fabricated from the preform shown in Fig. 2-2(c). The fiber features a central 100μm-thick copper wire, as well as an exposed conductive plastic electrode on the fiber surface. (b) To perform electrical characterization of the fibers, embedded copper wire is used as the first electrical probe, while the second electrical probe is an aluminum foil wrapped around the fiber conductive surface. The inset is an enlarged view of the fibers with single and double copper wire electrodes.

2.2 Electrical properties of the soft capacitor fibers

2.2.1 Setup for characterization of the isolated capacitor fiber

To characterize electrical properties of our capacitor fibers we used a measurement circuit presented in Fig. 2-4, where the fiber capacitor is connected to a function generator (GFG-8216A, Good Will Instrument Co., Ltd) through the reference resistor R_{ref} = 480 kΩ. The function generator provides a sinusoidal signal of tunable frequency ω=[0.3Hz-3MHz]. An oscilloscope (GDS-1022, Good Will Instrument Co., Ltd) measures the input voltage V_{Ch1} (ω) on channel 1 and the output voltage over the reference resistor V_{Ch2} (ω) on channel 2. A 10X probe (GTP-060A-4, Good Will Instrument Co., Ltd) was used to acquire the experimental data. The voltage produced by the function generator is fixed and in the whole frequency range of interest equals to V_{Ch1} = 2V. In our experiments we measured both the amplitudes and the phase difference between channels 1 and 2. Due to high resistivity of our fibers and also to fit the experimental data at higher frequencies (ω>1kHz), we have also to take into account the effective impedances of an oscilloscope.

In this section we present the properties of fiber capacitance and resistance as a function of various fiber geometrical parameters. Most of the measurements presented in this section were performed on fibers featuring a single copper electrode in their cores, while the second electrode is formed by the plastic conductive layer on the fiber surface (see Fig. 2-2(c)). The fiber was co-drawn with a 100 μm-thick copper wire in its center. In the preform, both conductive layers are 75 μm thick, while the two insulating layers are made of 86 μm thick LDPE films.

To characterize capacitance fibers we used embedded copper wire as the first electrical probe, while the second electrical probe was made by wrapping aluminum foil around a part or the whole of the fiber (Fig. 2-3).

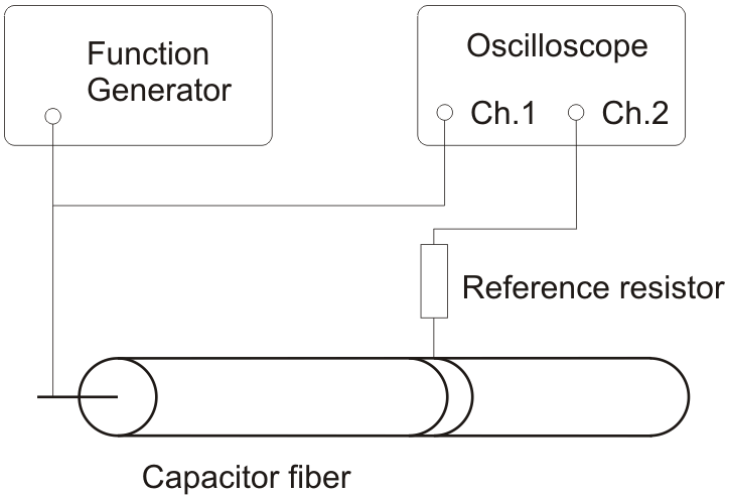

Fig. 2-4 Schematic of the measurement setup

2.2.2 RC ladder network model of a soft capacitor fiber fully covered with a foil probe

The high resistivity of the conductive composite films endows the capacitor fiber with a distributed response. Particularly the fiber electrical properties can be well described by a RC ladder circuit. First, we consider the case when the fiber outer electrode is fully covered with a highly conductive foil probe. In this case, the problem becomes two dimensional (no longitudinal currents) and an RC ladder circuit presented in Fig. 2-5 describes transverse currents in the capacitor crossection.

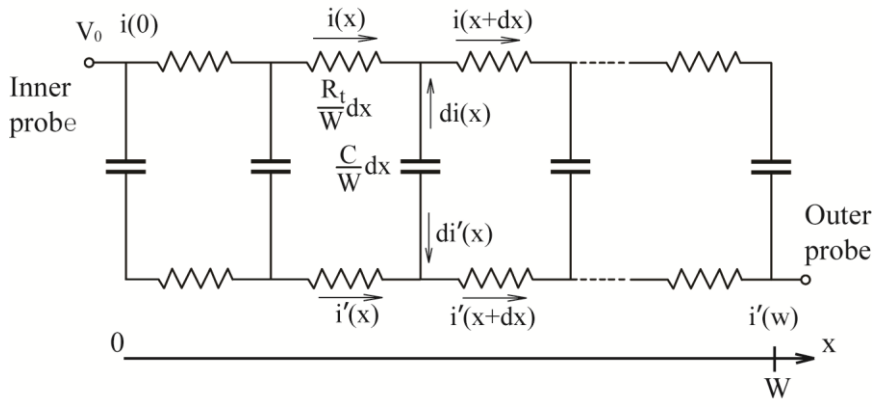

Fig. 2-5 Ladder network model of the capacitor fiber fully covered with a foil probe.

In Fig. 2-5 a schematic of the ladder model is presented where R_t corresponds to the transverse resistance of a single conductive film spiralling from the fiber core towards its surface. The value of the transverse resistance can then be approximated as:

$$R_t \approx \rho_v \frac{W}{Ld_c} \tag{2.1}$$

where ρ_v is the volume resistivity of the conductive films, L is the length of the fiber, W and d_c denote respectively the width and thickness of the conductive electrodes wrapped in the fiber crossection (see Fig. 2-2). To measure transverse resistance one has to ensure that there are no longitudinal (along the fiber length) currents in the fiber. Practically, to deduce transverse resistance one covers the outer fiber electrode (high resistance electrode) with a metallic foil, and then measures fiber AC response by applying the voltage between the inner copper electrode and the outer metallic foil.

For the longitudinal currents, fiber resistance will be:

$$R_l \approx \rho_v \frac{L}{Wd_c} \tag{2.2}$$

which for longer samples ($L > W$) is much higher than the transverse resistance.

To measure the longitudinal resistance one has to ensure that there are no transverse (perpendicular to the fiber length) currents in the fiber. Practically, it is difficult to measure the longitudinal resistance directly. In principle, if the electrode length (fiber length) is much longer than the net width of a conductive electrode wrapped in the fiber crossection, longitudinal resistance can be deduced from the AC measurement where high resistance outer electrode of a fiber is grounded on one end, while the inner high resistance electrode of the fiber is connected to a voltage supply at the other end. Note that the low resistance copper electrode has to be removed from the fiber for this measurement and DC measurements aren't possible as in the described configuration fiber acts as a capacitor. Clearly, when connecting to a fiber using a continuous probe (like foil) along the whole fiber length, fiber resistance will be dominated by its transverse component.

Another fundamental parameter that determines fiber performance is the fiber capacitance denoted as C in schematics Fig. 2-5. As thicknesses of the dielectric and conductive layers in the

fiber are hundred times smaller than the fiber diameter, fiber capacitance can be well approximated using an expression for the equivalent parallel-plate capacitor:

$$C \approx 2\varepsilon_0 \varepsilon \frac{WL}{d_i} \tag{2.3}$$

where ε is dielectric constant of the isolating films, ε_0 is permeability of the vacuum, d_i is thickness of the rolled isolating films.

As shown in Fig. 2-5, $i(x)$ and $i'(x)$ denote the current flowing in the conductive film connected to the inner probe and outer probe respectively. V_0 is the voltage difference between the inner probe and outer probe. We assume that the resistivity of the conductive film is a position-independant and frequency-indepent parameter. Appling Kirchhoff's Voltage Law (KVL) and Kirchhoff's Current Law (KCL) to the ladder circuit leads to the following equations:

$$\int_0^x \frac{R_t}{W} i(l)\,dl + \frac{W}{j\omega C}\frac{di'(x)}{dx} + \int_x^W \frac{R_t}{W} i'(l)\,dl = V_0 \tag{2.4}$$

and

$$di(x) = -di'(x) \tag{2.5}$$

With boundary conditions

$$i(0) = i'(W) \text{ and } i'(W) = 0 \tag{2.6},$$

equations (2.4), (2.5) and (2.6) can be solved analytically, and yields the following expressions for the effective transversal capacitance and effective transversal series resistance:

$$C_F(\omega) = -\frac{1}{\omega R_t \cdot Im\left(f(B)\right)} \tag{2.7},$$

$$R_F(\omega) = \frac{R_t}{2} + R_t \cdot Re\left(f(B)\right) \tag{2.8},$$

where

$$f(B)=\frac{1+\cosh(B)}{B\cdot\sinh(B)};\quad B=\sqrt{2j\omega R_t C}$$

Note at low frequencies, i.e. $B\rightarrow 0$, equations (2.7) and (2.8) reduce to the frequency-independent values as follows:

$$C_F = C,\ \ R_F = \frac{2}{3}R_t \tag{2.9}$$

2.2.3 Frequency dependent response of the capacitor fibers

As predicted by equations (2.7) and (2.8), effective capacitance and effective resistance of the capacitor fibers are dependent on the operational frequency, with limiting values at low frequencies given by (2.9). In this section we present results of experimental studies of the frequency dependent response of the capacitor fibers. To interpret correctly the measured response V_{Ch2} (ω) of the electric circuit it is important to take into the consideration the complex impedance of the oscilloscope and the electric probe used in the characterization. This is mainly due to the relatively large resistance of our fibers. One also has to be aware that conductive films used in the fiber fabrication can show significant frequency-dependence of their electrical properties. For example it has been reported [74] that near the percolation threshold the resistivity of CB/polymer films decreases with increasing frequency. To find the effective circuit parameters of an oscilloscope we first measured the response of a known resistor having a similar resistance as that of a fiber (~477 kΩ). We noted that complex impedance of the measuring circuit (oscilloscope) becomes important only at frequencies higher than 100 kHz. We then studied frequency response of the conductive film, and found that its resistivity is frequency independent below 300 kHz. Therefore, in all the experiments that followed we have operating frequencies lower than 100 kHz.

In Fig. 2-6 we present experimentally measured frequency dependent fiber resistance and capacitance of a fiber fully covered with a foil probe and with diameter of 0.93 mm and length of 137mm. At low frequencies both C_F and R_F are virtually constants, while they decrease at frequencies higher than 1 kHz. This behavior is similar to that of a standard electrolytic capacitor

and can be well explained by the RC ladder network model with a characteristic response frequency of $1/(R_tC)$~4 kHz. We can also see that equations (2.7) and (2.8) provide very good predictions of the experimental data by assuming C=9.4 nF and R_t=26 kΩ in the model.

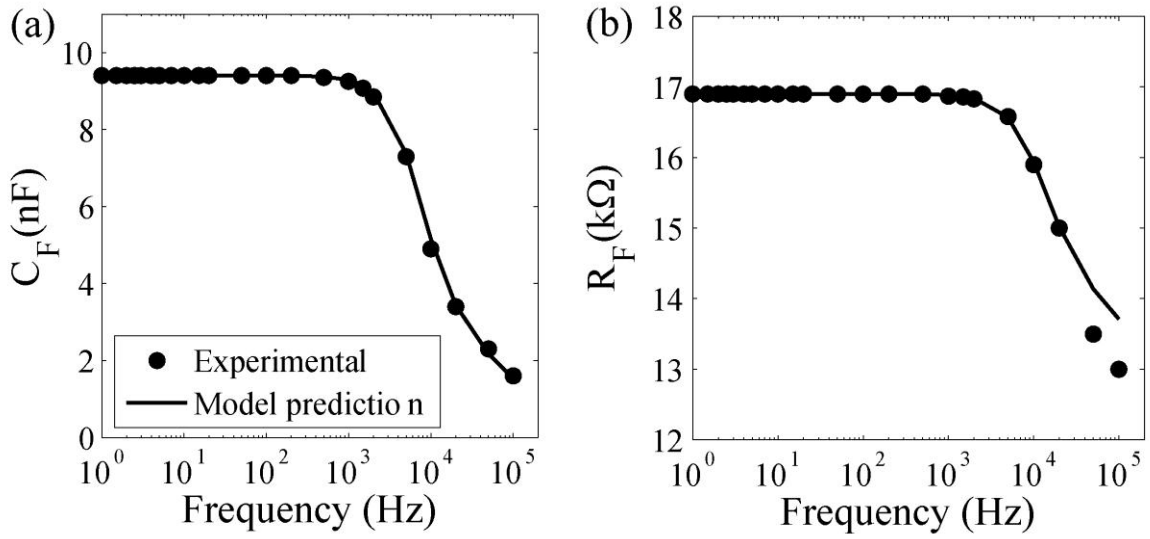

Fig. 2-6 Comparison of experimental data and model predictions of frequency responses of a fiber capacitor. (a) Effective capacitance vs. frequency. (b) Effective resistance vs. frequency.

2.2.4 Effect of the capacitor fiber length

In order to study dependence of the fiber properties as a function of the fiber length, we have used two fiber samples of different length that were drawn from the same preform. Sample #1 and sample #2 had outer diameters of 920-980 μm and 720-760 μm respectively. Both samples were drawn from the same preform at speeds around 100 mm/min at 180℃. The two samples were then cut into sections of different lengths ranging between 10 cm and 60 cm, and then wrapped with an aluminum foil with 100% coverage ratio. The experiments were conducted at low frequencies (ω<1 kHz), so that effective capacitance and resistance can be considered as constant. In Fig. 2-7(a) we present measured fiber capacitance as a function of fiber length and observe a clear linear dependence. From this data we see that for all the fibers the capacitance per unit length is around 69 nF/m (inset in the Fig. 2-7(a)), which is very close to the value of 69.5 nF/m measured for the capacitance of the fiber preform. This finding is easy to rationalise from equations (2.3) and (2.9). As W/d_i is constant during drawing (because of the largely

homologous drawing), hence, C_F/L should be the same for any fiber produced from the same preform, regardless of the fiber size. The reason why our fibers can obtain large capacitance is because the value of W/d_i is much larger than that of a coaxial cable with one capacitive layer. In contrast, fiber resistance decreases inversely proportional to the fiber length. In fact, it is rather the product $R_F \cdot L$ which is approximately constant, as shown in the inset of Fig. 2-7(b). Equations (2.1) and (2.9) indicate that if ρ_v is constant $R_F \cdot L$ should also be a constant because W/d_c is the same for fibers drawn from the same preform. However, we also find that the thinner fiber shows a larger value of $R_F \cdot L$. This diameter dependency is implied in the volume resistivity ρ_v in equation (2.1). It is reported that the resistivity of CB/polymer composites increase as the material is stretched, and the value is proportional to the elongation ratio in logarithm scale [75], [76]. Thus we observed that the thinner fiber has a larger $R_F \cdot L$ value.

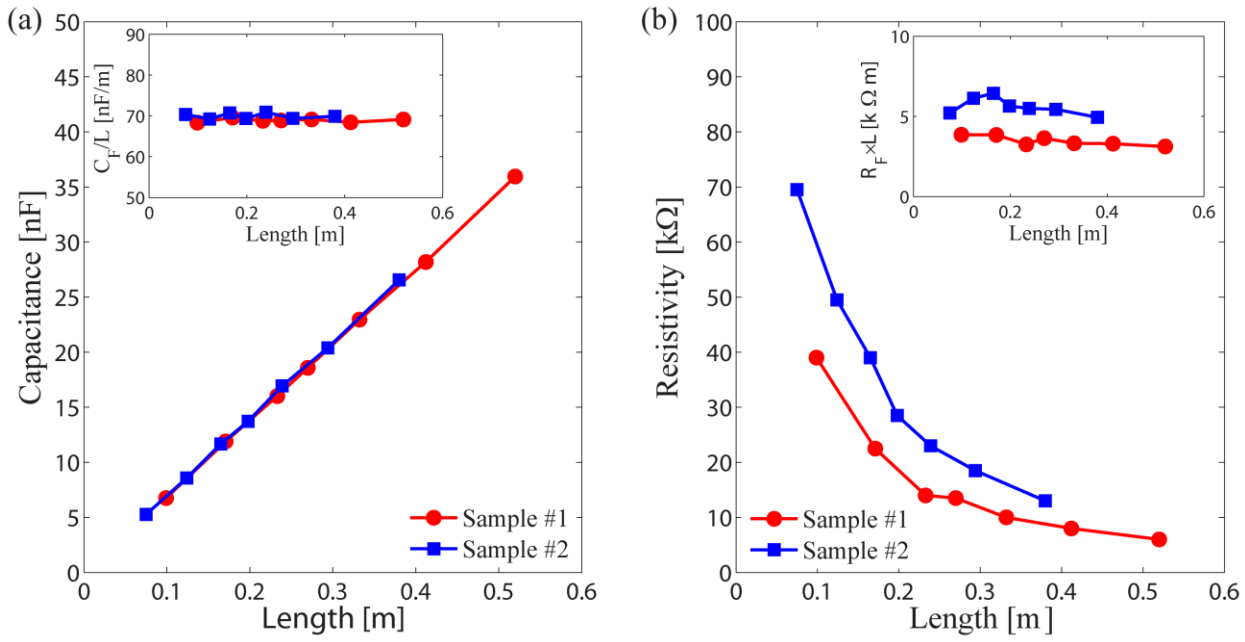

Fig. 2-7 Dependence of the (a) fiber capacitance and (b) fiber resistivity on fiber length. Red and blue data sets correspond to the two fiber samples of different diameters drawn from the same preform. Insets: dependence of the (a) fiber capacitance per unit length C_F/L and (b) fiber resistivity factor $R_F \cdot L$ on the fiber length.

2.2.5 Effect of the temperature of operation on the fiber electrical properties

The effect of the temperature of operation on the electrical properties of a capacitor fiber is presented in Fig. 2-8. Sample #1 was 135 mm long and had a diameter of 840 μm, while sample #2 was 133 mm long and had a diameter of 930 μm. To control the temperature of the two samples they were fixed on top of a hot plate. Our measurements at low frequencies show that fiber capacitance per unit length remains almost independent of the temperature of operation, while fiber resistivity increases rapidly as the temperature rises. This result is in good correspondence with the recent reports on positive temperature coefficient [77], [78] for the resistivity of the composites of carbon black and LDPE in the 0℃ to 100℃ temperature range. The effect of thermal expansion and a consequent increase of the average distance between carbon black particles are thought to be the main reasons for the positive temperature coefficient of the conductive polymer composites. This interesting property promises various applications of capacitor fibers in self-controlled or self-limiting textiles responsive to temperature or heat.

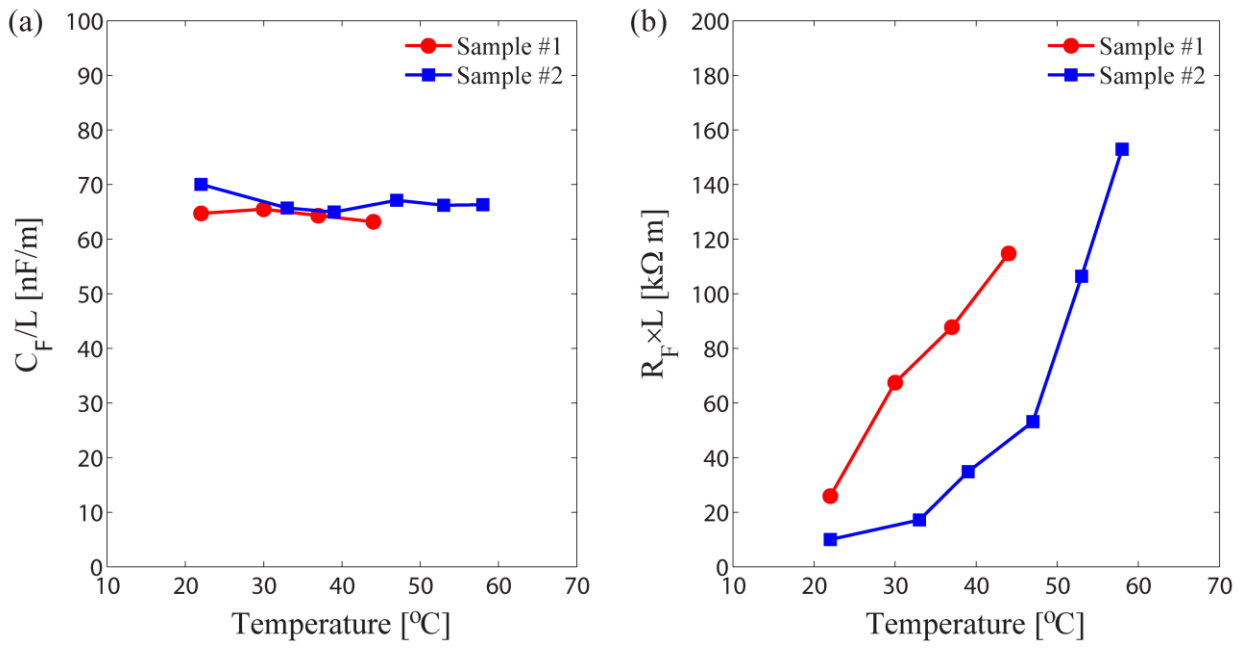

Fig. 2-8 Effect of the temperature of operation on electrical properties of a capacitor fiber. (a) Capacitance per unit of length C_F/L. (b) Resistivity factor RF•L. Sample #1 has a diameter of 840 μm and a length of 135 mm. Sample #2 has a diameter of 930 μm and a length of 136 mm.

2.2.6 Effect of the fiber drawing parameters

Electrical performance of the capacitor fibers is equally affected by the fiber geometrical parameters and by the fiber material parameters. In this section we show that fiber fabrication parameters such as fiber drawing temperature and fiber drawing speed can have a significant effect on the fiber resistivity, while also somewhat affecting the fiber capacitance. Generally, capacitor fibers presented in this work can be drawn at temperatures in the range of 170℃-185℃ with drawing speeds ranging from 100 to 300 mm/min.

Generally, we find that the fiber capacitance C_F/L is largely independent on the fiber diameter and drawing parameters, and equals to that measured directly in the fiber preform. In contrast, fiber resistivity parameter $R_F \cdot L$ is significantly affected by the drawing parameters. Particularly, from equations (2.1), (2.3) and (2.9) we can relate fiber capacitance per unit length and fiber resistivity parameters as:

$$\frac{R_F L}{C_F / L} \propto \frac{\rho_v}{\varepsilon_0 \varepsilon} \tag{2.10}$$

While fiber capacitance is indeed almost independent of the fiber geometrical and processing parameters, fiber resistivity is strongly influenced by them. This can be rationalized by concluding that bulk resistivity of the carbon black polymer composite can change significantly during drawing procedure from its original value in the fiber preform. To further validate our observation that drawing at lower temperatures results in higher resistivities we performed a set of stretching experiments at room temperature on the planar conductive films. It was found that the resistivity of the conductive film increases as much as by two orders of magnitude from its original value when the films were stretched unheated to about two times of their length. Similar observation has been reported in the literature for carbon black filled polymers and polymer composites [75], [76].

Conclusions of these experiments can be rationalized as follows. During the drawing process the conductive polymer composite in the preform undergoes various processing stages including heating, melting, stretching, annealing and cooling. The stretching increases the distance between the individual carbon black (CB) particles in the stretching direction, thus disrupting the conductive network. During the annealing above glass transition temperature, carbon black

particles aggregate together through Brownian motion and form a continuous network. The destruction and reconstruction of the conductive network is highly dependent on the concentration and properties of CB and processing parameters such as mixing strength, temperature and time and the annealing temperature and time, etc. [79], [80]. If the fiber is drawn at a lower temperature and with a higher speed, the stronger viscous stress of the polymer matrix may disintegrate CB particles and decrease their aspect ratio, thus making the conductive network more difficult to be formed. The annealing conditions have direct influences on the formation of the conductive network [80]. The rising of the annealing temperature decreases the viscosity of the matrix polymer, thus facilitating the movement and aggregation of the CB particles. This, in turn, reduces the time needed for the CB particles to build up a conductive network. It is well reported that the resistivity of polymer composites filled with carbon black [80], [81] or carbon nanotube [82] decreases as the annealing temperature and time increase. This explains our experimental observation about lower drawing speeds resulting in lower fiber resistivities; this is because a lower drawing speed leads to a longer annealing time in the furnace. In addition, a lower drawing speed corresponds to a weaker stretching and slower deformation. This not only avoids CB particles to be disintegrated but also provides them with more time to create a conductive network before cooling down to the room temperature.

2.3 Capacitor fiber as a 1D distributed touch sensor

In this section we study properties of the individual soft capacitor fiber as a one-dimensional tactile sensor integrated into textile base. To ease the integration and connection of the fibers a small-diameter (typically 50-150 μm) copper wire was embedded into the fiber during the drawing process by passing it inside of the fiber preform (see Fig. 2-9) central hole and letting the preform to collapse around the wire in the neckdown region.

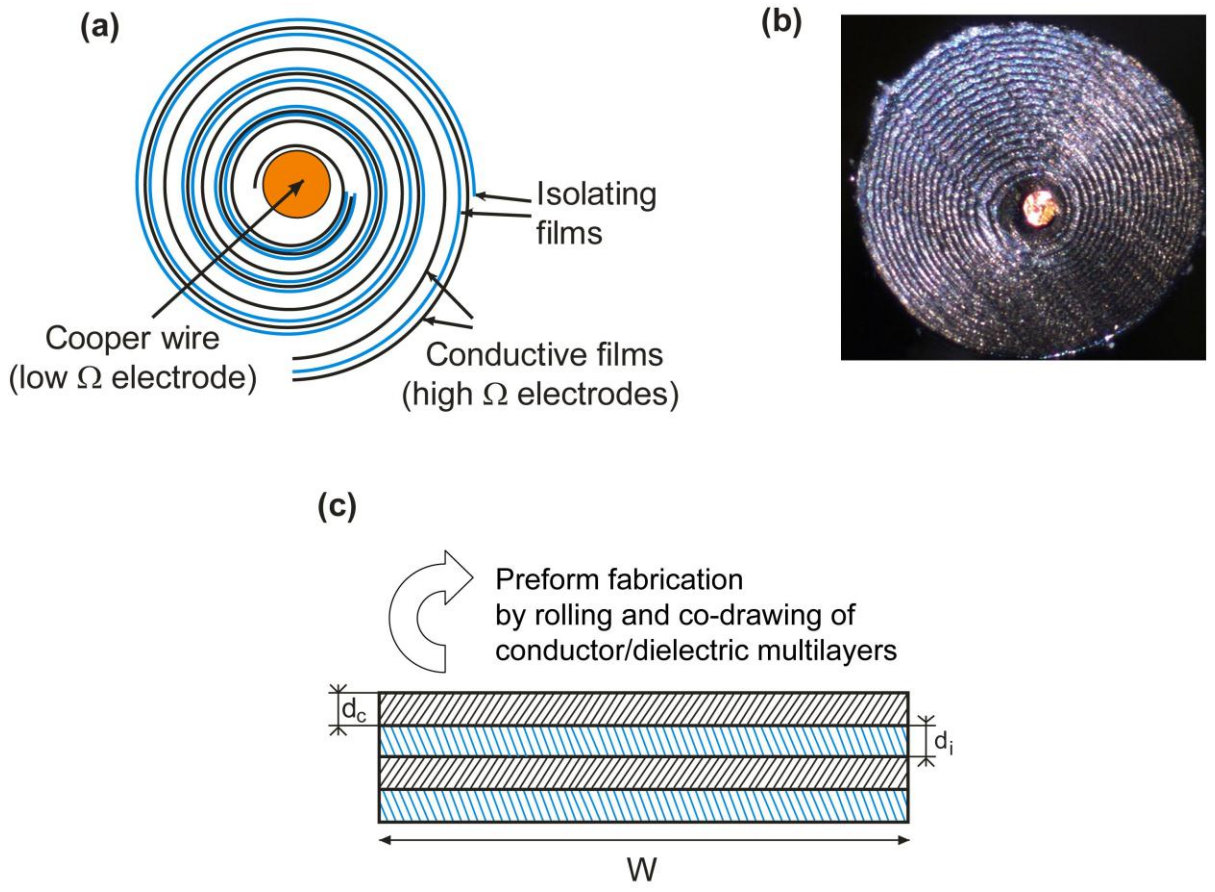

Fig. 2-9 (a) Schematic of a capacitor fiber featuring a spiraling multilayer comprising two conductive and two isolating films. Black curves represent two conductive films, while blue curves represent isolating films. (b) Photo of the crosssection of a drawn capacitor fiber with a cooper wire embedded in the center. (c) Fiber preform is made by co-rolling four polymer layers (2 conductive and two isolating) into a swiss-roll structure. The number of resultant layers in a spiral structure is proportional to the width of the unrolled multilayer. In the drawn fiber, thicknesses of the conductive d_c and isolating d_i layers can be smaller than 10μm, while the unwrapped width W of the layers fitting into a 1mm diameter fiber can be in excess of 3cm.

For the reader unfamiliar with the fiber drawing procedure we would like to explain that neckdown region is a “transitional” region between the preform and the resulting fiber, where the preform converges to the size of the resulting fiber. Introduction of a copper wire into the fiber drawing process actually improves the fiber drawability. In this configuration, copper wire in the fiber center serves as a low resistivity electrode attached to one of the two high resistivity conductive plastic electrodes of a fiber capacitor. The other high resistivity conductive plastic electrode of a fiber is brought to the fiber surface to ease connection. Typical fibers fabricated

using the above-mentioned fabrication procedure have a sub-millimeter diameter, contain at least 30 layers, and have a typical capacitance of 100 nF/m, which is almost three orders of magnitude higher than that of a standard coaxial cable of a comparable diameter.

High resistivity of the conductive polymer electrodes together with high capacitance endows the fiber with interesting electrical properties, which as we will see in what follows, makes the fiber well suited for distributed sensing applications of touch. In a typical implementation of a touch sensor, we ground the outer fiber electrode (high Ω electrode in Fig. 2-9) on one end, while applying the AC voltage to the copper wire (low Ω electrode in Fig. 2-9) on the other end (see Fig. 2-10). We then read out the voltage on the fiber outer electrode (high Ω electrode) at the same end where the copper wire is connected. In our experiments we found that the read out voltage is highly sensitive to the position of the touch along the fiber. In the following we describe basic principles behind touch sensing using a single capacitor fiber and then consider a theoretical model that describes capacitor fiber response to the touch.

2.3.1 Electrical response of a single capacitor fiber

To characterise a single fiber we use the general electrical layout outlined earlier. Particularly, a sinusoidal signal of voltage amplitude V_0 and constant frequency (10 Hz-10 kHz) is provided by an external function generator and is applied to the copper wire electrode of a fiber (see Fig. 2-10). Voltage response is acquired using a sliding contact on the outer electrode of a fiber (high Ω electrode). The sliding contact is connected to the oscilloscope as before through a 10X probe. This arrangement allows measuring the voltage distribution along the fiber length both when the fiber is touched or not. As a human body is largely composed of conductive electrolytes covered with a layer of dielectric skin, the human body can be approximated with an equivalent electrical circuit comprising a resistor connected in series to a capacitor. Typical values of an effective resistance and capacitance are 1.44 kΩ and 150 pF respectively. In our experimental studies of a single fiber response to touching, we use an equivalent human probe with these effective electrical parameters to guarantee repeatability between measurements and to simplify theoretical interpretation of the acquired data.

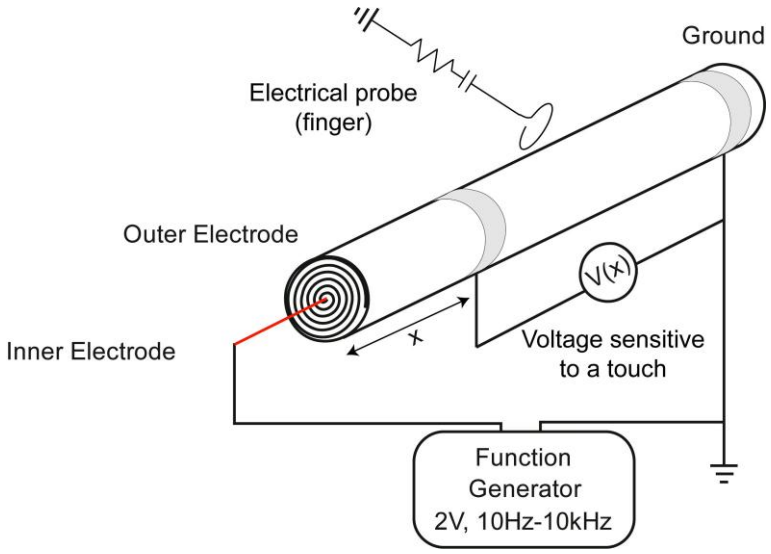

Fig. 2-10 Schematic of a 1D slide sensor based on a single capacitor fiber.

In Fig. 2-11 we present voltage distribution along the fiber length for an isolated fiber (Fig. 2-11(a)), and for the fiber that is touched with an equivalent human probe (Fig. 2-11(b)). Here *x/L* represents the normalised position of a sliding contact along the fiber length. Fiber length used in our experiments was L=12.3cm. $|V(x)/V_0|$ represents the voltage measured by the sliding contact along the outer electrode of a capacitor fiber. When using equivalent human probe (Fig. 2-11(b)), we fix it at the position x/L=0.3. Different data sets in Fig. 2-11 correspond to the four different frequencies of a function generator used in our measurements (10 Hz, 100 Hz, 1 kHz, 10 kHz).

In the DC case (not shown in the figures), voltage along the outer electrode of a capacitor is constant and zero as the outer high-resistive electrode provides a DC-connection to ground. For an isolated fiber (Fig. 2-11(a)) in the AC case, voltage distribution along the fiber length shows the same trend at all frequencies. Particularly, it saturates exponentially fast from zero at the grounded end to some maximal value at the other end of the fiber.

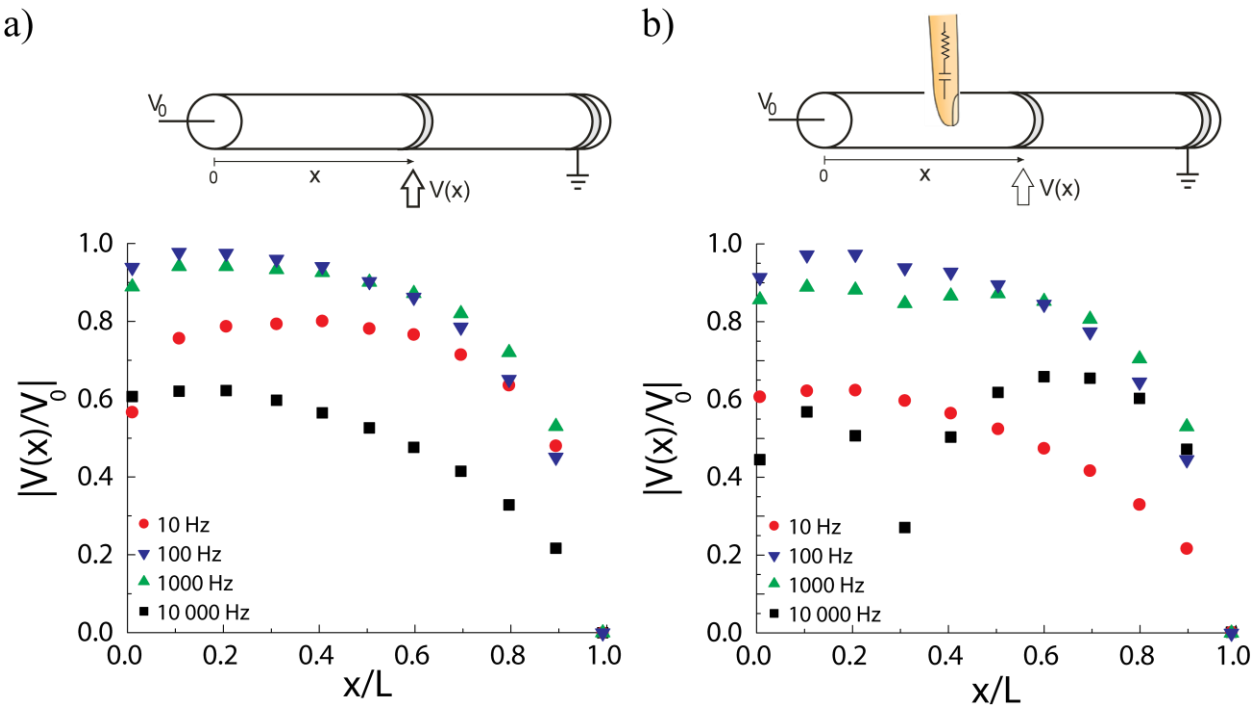

Fig. 2-11 Voltage distribution along the outer fiber electrode for (a) an isolated fiber (b) a fiber touched with an equivalent human probe. Four data sets correspond to the different driving frequencies of 10 Hz, 100 Hz, 1 kHz and 10 kHz. Voltage distribution along the fiber touched with a probe shows dip in the vicinity of a touching position.

From Fig. 2-11(b) it is clear that when operating at higher driving frequencies the touch position can be determined from the dip in the voltage distribution along the fiber outer electrode. For practical implementation of a slide sensor, it is, however, inconvenient to require the knowledge of the voltage distribution across the whole fiber length. Therefore, the important question is whether position of the touch can be determined by continuously measuring the voltage at a single fixed point on the fiber outer electrode. To answer this question in Fig. 2-12 we present the value of voltage as measured at the fiber extremity ($x = 0$) as a function of the touch position along the fiber. Now *x/L* represents the touch position of the equivalent human probe, while $|V(0)/V_0|$ represents the voltage measured at the fiber end opposite to the grounded end. We observe that for driving frequencies above 100 Hz, the voltage at the fiber extremity changes significantly depending on the position of touch. In turn, this allows building a 1D sliding sensor with a convenient acquisition procedure based on a single point measurement.

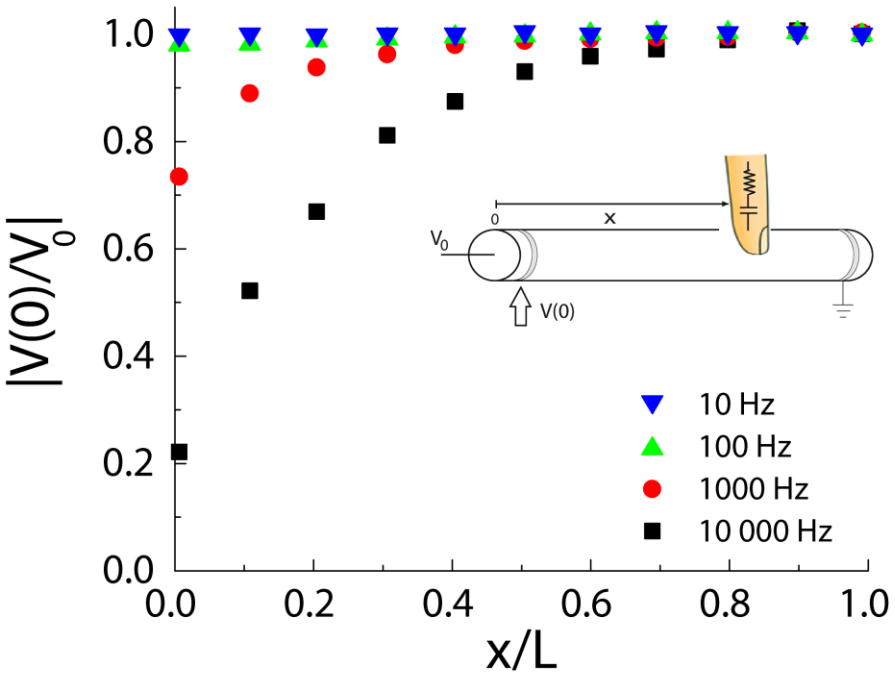

Fig. 2-12 Voltage measured at the extremity of a capacitor fiber opposite to the fiber grounded end.

2.3.2 RC ladder network model for the capacitor fiber featuring one highly conductive, and one highly resistive electrodes

To model electrical response of the capacitor fibers we start with an RC ladder network presented in the Section 2.2.2 and first consider a stand-alone capacitor fiber without touching. As before (eq. (2.1), (2.2)) we define the conductive polymer electrode transverse resistance as $R_t \approx r_t/L$, where the electrode resistivity is $r_t = \rho_\upsilon W/d_c$. Longitudinal resistance is given by $R_l \approx r_l L$, where $r_l = \rho_\upsilon/(Wd_c)$ is the electrode longitudinal resistivity. Finally, the total fiber capacitance is proportional to the fiber length, while the fiber capacitance per unit length is simply $C_t \approx 2\varepsilon_0 \varepsilon W/d_i$ (eq. (2.3)), where d_i is the thickness of the isolating films in the fiber, ε is the dielectric constant of the isolating films, ε_0 is permeability of the vacuum.

We note that relatively high capacitance of our fibers is due to small thickness of the isolating films, and large net width of the conductive layers. Thus, a typical fiber features

conductive and isolating layers with thicknesses smaller than 10 μm, while the net width *W* of the layers wrapped into a 1 mm diameter fiber can be in excess of 3 cm.

Now let us consider a capacitor fiber as a sequence of thin crossections of length *dx* (Fig. 2-13(a)) each having a longitudinal resistance $dR_l = r_l\, dx$ for the outer (surface) electrode. We then consider electrical response of an individual crossection, while assuming that along the fiber length the individual fiber sections are connected via longitudinal resistance elements dR_l (Fig. 2-13(b)). Electrical response of an individual fiber crossection is modeled as an RC network where transverse resistance elements $dR_t = r_t / dx$ are connected via capacitance $dC_t = C_t\, dx$ elements.

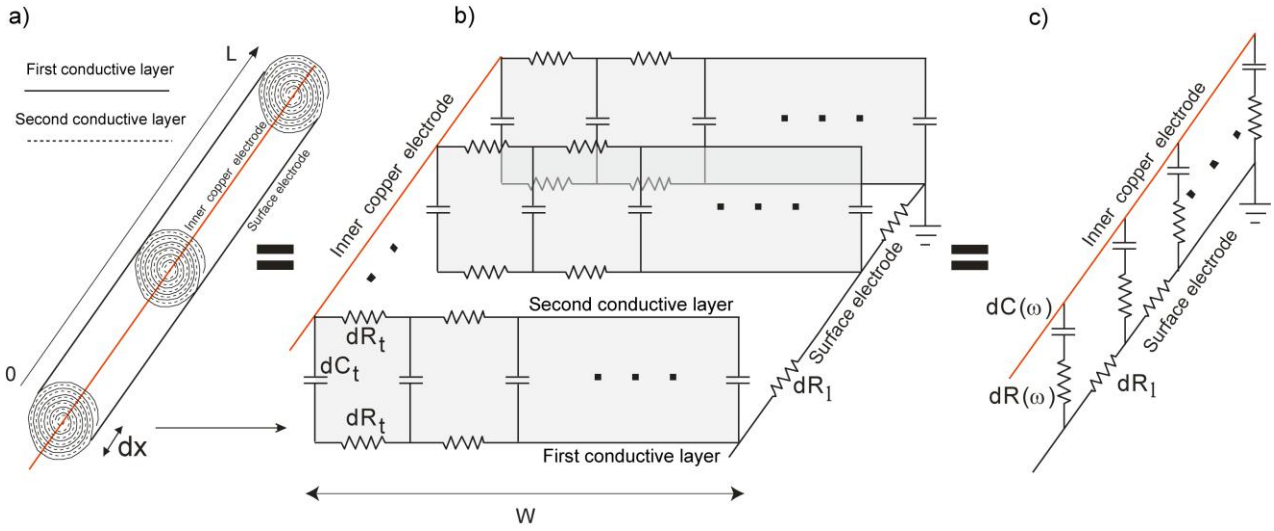

Fig. 2-13 Ladder RC network model of a stand-alone capacitor fiber. (a) The fiber is modeled as a sequence of fiber crossections of small length dx connected in series via longitudinal resistive elements (high resistivity outer electrode), while we assume that the inner copper electrode has a constant potential along its length. (b) Electrical response of an individual fiber crossection is modeled as an RC network where transverse resistivity elements are connected via capacitance elements. (c) Also dR_l on the scheme above corresponds to longitudinal resistance element, $dR(\omega)$ and $dC(\omega)$ are frequency dependent resistance and capacitance of an individual fiber crossection of length *dx*. One can show that equivalent circuit that describes electrical response of an individual fiber crossection is given simply by the frequency dependent resistivity connected in series with frequency dependent capacitance. Finally, electrical response of a fiber is modeled as another RC network with frequency dependent resistivity and capacitance.

In Section 2.2.2 we have shown that equivalent circuit that describes electrical response of an individual fiber crossection of length *dx* is given by the frequency dependent resistance $dR(\omega)$ connected in series with frequency dependent capacitance $dC(\omega)$, where:

$$dC(\omega) = -\frac{dx}{\omega r_t \cdot \mathrm{Im}\left(f(B)\right)}, \tag{2.11}$$

$$dR(\omega) = \left(\frac{1}{2} + \mathrm{Re}\left(f(B)\right)\right)\frac{r_t}{dx}, \tag{2.12}$$

and $f(B) = \dfrac{1+\cosh(B)}{B\cdot\sinh(B)}$; $B = \sqrt{2j\omega \cdot r_t C_t}$.

Electrical response of a stand-alone fiber can, therefore, be modeled as another RC ladder with frequency dependent $dR(\omega)$, $dC(\omega)$, and frequency independent parameters dR_l (see Fig. 2-13(c)).

Now that the model for a stand-alone capacitor fiber is defined, we modify it slightly in order to analyse a 1D slide sensor. Particularly, the fiber is assumed to be touched at a position x_b with a finger having effective electric parameters R_b=1.44 kΩ, C_b=150 pF. Moreover, to simplify comparison with experiment we include in our model the effective circuit of an oscilloscope probe used in our measurements. The probe is attached at a position x_p on the fiber surface (see Fig. 2-14), and the effective circuit parameters of a probe and oscilloscope are R_p=10 MΩ, C_p=200 pF. The necessity to include effective circuit of a probe into the model comes from the realization that resistance of a standard 10X probe (10 MΩ) used in our experiments has the same order of magnitude as the transverse resistance of the short fiber segments used in our studies. For example, transverse resistance of the 10 cm-long fiber pieces typically ranges in 0.1 - 1 MΩ. Moreover, one can show that at frequencies lower than $\nu \approx 1/\left(2\pi R_p C_b\right) \approx 100\ Hz$ or higher than $\nu \approx 1/\left(2\pi R_b C_p\right) \approx 55\ kHz$, the effective impedance of a probe becomes smaller than that of a finger, therefore the probe effective circuit has to be included into the model to accurately explain experimental measurements.

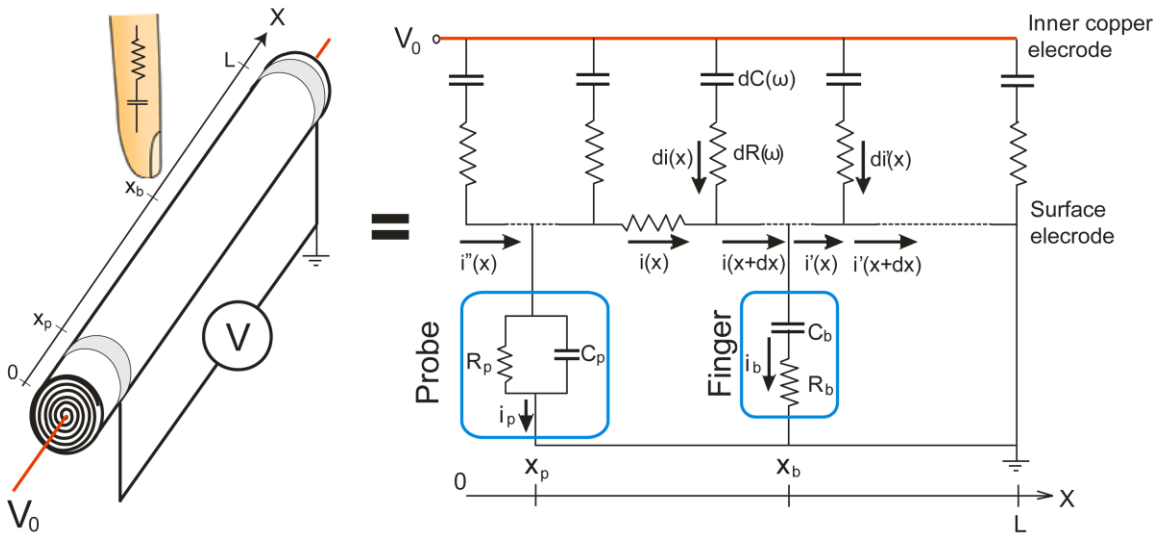

Fig. 2-14 The ladder network model of a 1D slide sensor. The fiber is assumed to be touched at a position x_b with a finger having effective electric parameters R_b, C_b. Moreover, to simplify comparison with experiment we include in our model the effective circuit (with parameters R_p, C_p) of an oscilloscope probe used in our measurements; the probe is attached at a position x_p.

In Fig. 2-14 we distinguish three parts of an RC latter network. The first part is located to the left of the probe, where i"(x) denotes the longitudinal current flowing in the polymer conductive film, while di"(x) denotes the transverse current flowing in the thin section of length dx. To the right of the probe, while still before the finger touch position the longitudinal ant transverse currents in the polymer electrode are denoted as $i(x)$ and $di(x)$. Finally, to the right of the touch position the corresponding currents are i'(x) and di'(x). V_0 is the voltage difference between the inner copper electrode and the outer electrode at $x=L$. We also assume that the fiber material parameters are position and frequency independent. Furthermore, we consider that that the probe is attached to the left of a touch position $x_p<x_b$. We now apply the Kirchhoff's voltage law and current conservation law to the ladder circuit to arrive at the following equations for any position x along the fiber. Thus, using Kirchhoff's voltage law we get:

$$
\begin{aligned}
&0 < x < x_p \quad ; \quad di''(x)\left(\frac{1}{j\omega\, dC(\omega)} + dR(\omega)\right) + \int_x^{x_p} r_l\, i''(l)\, dl = V_0 - V(x_p) \\
&x = x_p \quad ; \qquad i_p \frac{R_p}{1 + j\omega C_p R_p} = V(x_p) \\
&x_p < x < x_b \quad ; \quad di(x)\left(\frac{1}{j\omega\, dC(\omega)} + dR(\omega)\right) + \int_x^{x_b} r_l\, i(l)\, dl = V_0 - V(x_b) \\
&x = x_b \quad ; \qquad i_b\left(\frac{1}{j\omega C_b} + R_b\right) = V(x_b) \\
&x_b < x < L \quad ; \quad di'(x)\left(\frac{1}{j\omega\, dC(\omega)} + dR(\omega)\right) + \int_x^{L} r_l\, i'(l)\, dl = V_0
\end{aligned}
\quad . \tag{2.13}
$$

Using the current conservation law we get:

$$
\begin{aligned}
&0 < x < x_p \quad ; \quad i''(x) + di''(x) = i''(x + dx) \\
&x = x_p \quad ; \qquad i''(x_p) = i(x_p) + i_p \\
&x_p < x < x_b \quad ; \quad i(x) + di(x) = i(x + dx) \\
&x = x_b \quad ; \qquad i(x_b) = i'(x_b) + i_b \\
&x_p < x < L \quad ; \quad i'(x) + di'(x) = i'(x + dx)
\end{aligned}
\quad . \tag{2.14}
$$

Finally, the boundary conditions are:

$$
i''(0) = 0 . \tag{2.15}
$$

To solve these equations, we can first differentiate equations (2.13) with respect to x to obtain three similar second order differential equations with respect to i, i' or i'' of the following form:

$$
\frac{d^2 i(x)}{dx^2}\left(\frac{1}{j\omega\, dC(\omega)/dx} + dx \cdot dR(\omega)\right) - r_l\, i(x) = 0 . \tag{2.16}
$$

Then, in each of the three sections of the fiber, we can write solution for the currents as:

$$
i = C_1 e^{\tilde{B}x} + C_2 e^{-\tilde{B}x} \quad ; \quad i' = C_3 e^{\tilde{B}x} + C_4 e^{-\tilde{B}x} \quad ; \quad i'' = C_5 e^{\tilde{B}x} + C_6 e^{-\tilde{B}x} \quad , \tag{2.17}
$$

where:

$$\tilde{B} = \sqrt{\frac{r_l}{\left(\frac{1}{j\omega dC(\omega)/dx} + dx \cdot dR(\omega) \right)}} = \sqrt{\frac{r_l}{r_t\left(\frac{1}{2} + f(B) \right)}}, \tag{2.18}$$

and B, $f(B)$ are defined in (2.11) and (2.12). Substitution of the expressions (2.17) into the remaining equations (2.13), (2.14) and (2.15) results in a set of linear equations from which the constants, C_1-C_6 can be determined. Finally, from the known current distributions voltage distribution in the given position *x* measured from the surface electrode can be easily found as:

$$V(x) = V_0 - \frac{d^2 i(x)}{dx^2}\left(\frac{1}{j\omega dC(\omega)/dx} + dx \cdot dR(\omega) \right). \tag{2.19}$$

2.3.2.1 Comparison of experimental data with predictions of a theoretical model

In Fig. 2-15 we present experimental data and theoretical RC ladder model (2.13)-(2.19) prediction for the dependence of voltage measured at x_p=0 as a function of the equivalent human probe touch position x_b. In each graph, different set of curves correspond to distinct fibers which are different from each other in a single parameter. Thus, in Fig. 2-15(a) we present measurements of three fibers which were drawn using preforms containing different number of conductive layers, and as a consequence, having different capacitance *C*. The preforms were drawn using the same temperature profile and drawing speed so as to guarantee similar values of the bulk resistivity of the polymer electrodes. Then, the fiber geometrical parameters such as layer thicknesses, electrode width and fiber length were measured using the optical microscope. Parameters of the oscilloscope effective circuit were measured independently. Finally, bulk resistance of the conductive layers in a fiber was measured, as described in Section 2.2.2, by wrapping the fiber outer electrode into a foil and then extracting the transverse resistance and, consequently, the bulk resistance of conductive layers from the fiber AC response. In this arrangement the currents are purely transverse and RC ladder model was shown (in Section 2.2.2) to give precise fits for the bulk resistivity parameter. We then use all these model parameters found in the independent measurements to predict the response of the fiber to the

touch. From Fig. 2-15(a) we see that at the operating frequency of 10 kHz the experimental curves are very well described by the RC ladder model which does not use any fitting parameter.

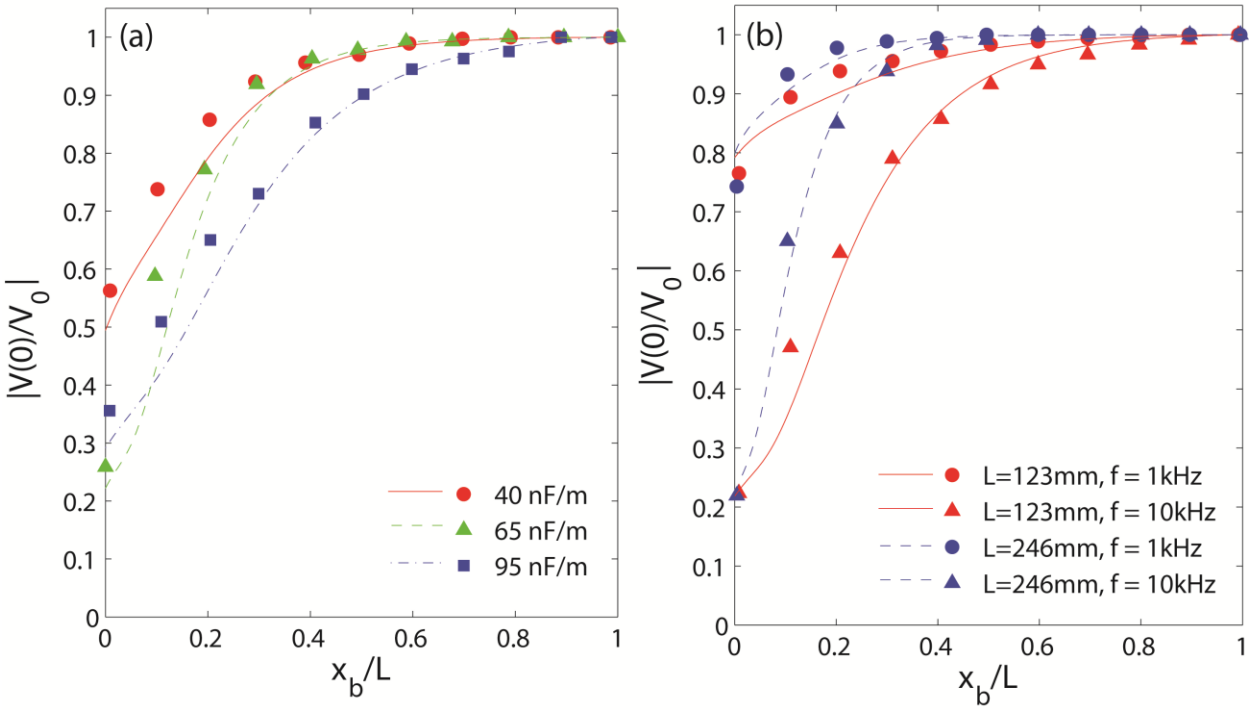

Fig. 2-15 Fiber response to the touch of the equivalent human probe - comparison between predictions of the RC ladder model and experimental data. (a) Response at 10 kHz of the three distinct fibers of the same length and different capacitances C_t=40 nF·m^{-1}, C_t =65 nF·m^{-1}, C_t =95 nF·m^{-1}. The rest of the geometrical and electrical parameters of the fibers are similar to each other. (b) Response at 1 kHz and 10 kHz of the two distinct fibers of the different lengths. The rest of the geometrical and electrical parameters of the fibers are identical to each other as shorter fiber was obtained by cutting a longer fiber in half.

Similarly, in Fig. 2-15(b) we present fiber response to the touch for two identical fibers of different length. In these experiments we first use the fiber of 24.6 cm of length and then cut it in half to 12.3 cm and repeat the measurement. The rest of the input parameters necessary for the use of a theoretical model were measured as described above. From the figure we see that fiber response is very well described by the RC ladder model both at 1 kHz and 10 kHz operating frequencies. Moreover, we see that this particular fiber becomes insensitive to touch if the touch point x_b is further than 10 cm from the measuring point x_p.

The measurement of fiber response as a function of fiber length presented in Fig. 2-15(b) brings about an important question about the maximal length of a 1D slide sensor, and about the

optimal frequency of operation. We note that the functional form of the currents (equation (2.17)) flowing between the probe and the measurement point is exponential with the characteristic length:

$$\tilde{L} = \frac{1}{\mathrm{Re}(\tilde{B})} = \frac{W}{\sqrt{2}} \frac{1}{\mathrm{Re}\left(\left(1+2f\left(B\right)\right)^{-\frac{1}{2}} \right)}, \tag{2.20}$$

where we used $\sqrt{r_t / r_l} = W$ - the total width of the rolled electrodes. We now use asymptotic expansions of the function $f(B)$:

$$f(B) = \frac{1+\cosh(B)}{B \cdot \sinh(B)} \underset{B=\sqrt{2j\omega \cdot r_t C_t}}{=} \begin{cases} \frac{1}{B} & ; \quad \omega \gg \frac{1}{r_t C_t} \\ \frac{2}{B^2} & ; \quad \omega \ll \frac{1}{r_t C_t} \end{cases}, \tag{2.21}$$

to get the following limiting values for the characteristic length of the current decay:

$$\tilde{L} = \frac{W}{\sqrt{2}} \begin{cases} 1 & ; \quad \omega \gg \frac{1}{r_t C_t} \\ \frac{1}{\sqrt{\omega r_t C_t}} & ; \quad \omega \ll \frac{1}{r_t C_t} \end{cases}. \tag{2.22}$$

Note that for the slide sensor of length L to be sensitive along its whole length we have to require that $L \sim \tilde{L}$. From the expression (2.22) we can see that at high frequencies $\omega \gg 1/\left(r_t C_t\right)$ the maximal sensor length is limited by the net width of a polymer electrode wrapped into the fiber crossection. Note that for most of our fibers the region of high frequency is in the vicinity or above 1 kHz. Furthermore, in a typical fiber of *D*=1 mm diameter, we can currently fit *N*~10-50 turns of the conductive electrode, which results in the net width of a conductive electrode in the fiber $W \sim \pi D N \sim 3cm - 15cm$. Therefore, for the operation frequencies in the vicinity or above 1 kHz, the maximal length of the capacitor fiber-based slide sensor is currently limited to several tens of centimeters.

In principle, operating at lower frequencies allows to match the fiber length and characteristic current decay length $L \sim \tilde{L}$ for any desired length of the fiber. This, however, demands very low

operation frequencies $\omega \sim (W/L)^2 / (r_t C_t)$ that even for a relatively short 1m-long fiber can be as low as 1-10 Hz. Operation at low frequencies, however, is prone to strong electrical interferences and noise. Moreover, at low frequencies ~1Hz the finger has very large impedance $\gg 1\ \mathrm{M\Omega}$, which is mismatched with that of our fiber. This makes the sensor of very low sensitivity at low frequencies.

2.3.3 Interpreting electrical data from a single fiber touch sensor

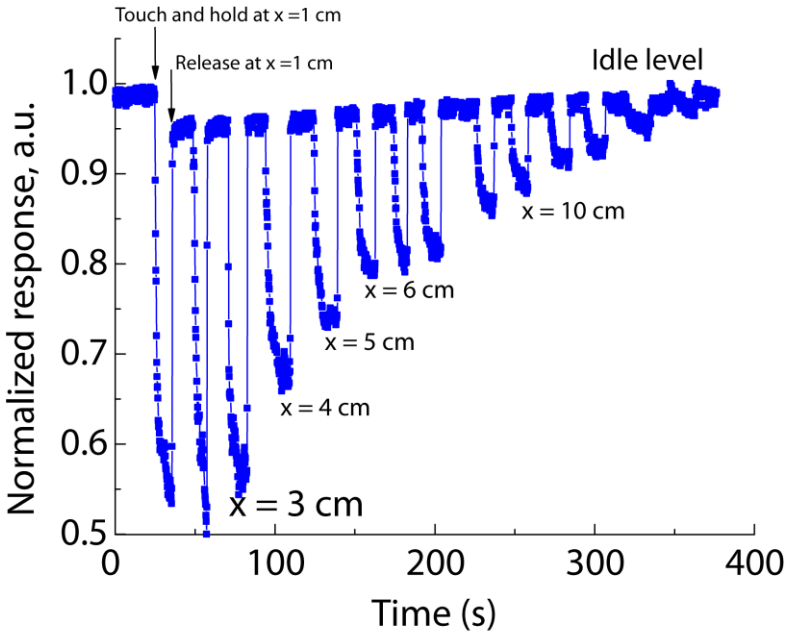

Fig. 2-16 Typical time resolved response of a 1D slide sensor. Dips in the measured voltage correspond to the touch and release events.

Finally, a 1D slide sensor was characterized in a realistic setting with a student touching the sensor consecutively at different positions along the fiber length. At this time the sensor was touched with an actual finger and not an equivalent probe. Driving frequency was 1 kHz and it was provided by the analogue output of an ADC card. The same card was also employed as a signal acquisition unit with an acquisition rate of 20 kHz. Such high acquisition rates were only used for the purpose of resolving the time response of a sensor and in practice significantly

slower acquisition rates (<10 Hz) could be used. To deduce the touch position we continuously measured the voltage at the endpoint of the fiber outer electrode. Fig. 2-16(b) presents an example of the measured voltage as a function of time. To operate the sensor we first record for several seconds the voltage level ("idle" level) without touching the fiber. We then touch the sensor at $x = 1\,cm$ from the fiber end. At the moment of touch the signal drops very fast (in a matter of 1s) to almost its equilibrium value, this is followed by a much slower (~10 s) relaxation to the actual equilibrium value. We believe that the fast time scale corresponds to a pure electrical response of a fiber, while the slow time scale corresponds to small pressure induced changes in the fiber electrical parameter due to fiber deformation under touch. As soon as the finger is removed, the signal returns back to the "idle" level in a matter of 0.2 s. Next, by touching, holding, and releasing the fiber at various positions along its length we can record a complete calibration curve. Then, the position of touch can determined from the voltage level at the bottom of dips corresponding to touching events. This is of course the simplest implementation of a touch sensor. To avoid person-dependent calibration of the sensor one can, for example, perform two voltage measurements from opposing sides of a fiber (by simultaneously flipping the ground from one side to the other), then use analytical models to extract the effective electrical parameters of a human figure and find touch position.

2.3.4 Effect of the fiber length on sensitivity

To study the effect of fiber length on its sensing performance, we take two pieces of fibers, named sample #1 and sample #2, from the same batch of drawing. Sample #1 with a length of 123 mm is a part of sample #2 with a length of 246 mm. Thus they share the same electrical and geometric parameters. The samples have an equal diameter around 1.1mm. The geometric parameters, such as the thickness and width of films (d_c, d_i and W), can be measured from microscopic observations or calculated from the preform geometry and draw-down ratio. The fiber's electrical parameters were characterised independently by the method reported in reference [80].The measured capacitance per unit length for both fibers equals 93 nF m^{-1}. The volume resistivity of the conductive film, calculated from transverse resistivity r_t, equals 4.5 Ωm. Fig. 2-15(b) also shows a comparison of the experimental data and model predictions for sample

#1 and #2 at frequencies of 1k and 10 kHz. The data below 100 Hz are not displayed because the disturbance caused by finger touch at these frequencies is very small.

We can see that both fibers exhibit a voltage drop at the left end, which becomes more prominent as frequency goes higher. This phenomenon is precisely predicted by the model. In order to find the reasons that cause this observation, we made calculations by a model without the oscilloscope in the circuit, or simply set the value of C_p extremely small and the value of R_p extremely higher in the present model. The result shows that if we neglect the effect of the oscilloscope the voltage becomes a constant without any drop when the measurement point approaches the left end of the fiber. This implies that this voltage drop on the left end of the fiber is rather caused by the decreased impedance of the oscilloscope at higher frequencies than by the fiber itself. As we can see from Fig. 2-15(b) the longer fiber, denoted by the blue color, has a longer part in the middle where the voltage is constant, while the short fiber, denoted by the red color, has a greater part of its length with a changing voltage. This can be rationalized by the distributed nature of the fiber. The edge effect becomes more dominant when the fiber length decreases. In Fig. 2-15(b) we compare the effect of frequency on the fiber performance. For both fibers the overall voltage decreases as frequency increases, which is related to the capacitance and resistance of the fiber.

2.3.5 Effect of the operational frequency on sensitivity

The maximal voltage amplitude at the outer fiber electrode is strongly dependent on the operation frequency and it reaches its maximum at frequencies between 100 Hz - 1 kHz. When fiber is touched with an equivalent human probe, voltage distribution along the fiber outer electrode shows high sensitivity to the operation frequency (Fig. 2-11 (a)-(b)). Thus, at low driving frequencies (10 Hz, 100 Hz) voltage distribution along the fiber outer electrode is virtually unchanged by the touch. At higher frequencies (above 100 Hz) a dip appears in the voltage distribution in the vicinity of the point of contact with an equivalent human probe. Finally, at high frequencies (above 1 kHz) this dip becomes very pronounced and easy to detect. Overall frequency response of the capacitor fiber can be understood from the basic electric circuit theory. Thus, the fiber used in these experiments had capacitance per unit length of

C_t=93 nF/m and transverse resistance per unit length of R_t = 14.5 kΩ·m (bulk resistance per unit length of conductive layers 4.8 Ω·m). The characteristic frequency associated with a corresponding RC circuit is $\nu = 1/(2\pi R_t C_t) = 120\ Hz$. Electric response of a capacitor fiber is, in fact, that of a high pass filter. Namely, at frequencies well below 120 Hz the fiber operates in a quasi-DC regime where it simply breaks the electrical circuit. Fiber response to the touch is, therefore, minimal at low frequencies. At frequencies comparable or higher than 120 Hz the capacitor fiber acts as a distributed complex impedance with relatively low resistance. At these higher frequencies touching the capacitor fiber can modify significantly the local current flows and voltage distributions, thus resulting in sensitivity of its various electrical parameters to touching.

2.4 Fully woven 2D touch pad sensor using 1D array of capacitance fibers

2.4.1 Sensor design and fabrication

Soft, while highly elastic mechanical nature of the fibers makes them easy to use in the conventional weaving process (Fig. 2-17(b)). In our laboratory we have used a table Dobby loom (Leclerc Voyager 15¾" 4s) to weave the fibers into a wool-based textile matrix (see (Fig. 2-17(b)). The resulting 15x10 cm woven touchpad contained 15 capacitor fibers, each of 12 cm long (Fig. 2-17(c)).

In our experimental setup we use the same connection as described earlier: the inner (low Ω) electrodes of all the fibers (copper wires) are connected to the analogue voltage source integrated into the Analog-to-Digital Convertor (ADC) card providing a sinusoidal signal at 1 kHz with amplitude of 4 V (see Fig. 17 b)). The outer (high Ω) electrodes of the fibers are connected to the individual channels of the ADC card (National Instruments USB-6343 X-series DAQ) in order to measure the voltage at their endpoints. The connections are made using thin cooper wires (0.120 μm-diameter) and secured with a conductive epoxy.

We have already shown in section 4 that the read out voltage measured at the end of the individual fiber is highly sensitive to the position of the touch along this fiber, which in this case

acts like a tactile slide sensor. Thus, a one dimensional sensor array integrated into the textile allows us building a touchpad sensor that can localise in two dimensions the position of touch (Fig. 2-17(c)). In practice we use the ADC board plugged into a PC to acquire the signal from all the fibers and the touch position can then be monitored on the computer screen via custom LabVIEW software.

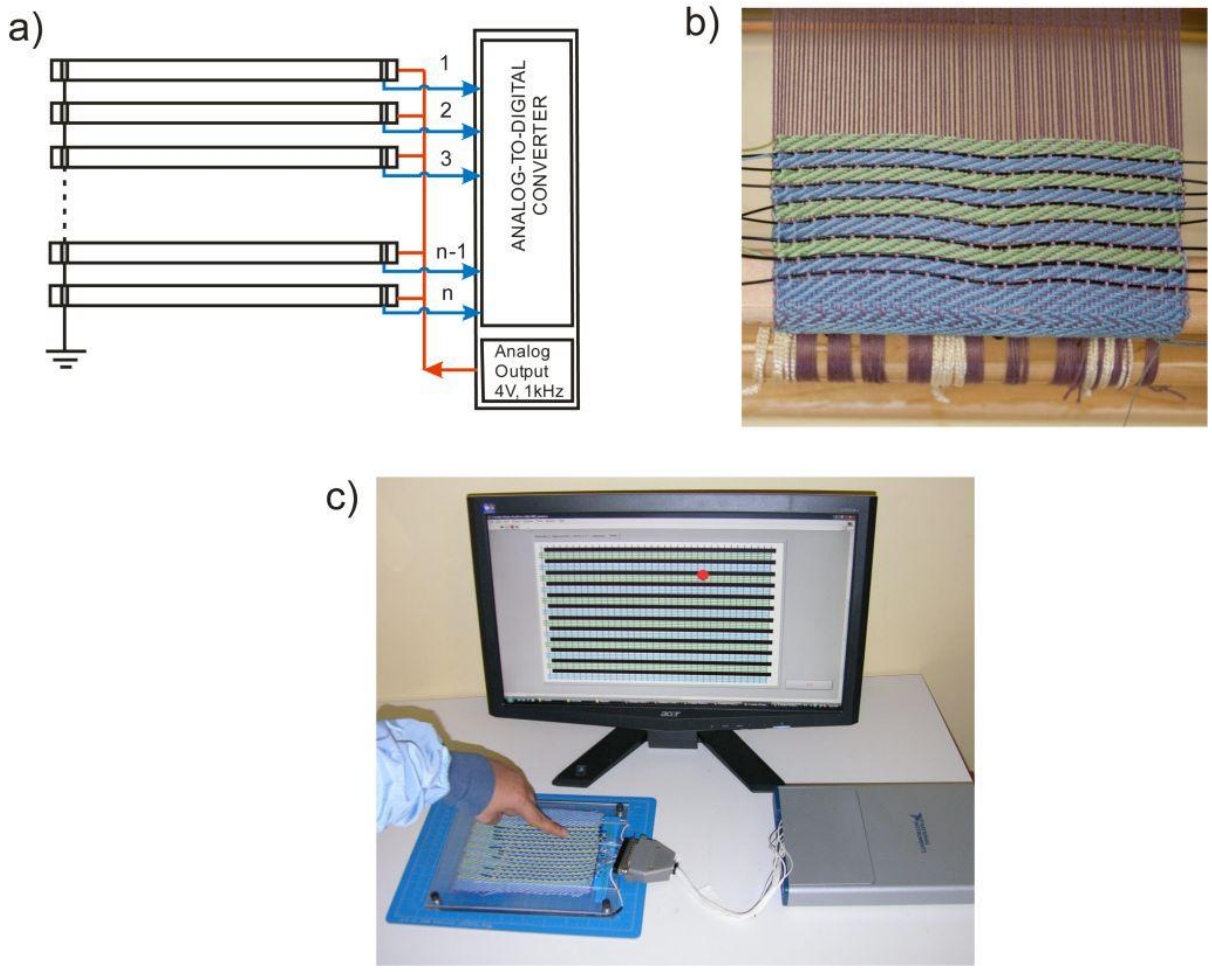

Fig. 2-17 The woven touchpad sensor. (a) Schematic representation of the woven 2D touchpad sensor featuring a one dimensional array of the capacitor fibers. All the connections to and from the fibers are done using a 120 μm-diameter cooper wire (denoted by red lines). Fibers in the array have the common ground and a common source, however, they are interrogated individually. Analog output of the ADC board is used as a function generator that provides a sinusoidal signal at 1 kHz with an amplitude of 4 V. (b) Weaving a two dimensional touchpad sensor on a Dobby loom. (c) Photograph of the woven touchpad connected to the ADC board, as well as the monitor image of a textile with an interpreted touch position.

2.4.2 Cross-talk and channel calibration

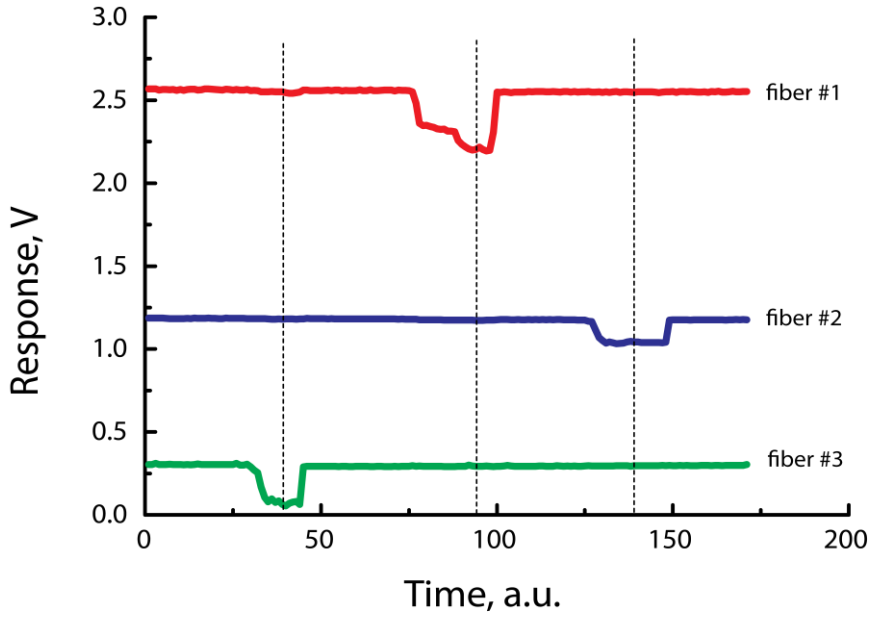

Fig. 2-18 Recorded voltage response as a function of time for the three neighboring fibers in the woven touchpad. No detectable cross-talk between the fibers was observed. Dips on the graphs correspond to the individual touch events that take place at different moments in time.

Finally, we address the question of crosstalk between the fibers in the woven 2D touchpad sensor. As discussed earlier, the sensor comprises a 1D fiber array separated by 1cm of textile and is presented in Fig. 17. In principle, false responses in our system could be induced by cross-talk between individual fibers that may lead to interference effects between measured signals. In this case the electrical signal at one channel may induce the signal at the other channel which might be detected as a false touch. In Fig 18 we show an example of a typical recorded voltage response as a function of time for the three neighboring fibers in the touchpad. No detectable cross-talk between the fibers was observed during recording. Dips on the graphs correspond to the individual touch events that take place at different moments in time. As can be seen in Fig. 18, after each touch and release, all the sensor channels successfully return back to the idle state. One can notice that fibers in Fig. 18 have different idle levels, which is explained by the fact that all of them have slightly different resistance and capacitance so the real (not normalized) signal is presented mainly for the demonstration purposes. Despite of the fact that in the simplest

interrogation configuration each individual fiber incorporated into the textile is not multi-touch sensitive (only the closest to the outer electrode touch will be detected), the absence of inter-channel cross-talk enables simultaneous interrogation of the individual slide sensors. In this sense a 2D touchpad has a partial multi-touch functionality.

2.5 Conclusions

In conclusion, we have described fabrication, electrical characterization and integration into tactile sensors of the novel all-polymer soft capacitor fibers. The capacitor fibers featuring relatively high capacitance and resistance were fabricated using fiber drawing technique. For the ease of connectorization, a thin copper wire was integrated into the fiber core during drawing procedure. Soft-capacitor fibers have a typical capacitance per unit length of 69 nF/m, and a typical resistivity parameter of 5 kΩ•m. Our measurements and theoretical modeling show that the fiber capacitance is a very stable, geometry defined parameter independent of the fiber diameter, and fiber fabrication parameters. In contrast, fiber resistivity has a very strong positive temperature coefficient, it is highly sensitive to stretching, and it is strongly dependent on the fiber drawing parameters.

Next, an individual capacitor fiber was demonstrated to act as a slide sensor that allows determining the touch position along its length by measuring the fiber AC response at a single point at the fiber surface. Electrical response of such a sensor was described by the RC ladder model, with the modelling data in excellent agreement with experimental observations.

Developed capacitor fibers are soft, small diameter, lightweight and do not use liquid electrolytes, thus they are ideally suited for the integration into textile products. At the end of the chapter, we have demonstrated that by weaving a one dimensional array of capacitor fibers (in parallel to each other) a fully woven 2D touchpad sensor could be build. Performance of a touchpad sensor was then characterised and the absence of the inter-channel crosstalk was confirmed. We also note that a 2D touchpad has a partial multi-touch functionality.

CHAPTER 3

FLEXIBLE, SOLID ELECTROLYTE-BASED LITHIUM BATTERY FOR SMART TEXTILE APPLICATION

As it was mentioned earlier, development of soft electronics, such as fiber sensors presented in the previous chapter, should go hand in hand with the development of compliant (soft) wearable energy sources that would power soft electronic circuits and actuators. In our group two important improvements towards fabrication of a flexible, extrudable, and environmentally safe battery for smart textiles were achieved. The first one involves processing of both electrode binders and polymer electrolytes with aqueous solution rather than with organic solvents. This leads to an environmentally friendly process for the electrode and polymer electrolyte fabrication. The second improvement is the extensive use of a thermoplastic solid electrolyte both in the electrodes and a separator layer. This allows, in principle, fabrication of a battery preform that can be then drawn into a battery fiber.

3.1 Fabrication and characterization of the solid electrolyte battery

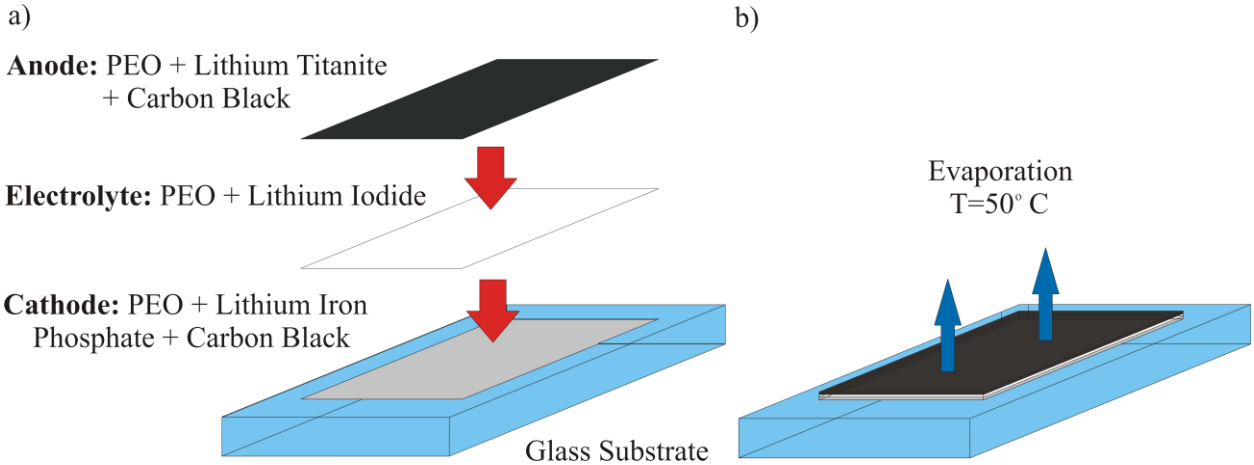

Fig. 3-1 Fabrication procedure of the all-solid flexible battery a) First cathode film is created and completely dried, then a solution for the separator layer was poured onto the cathode layer and a two-layer system is created after drying. Finally, the cathode layer mix was poured onto the two layer system and dried.

Anode, polymer electrolyte and cathode films are all prepared separately. The anode and cathode fabrication starts with mixing the appropriate amounts of $Li_4Ti_5O_{12}$ or $LiFePO_4$ powder, PEO or PVDF powder (acting as binders), as well as electron conductive carbon black powder. The powder mix is then added into the PEO dissolved either in the aqueous or acetonitrile solution, and then mixed using magnetic stirrer. The resulting slurry is deposited onto a glass substrate, dried in the hood under the horizontal air flow, and then in the vacuum oven at 50ºC (overnight) to get the anode and cathode films.

In order to fabricate the electrolyte layer appropriate amounts of polymer and Li salt were first dissolved in aqueous (majority of experiments) or organic solvents (control experiments). These solutions were then poured either onto the glass substrate to cast a film or directly onto the anode or cathode films to make a multilayer film. The polymer electrolyte films were first dried in the hood under the horizontal air flow, followed by drying in the vacuum oven.

To assemble the battery, anode film was created and completely dried, then a solution for the separator layer was poured onto the anode layer and a two-layer system was created after drying. Finally, the cathode layer mix was poured onto the two layer system and dried.

3.1.1 Characterization methods

The conductivities of polymer electolytes were measured by electrochemical impedance spectroscopy using a potentiostat from Princeton Applied Research (model PARSTAT 2273). The test cell comprised two copper or aluminium electrodes with the area of ~1.26 cm^2. The thickness of the polymer electrolyte layers was measured using a caliper so that the conductivity could be obtained from the resistance.

Cyclic voltammetry (CV) was used to characterize the electrochemical activity of the electrode material. The cyclic voltammetry was measured with the same copper electrodes and the same potentiostat as in the electrical conductivity test.

Charge-discharge test was used to characterize the reversibility of the battery system. Cu and Al foils with the area of 1 cm^2 were used as electron conductors for cathode and anode films respectively. Constant current method (±0,02, ±0,05 or ±0,1 mA) was used in the test with the maximum charge or discharge time fixed at 0.5 hour. For the woven battery, charge-discharge

characterisation is performed using 0.1mm-diameter Cu and Al wire electrodes woven at the time of sample preparation. The wires were held firmly at the appropriate faces of the battery stripes with the cotton threads.

Wide angle X-ray diffraction (WAXD) was used to characterize the crystallinity of polymer electrolytes and the crystal structure of the electroactive materials. The WAXD measurements were carried out using a Bruker AXS diffractometer (Siemens Kristalloflex 780 generator) operated at 40 kV and 40 mA, using the Cu Kα (0.1542 nm) radiation collimated by a graphite monochromator and a 0.5 mm pinhole. The diffraction patterns were recorded by a HI-STAR area detector.

3.2 Properties of the polymer electrolyte

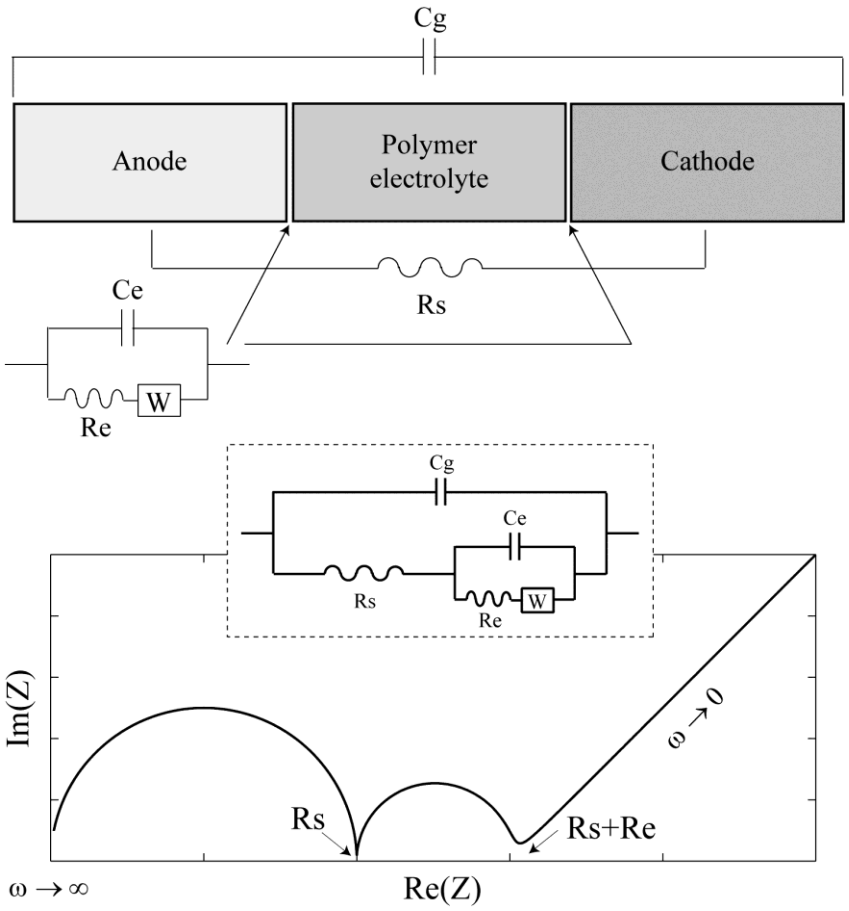

Fig. 3-2 The complex equivalent circuit for the battery system with polymer electrolytes. C_g is the geometrical capacitance, R_s is the polymer electrolyte resistance, C_e is the electrode and electrolyte interfacial capacitance and R_e is the electrode/electrolyte interfacial resistance, W is the Warburg impedance.

One of the key parameters affecting performance of a solid battery is the bulk electrolyte conductivity which characterizes ionic mobility in polymer electrolytes. The higher is the conductivity the more effective is the ion transfer across the battery. In a solid battery, the impedance between electrode/electrolyte interface, such as double layer capacitance C_e as well as charge transfer resistance R_e, must be considered in addition to the bulk electrolyte resistance R_s. To understand the battery performance, one typically assumes a certain effective electrical circuit of a battery such as the one shown in Fig. 3-2.

Detailed analysis of the equivalent circuit in Fig. 3-2 shows that complex part of the battery impedance will have two minima, one at lower frequencies with the corresponding value of the real part $R_e(Z)=R_s+R_e$, and the other one at higher frequencies with the corresponding value of the real part $R_e(Z)=R_s$. By measuring the bulk electrolyte resistance R_s of a film sample and knowing the film thickness, one can extract the bulk electrolyte conductivity.

Addition of Li salts (such as LiI or $LiCF_3SO_3$) into the polymer electrolytes increase dramatically the electrolyte ionic conductivity. Addition of the low molecular weight PEG further increases the ionic conductivity; however, it has a much weaker influence on the conductivity when compared to the prior case without Li salts. The most important effect of PEG is however on the mechanical properties of the resultant films. Pure PEO films are highly crystalline and relatively rigid with a well-defined melting temperature. Adding Li salts reduces crystallinity of PEO and for low concentration of salts the mix becomes soft and rubber like. At higher concentration of salts, however, the films lose their elasticity and start crumbling. Adding low molecular weight PEG into the PEO/Li salt combinations results in softer more flexible films even at high salt concentrations.

Polymer electrolytes play three important roles in the battery. First, it is a lithium ion carrier; second, it is a separator between the two electrodes, which eliminates the need for an inert porous separator; third, it is a binder and an adhesive that ensures good mechanical and electrical contact with electrodes. As we have mentioned earlier, pure PEO films are highly crystalline and relatively rigid, while the ones with Li salts are more rubber like, especially the ones with low molecular weight PEG. The highly amorphous structures might facilitate ionic conductivity of the polymer electrolytes, and have a soft artificial leather-like feel, which is beneficial for the applications in wearables. At the same time, semi-crystalline structures with a controllable

degree of crystallinity produces films with better mechanical properties and drawability. To control the degree of crystallinity we study adding the urea in the polymer composition. It has been reported that adding urea into the PEO film promotes crystallinity via formation of the highly crystallized complexes [83], [84]. Overall we observe that adding urea promotes rigidity in the otherwise rubber-like films containing PEO-Li salt compositions, which can be highly beneficial for extrusion or drawing of these materials. Finally, in **Table 1** we present the ionic conductivity of compounds containing different molar ratios of urea in the PEO.

Li salt	PEG ratio (y)	Urea ratio	Ionic conductivity
	0	0	3.50×10^{-9}
-	0.1	0	7.90×10^{-9}
-	0.25	0	2.28×10^{-8}
-	0.50	0	1.54×10^{-7}
LiI	0	0	1.67×10^{-4}
LiI	0.33	0	2.97×10^{-4}
LiI	0.50	0	9.23×10^{-4}
LiI	0.67	0	4.27×10^{-4}
LiI	0	0.4	2.16×10^{-5}
LiI	0	0.69	1.28×10^{-5}
$LiCF_3SO_3$	0	0	2.05×10^{-4}
$LiCF_3SO_3$	0.33	0	1.57×10^{-4}
$LiCF_3SO_3$	0.50	0	3.33×10^{-4}
$LiCF_3SO_3$	0.67	0	5.03×10^{-4}
$LiCF_3SO_3$	0	0.4	1.22×10^{-5}
$LiCF_3SO_3$	0	0.69	7.80×10^{-6}
$LiPF_6$	0	0	3.88×10^{-5}
$LiPF_6$	0	0.4	6.02×10^{-5}
$LiPF_6$	0	0.69	1.60×10^{-5}
$LiClO_4$	0	0	2.31×10^{-5}
$LiClO_4$	0	0.4	4.11×10^{-5}
$LiClO_4$	0	0.69	1.30×10^{-5}

Table 1. Ionic conductivity of (1-y)PEO-yPEG-LiX (X=I-, CF_3SO_3-, PF_6- and ClO_4-) at room temperature. The molecular weight of PEO and PEG are 4,000,000 and 400 g/mol, respectively. The molar ratio of PEO(PEG):LiX is kept at 6:1 for all the samples, the urea molar ratios are 0.4 and 0.69 respectively, corresponding to the two complexes formed with PEO.

We find that for PEO-$LiClO_4$ and PEO-$LiPF_6$ compounds, the ionic conductivities are comparable to each other with or without urea. However, for PEO-LiI and PEO-$LiCF_3SO_3$

compounds ionic conductivity drops by an order of magnitude when urea is added. In all the cases, of the two samples with different ratios of urea, the one with smaller urea content (samples of lower crystallinity) has consistently higher conductivity that the one with higher urea content (samples of higher crystallinity).

3.3 Properties of the flexible electrodes

In a standard battery, to form the electrodes one typically uses powder compositions of various electroactive materials mixed with small amounts of a binder. The electrode pallets are then created by forming the powder mix under press. In our case, the goal is to create extrudable/drawable electrodes, therefore, a larger quantity of polymer binder materials has to be used in order to obtain the desired thermo-mechanical properties of the electrode material. Plus battery electrode has to exhibit simultaneously good electron and ionic conductivities. So in the case of a cathode $LiFePO_4$ was used but as it exhibits low electron conductivity, electron conductors had to be added into a cathode compound. In case of the anode $Li_4Ti_5O_{12}$ was used.

In Fig. 3-3 examples of electrodes and battery samples prepared by solution casting method using PEO as a binder and carbon black as electron conductive material are presented. The cathode, anode, polymer electrolytes and complete batteries are all soft and highly stretchable; moreover, they have a feel and appearance of artificial leather, which is highly appropriate for applications in wearables. The 1cm x 10cm battery strips cut from the planar film samples have very robust mechanical properties, and can be easily weaved into textiles.

The electron and ionic conductivities have been measured with the DC and AC methods respectively. The electronic conductivities of both the cathode and anode were $\sim 1\times10^{-4}$ Scm^{-1}, which is much higher than those of pure PEO, $LiFePO_4$ or $Li_4Ti_5O_{12}$ powders. However, compared to the conventional electron collecting materials, such as copper or aluminium, the electronic conductivity of the soft electrodes is still very small.

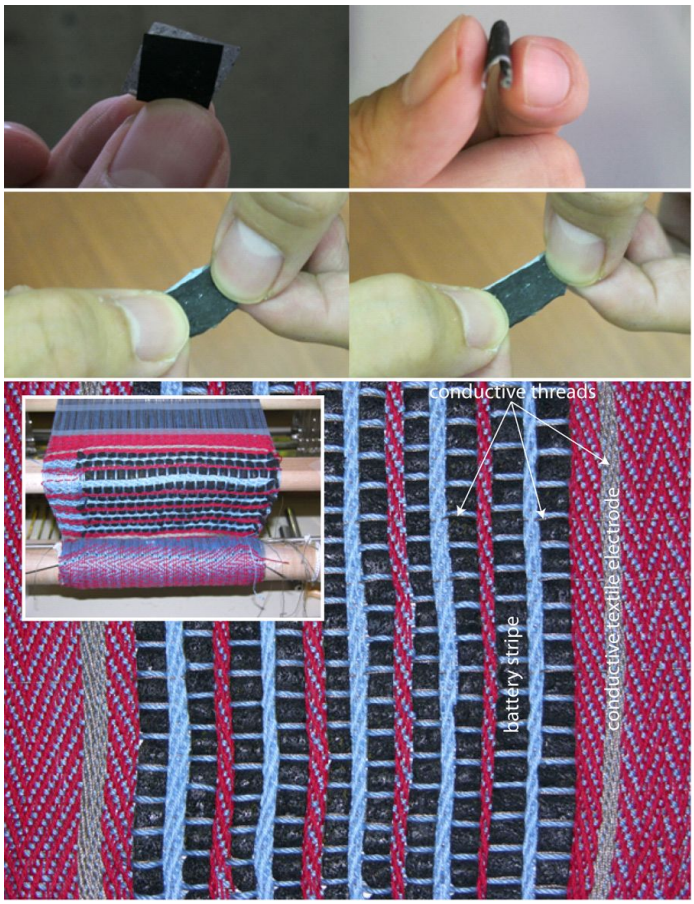

Fig. 3-3 Top row: photographs of a flexible battery made of binding individual cathode, anode and polymer electrolyte films. Middle row: resulting battery is highly stretchable. Bottom row: battery stripes (black) woven into a textile (blue and red cotton threads) using Dobby loom. The stripes are connectorized in series with conductive threads (metallic brown). Two textile electrodes are formed by the conductive threads at the textile extremities.

To investigate the effect of PEO ratio on the properties of electrodes, two types of samples were prepared. The first series of samples has low PEO content (less than 5%) where PEO acts mainly as a binder material to hold the powder together as in the conventional Li battery. In particular, the powder cathode and anode are composed of 87% $LiFePO_4$ or $Li_4Ti_5O_{12}$ and 13% carbon black, then binded with a few drops of 5% PEO solutions. The second series of samples has high PEO content (above 25 %) and the resultant electrodes are flexible films. In these samples the cathode and anode films are composed of 37.5% $LiFePO_4$ or $Li_4Ti_5O_{12}$, 50% PEO and 12.5% carbon black. Typical result of the cyclic voltammetry measurements is presented in Fig. 3-4.

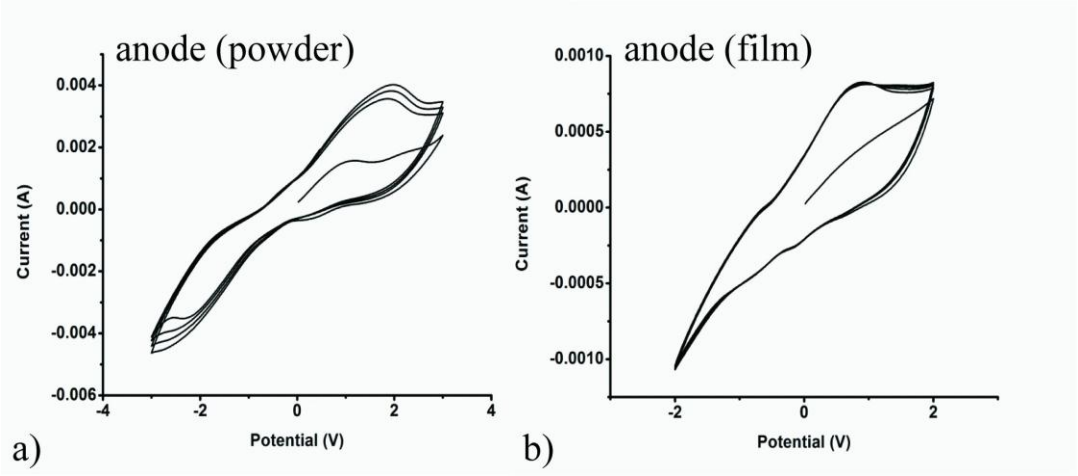

Fig. 3-4 The cyclic voltammetry results of a) anode powder sample, b) anode film sample

An anode made of pressed powder exhibits an oxidation current peak which is much larger than that of an anode film with high PEO content. Similar effect is observed for the powder and film cathodes. While voltammetry results indicate that large resistance is indeed brought by the high PEO content, at the same time they also show that reversibility of a film battery is at least as good as the reversibility of the powder-based battery. This is judged from the good repeatability of the I(V) curves during 5 cycles of the voltammetry experiment.

3.4 Electrochemical properties of flexible batteries

3.4.1 Open circuit voltage measurements

In this section we report performance of several batteries assembled with various material choices for anode, cathode and electrolyte. Based on our measurements, we conclude that $LiFePO_4$, $Li_4Ti_5O_{12}$, PEO material composition presents a viable flexible all-solid battery system; however, the registered voltage is always significantly lower than the theoretical value of 1.8 V.

Li salts and electrolyte types	PEG ratio (y)	Urea ratio	Electrode Types	OCV (V)
LiI solution	0.50	0	powder	1.00
$LiPF_6$ solution	0	0	powder	1.00
$LiPF_6$ solution	0	0	film	0.72
$LiCF_3SO_3$ solution	0	0	film	0.70
$LiCF_3SO_3$ film	0	0	powder	0.50
LiI film	0	0	powder	0.32
LiI film	0.33	0	powder	0.36
LiI film	0.50	0	powder	0.52
LiI film	0.67	0	powder	0.56
LiI film	0	0.40	powder	0.63
LiI film	0	0.69	powder	0.52
LiI film	**0**	**0.69**	**film**	**0.50**
LiI film	**0.50**	**0**	**film**	**0.45**

Table II. Open circuit voltage measured with various electrolytes (polymer solution and polymer solid) and two types of electrodes (powder electrode and film electrode). LiI solution refers to aqueous solution, LiPF6 solution refers to the ethylene carbonate (EC) / ethylmethyl carbonate (EMC) (1:1) solution, $LiCF_3SO_3$ solution refers to the acetonitrile solution. The molar ratio of PEO1-y(PEGy): Li-X is kept at 6:1 for all the compositions.

All the batteries in our experiments can be characterised as those with powder pressed electrodes (no or little PEO) or film electrodes (high ratio of PEO binder). Moreover, in our experiments we compare battery performance when using solid electrolyte separator layer versus a filtration paper soaked in liquid electrolyte. Electrode and electrolyte types and compositions, as well as open circuit voltage (OCV) of the corresponding batteries are listed in **Table 2**.

First, we have tested performance of a battery comprising powder anode and cathode reported in the previous section, while using as a separation layer a filtration paper soaked either in PEO(PEG):LiI aqueous solution or PEO:$LiPF_6$ in the EC/EMC (1:1) solution. Not surprisingly, batteries comprising powder electrodes and liquid electrolyte showed consistently the best performance with the highest open circuit voltage ~1 V.

In the next set of experiments we have retained a filtration paper soaked in liquid electrolyte as a separator layer, while substituting powder pressed anode and cathode with film anode and cathode described in the previous section. Two types of liquid electrolited were tested including

PEO:$LiPF_6$ in the EC/EMC (1:1) solution and PEO:$LiCF_3SO_3$ in acetonitrile solution. In both systems, OCV dropped from ~1 V to ~0.7 V. This result correlates with the greatly reduced ionic and electronic conductivity of the PEO containing electrodes compared to the powder pressed electrodes.

Most pronounced effect on the OCV was observed when we have substituted liquid electrolyte-based separator layer with solid electrolyte film. In what follows, all the solid electrolyte films had the composition $PEO_{1-y}(PEG_y)$:Li-X, where a constant 6:1 molar ratio was used for the polymer to salt ratio. In the first set of experiments we have retained powder anode and cathode and used solid electrolyte films only as a separator layer. When using PEO:$LiCF_3SO_3$ electrolyte the OCV dropped to 0.5 V. However the reduction in case of a PEO:LiI electrolyte, for which the OCV was ~0.32 V, can be compensated by adding significant amounts of the low molecular weight PEG or urea into PEO:LiI electrolyte. Thus it was possible to increase the OCV to ~0.5-0.6 V. These results correlate perfectly with the ionic conductivity measurements presented in **Table 1**. Namely, higher OCV values are consistently achieved in systems with higher ionic conductivities of the solid polymer electrolytes used in a separator layer.

Finally, when substituting the powder pressed anode and cathode with their film homologues, no significant voltage drop was observed. This allowed us to obtain OCV of ~0.5 V in the all-solid battery systems comprised of solid electrodes separated with PEO:LiI electrolyte films that ether contained high ratios of low molecular weight PEG or urea. Although in both cases battery structure was rubber-like with mechanical properties mostly determined by the soft outer electrodes, urea containing batteries were tangibly firmer than those containing PEG.

3.4.2 Charge-discharge measurements

Although an open circuit voltage is an important indicator of the battery performance, the more important test is a charge-discharge cycling under loading. In Fig. 3-5 constant current (±0.02 mA, ±0.05 mA and ±0.1 mA) charge-discharge tests of the two 1cm x 1cm battery samples are presented, each sample contains the same PEO:LiI (6:1) polymer electrolyte separator layer. Copper and aluminium foils were used as electron collectors in the measuring cell. The film electrodes in the first battery sample (Fig. 3-5(a)) were prepared using PEO

(26.7%), $LiFePO_4$ or $Li_4Ti_5O_{12}$ (66.7%), and carbon black (6.6%) (by weight). The second sample featured film electrodes with higher concentration of PEO and carbon black, namely, PEO (50%), $LiFePO_4$ or $Li_4Ti_5O_{12}$ (37.5%), carbon black (12.5%). For the first sample with electrodes containing smaller amounts of PEO (see Fig. 3-5(a)), the discharge curves at currents 0.02 mA and 0.05 mA showed a continuous decay from ~0.5 V to ~0.1 V with no change in the discharge time after 5 cycles. At higher currents (0.1 mA) discharge time somewhat shortened during the first five discharges with the discharge voltage dropping to zero after 3 cycles. For the second sample with electrodes containing larger amounts of PEO (see Fig. 3-5(b)), at currents 0.02 mA and 0.05 mA the discharge curves first show an almost instantaneous drop from 0.4 - 0.5 V to ~0.3 V followed by a slow linear in time decay. No change in the discharge time is observed after 5 cycles at lower currents. At higher currents (0.1 mA) discharge time shortened significantly during the first five discharges with the discharge voltage dropping to zero already after the first cycle.

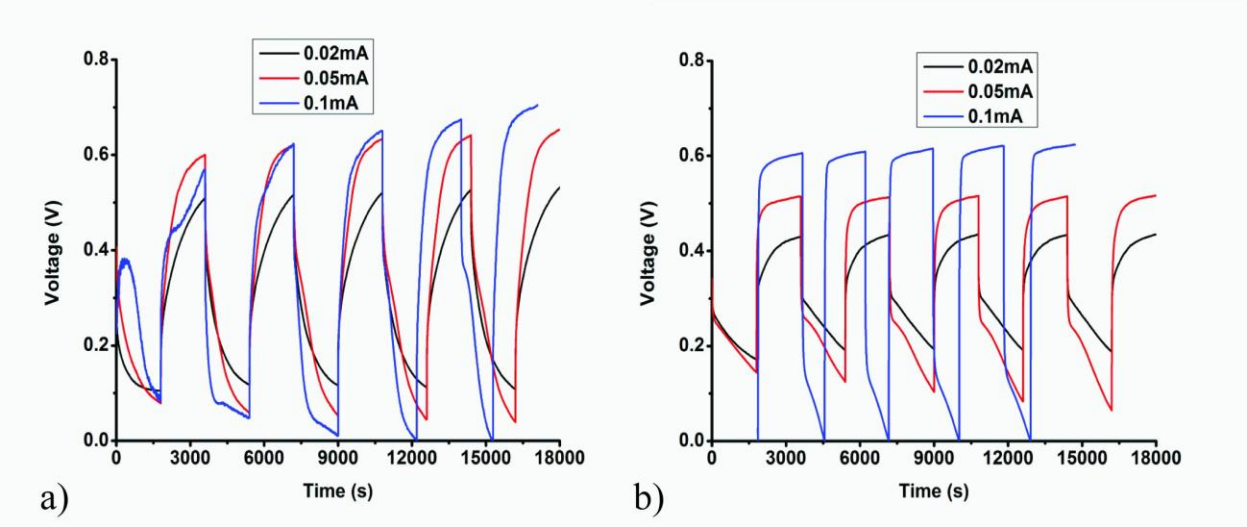

Fig. 3-5 Constant current charge-discharge curves of the two flexible batteries with a solid PEO:LiI polymer electrolyte separator layer. a) Electrodes with 26.7% of PEO. b) Electrodes with 50 % of PEO.

These and similar charge-discharge experiments consistently show that initial discharge voltage is higher and it decreases slower in battery samples featuring electrodes with lower amounts of PEO. At the same time, it appears that battery samples containing electrodes with higher amounts of PEO show a better performance at longer discharge times, where voltage

decrease is relatively slow and almost linear with time. Overall, these charge-discharge experiments indicate good reversibility of the solid electrolyte-based batteries developed in this work even though a typical measured discharge voltage ~0.2-0.3 V is much lower than the theoretical one of 1.8 V.

3.4.3 Effect of solvents and PEO on electrode structure.

One possible explanation of the fact that OCVs of all the film batteries are much lower than the theoretical value can be attributed to the changes in the physical and chemical structure of the electrodes after treatment of the pure powders of $LiFePO_4$ or $Li_4Ti_5O_{12}$ with solvents and addition of PEO. As a result, the electrochemical reaction at the interfaces between electrodes and electrolyte might change. Here we use WAXD to probe differences in the structure of pure $LiFePO_4$ and $Li_4Ti_5O_{12}$ powder electrodes versus film electrodes that contain significant amounts of PEO and were subject to solvent treatment.

In Fig. 3-6(a) we present WAXD results for cathode. Particularly, we compare diffraction peaks coming from the pure $LiFePO_4$ powder electrode to the diffraction peaks coming from the film electrode containing 37.5% PEO, 50% $LiFePO_4$, 12.5% carbon black and cast from the aqueous solution of PEO. For comparison, WAXD of a pure PEO powder sample is presented on the same plot. All the diffraction peaks of $LiFePO_4$ could be indexed with an orthorhombic structure (a=10.323 Å, b=6.003 Å and c=4.694 Å) (39, 40). From Fig. 3-6(a) we see that all the peaks in the film cathode can be related to the peaks of pure $LiFePO_4$ or PEO materials, which means that the chemical structure of a cathode film is similar to that of the basic elements used in its fabrication. Physical structure of the cathode is clearly semi-crystalline as judged from the broad and relatively intense background.

In Fig. 3-6(b) we present WAXD results for anode. There, diffraction peaks coming from the pure $Li_4Ti_5O_{12}$ powder electrode are compared to the diffraction peaks coming from the film electrode containing 37.5% PEO, 50% $Li_4Ti_5O_{12}$, 12.5% carbon black and cast from the aqueous solution of PEO. All the diffraction peaks of $Li_4Ti_5O_{12}$ could be indexed with a cubic spinel structure (a=b=c=8.376 Å) (41). From Fig. 3-6(a) we see that diffraction peaks corresponding to the anode film are quite different from those corresponding to the powder anode. For example,

the most intense band at ~37 º in the powder sample is missing in the film sample. Difference in the chemical and physical structure of an anode material after its treatment with aqueous solution of PEO can be one of the reasons why measured open circuit voltage is different from the theoretical prediction. Additionally in Fig. 3-6(b) we present WAXD results for a $Li_4Ti_5O_{12}$ powder sample treated with acetonitrile solution, and observe no change in the diffraction bands of an anode material. Finally we note that anode film shows high degree of crystallinity as judged from the low intensity of the broad background.

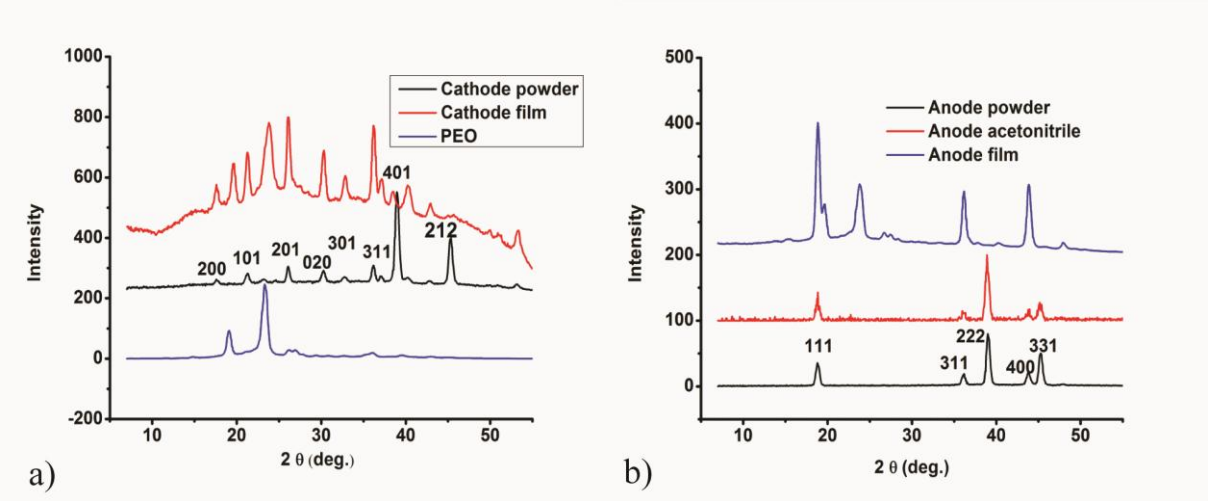

Fig. 3-6 WAXD results for the a) powder (no PEO) and film (50% PEO) cathode b) powder (no PEO) and film (50% PEO) anode.

3.5 Textile battery prototype performance

As it was shown above, operating voltage of a single flexible battery is relatively low (~0.3 V), but when several of them are connected in series, the net voltage can be large enough for practical applications. In Fig. 3-7 an example of a textile battery comprising 8 flexible battery strips woven together and connectorized in series to power up a 3 V LED is presented. This battery provides dim LED light for several hours and it can be recharged. The electrode compositions used in this sample are those described above with high content of PEO (50%). Charge-discharge curves for the textile battery were measured after connectorization of all the strips in series using copper and aluminium wires (one wire per strip per side). The charge-discharge curves showed stable discharging plateaus at ~2 V for lower currents of 0.02 mA and

0.05 mA, while at higher current of 0.1 mA the discharging voltage rapidly dropped to zero. At the same, very high values of the charging voltages 5.5, 7 and 8.5 V for the charging currents of 0.02, 0.05 and 0.1 mA indicate that the internal resistance of a textile battery is high. This is in part due to a relatively small contact area between the battery polymer electrode and the electron collector in the form of thin wires. Note that, in principle, charging voltages can be reduced by using metallic foils with large surface area as electron collectors instead of wires. However, in textile applications the most appropriate is to use wires or conductive threads as the electron collectors (see Fig. 3-3), as they can be naturally integrated during weaving.

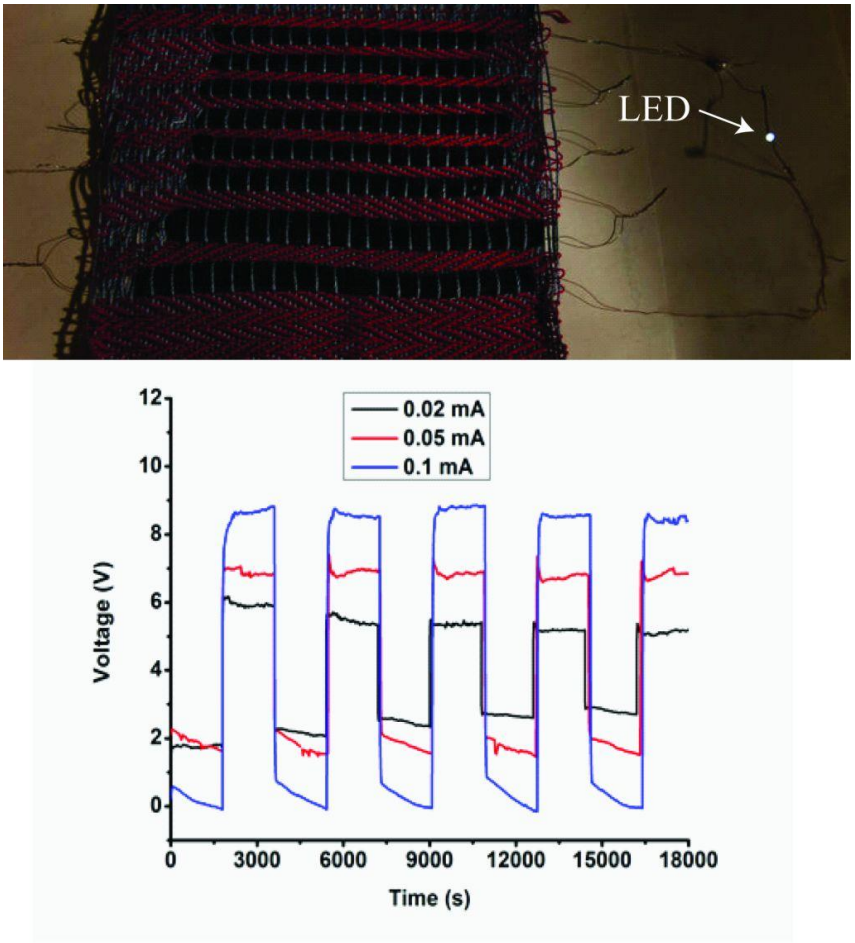

Fig. 3-7 Top: Textile battery is made of 8 battery stripes woven with cotton thread and connectorized in series using copper and aluminium wires (one per stripe per side) as electron collectors. The resultant battery is powerful enough to light up a 3 V LED for several hours. Bottom: the charge-discharge curves of the textile battery.

3.6 Conclusions

Flexible and stretchable film batteries for smart textile applications have been demonstrated with conventional Li battery materials including $LiFePO_4$ cathode, $Li_4Ti_5O_{12}$ anode and PEO solid electrolyte. By introducing large quantities of the thermoplastic PEO binder in the battery electrodes and separator layer one can potentially realise a fully extrudable/drawable battery system, which could allow direct drawing of battery fibers ideal for textile applications. Alternatively, it was experimentally demonstrated that flexible batteries can be first cast as sheets, then cut into thin strips, and finally integrated into textile using conventional weaving techniques. The electrochemical performance of the film batteries was extensively characterised and found to be poorer compared to the performance of batteries based on the powder electrodes and liquid electrolytes. At the same time, cycling performance of the solid film batteries was stable, and together with their soft leather-like feel and appearance, this makes such batteries well suitable for smart textile applications. Finally, the film batteries were made using environmentally friendly fabrication route, where in place of organic solvents only aqueous solutions were used to cast the electrodes and solid electrolyte separator film.

CHAPTER 4
GENERAL DISCUSSION, PERSPECTIVES AND CONCLUSIONS

As mentioned earlier, a truly smart textile should be completely autonomous with little or no maintenance required, and should be able to sense and respond to various non-trivial stimuli.

In our work, two smart textile concepts were investigated, namely, a touch sensitive textile pad and a flexible textile battery. These prototypes already cover two out of the three elements of a futuristic, fully autonomous smart-textile that would incorporate soft electronics (touchpad in our case), a power source (Li-ion battery in our case), and, finally, some kind of soft actuator.

One of the important aspects of any practical textile is its ability to withstand external factors including, for example, washing. Soft capacitor fibers developed in our group have durable plastic surfaces that would undoubtfully withstand the adverse effects of water and detergent during washing. At the same time, it remains to be seen if electric connections from the textile to outside electronics can be made durable enough to withstand several washing cycles.

Similarly, the electrochemical properties of flexible batteries could be significantly affected if no protective encapsulation layer is used on the battery surface, while introduced into the washing cycle. Further research into flexible encapsulation solutions is therefore needed to make the battery an attractive solution for textiles.

4.1 Touch sensitive textile

In our work, an individual soft capacitor fiber was demonstrated to act as a slide sensor that allows determining the touch position along its length by measuring the fiber AC response at a single point at the fiber surface. Electrical response of such a sensor was described by the RC ladder model, with the modelling data in excellent agreement with experimental observations. We then use this model for user oriented calibration procedure in order to build a fully woven 2D touchpad sensor that has a partial multi-touch functionality.

One of the principal difficulties that we have encountered in our work was the realisation that equivalent electric parameters of the human body vary strongly from person to person, and, therefore, for every new user we need to recalibrate the textile touchpad software. In practice it is done by sweeping a finger across all the fibers. After that calibration curves are recalculated

according to the theoretical model. In order to eliminate such a cumbersome calibration procedure one may consider measuring AC response at two points along the fiber instead of one. Comparison of these two measurements will not only make recalibration unnecessary but also increase precision of the detection of a touch position.

4.2 Flexible batteries

Presented fully solid flexible batteries proved to be very convenient for integration into textiles as they can be first cast as sheets, then cut into thin strips. Moreover, we used thermoplastic PEO base for the fabrication of the batteries which means that in principle one can create fully extrudable or drawable battery-fiber. Such fibers would be even better suited for integration in textiles.

As it was mentioned earlier, the main deficiency of the developed batteries is their much lower voltage than theoretically predicted. A big part of the problem lies in the optimization of the processing conditions used during the battery assembly, such as ambient atmosphere during assembly, solvent nature and evaporation rate, etc.

REFERENCES

[1] S. M. Park, C. Gopalsamy, R. Rajamanickam, and S. Jayaraman, "The Wearable Motherboard (c): A flexible information infrastructure or sensate liner for medical applications," in *Medicine Meets Virtual Reality: The Convergence of Physical & Informational Technologies: Options for a New Era in Healthcare*. vol. 62, J. D. Westwood, H. M. Hoffman, R. A. Robb, and D. Stredney, Eds., ed Amsterdam: I O S Press, 1999, pp. 252-258.

[2] S. Park, C. Gopalsamy and S. Jayaraman, "Fabric or garment with integrated flexible information infrastructure", *WO Patent Specification 9964657,* 1999.

[3] E.R. Post and M. Orth, "Smart fabric, or washable computing", *Proc. 1st Int. Symp. Wearable Computers* pp 167–8, 1997.

[4] R. Paradiso, A. Gemignani, E. P. Scilingo, D. De Rossi, and Ieee, "Knitted bioclothes for cardiopulmonary monitoring," in *Proceedings of the 25th Annual International Conference of the IEEE Engineering in Medicine and Biology Society*, Vols 1-4: A New Beginning for Human Health. vol. 25, ed, 2003, pp. 3720-3723.

[5] D. Marculescu, R. Marculescu, N. H. Zamora, P. Stanley-Marbell, P. K. Khosla, S. Park, S. Jayaraman, S. Jung, C. Lauterbach, W. Weber, T. Kirstein, D. Cottet, J. Grzyb, G. Troster, M. Jones, T. Martin, and Z. Nakad, "Electronic textiles: A platform for pervasive computing," *Proceedings of the IEEE*, vol. 91, pp. 1995-2018, Dec 2003.

[6] S. R. Anton and H. A. Sodano, "A review of power harvesting using piezoelectric materials (2003-2006)," *Smart Materials & Structures*, vol. 16, pp. R1-R21, Jun 2007.

[7] L. M. Swallow, J. K. Luo, E. Siores, I. Patel, and D. Dodds, "A piezoelectric fibre composite based energy harvesting device for potential wearable applications," *Smart Materials & Structures*, vol. 17, Apr 2008.

[8] T.L. Vigo and C.M. Frost, "Temperature-adaptable fabrics", *Text. Res. J.*, pp. 55737–43, 1985.

[9] X. X. Zhang, X. C. Wang, X. M. Tao, and K. L. Yick, "Energy storage polymer/MicroPCMs blended chips and thermo-regulated fibers," *Journal of Materials Science*, vol. 40, pp. 3729-3734, Jul 2005.

[10] M. Engin, A. Demirel, E. Z. Engin, and M. Fedakar, "Recent developments and trends in biomedical sensors," *Measurement*, vol. 37, pp. 173-188, Mar 2005.

[11] D. De Rossi, A. Della Santa, and A. Mazzoldi, "Dressware: wearable hardware," *Materials Science & Engineering C-Biomimetic and Supramolecular Systems*, vol. 7, pp. 31-35, May 1999.

[12] R. Paradiso, G. Loriga, and N. Taccini, "A wearable health care system based on knitted integrated sensors," *Transactions on Information Technology in Biomedicine*, vol. 9, pp. 337-344, Sep 2005.

[13] D. Morris, B. Schazmann, Y. Wu, S. Coyle, S. Brady, J. Hayes, C. Slater, C. Fay, K. T. Lau, G. Wallace, D. Diamond, "Wearable Sensors for Monitoring Sports Performance and Training", *5th International Summer School and Symposium on Medical Devices and Biosensors*, pp. 37-40, 2008.

[14] E. Drean, L. Schacher, F. Bauer, and D. Adolphe, "A smart sensor for induced stress measurement in automotive textiles," *Journal of the Textile Institute*, vol. 98, pp. 523-531, 2007.

[15] B. Gauvreau, N. Guo, K. Schicker, K. Stoeffler, F. Boismenu, A. Ajji, R. Wingfield, C. Dubois, and M. Skorobogatiy, "Color-changing and color-tunable photonic bandgap fiber textiles," *Optics Express*, vol. 16, pp. 15677-15693, Sep 29 2008.

[16] J. Berzowska, "Very slowly animating textiles: shimmering flower", *Proceedings SIGGRAPH '04 ACM SIGGRAPH 2004* Sketches, pp. 34, 2004

[17] J. Berzowska, M. Coelho, "Smoks: the memory suits", *CHI 2006: Extended Abstracts on Human Factors in Computing Systems*, pp. 538–543. ACM, New York, 2006.

[18] A. C. Siegel, S. T. Phillips, B. J. Wiley, and G. M. Whitesides, "Thin, lightweight, foldable thermochromic displays on paper," *Lab on a Chip*, vol. 9, pp. 2775-2781, 2009.

[19] A. Wakita, M. Shibutani "Mosaic textile: wearable ambient display with non-emissive color-changing modules", *Proceedings of the 2006 ACM SIGCHI International Conference on Advances in Computer Entertainment Technology*, p. 48. ACM, New York, 2006.

[20] M. A. Invernale, Y. Ding, and G. A. Sotzing, "The effects of coloured base fabric on electrochromic textile," *Coloration Technology*, vol. 127, pp. 167-172, 2011.

[21] S. Beaupre, J. Dumas, and M. Leclerc, "Toward the development of new textile/plastic electrochromic cells using triphenylamine-based copolymers," *Chemistry of Materials*, vol. 18, pp. 4706-4706, Sep 19 2006.

[22] R.S Cok, R.R. Bourdelais and C.J. Kaminsky, "Flexible resistive touch screen", *US Patent* 0212599 A1, 2004.

[23] P.W. Kalendra and W.J. Piazza, "Automatic calibration of a capacitive touch screen used with a fixed element flat screen display panel", *US Patent* 5283559, 1994.

[24] S. Lee, W. Buxton and K.C. Smith, "A multi-touch three dimensional touch-sensitive tablet", *Proceedings of the SIGCHI conference on Human factors in computing systems,* pp 21-5, 1985.

[25] J. Rekimoto, "SmartSkin: an infrastructure for freehand manipulation on interactive surfaces", *Proceedings of the SIGCHI conference on Human factors in computing systems*, pp. 113-120, 2002.

[26] P. Dietz and D. Leigh, "DiamondTouch: a multiuser touch technology", *Proceedings of UIST , the 14th Annual ACM Symposium on User Interface Software and Technology*, pp. 219-26, 2001.

[27] R. S. Dahiya, G. Metta, M. Valle, and G. Sandini, "Tactile Sensing-From Humans to Humanoids," *IEEE Transactions on Robotics*, vol. 26, pp. 1-20, Feb 2010.

[28] J. Engel, J. Chen, and C. Liu, "Development of polyimide flexible tactile sensor skin," *Journal of Micromechanics and Microengineering*, vol. 13, pp. 359-366, May 2003.

[29] M. E. H. Eltaib and J. R. Hewit, "Tactile sensing technology for minimal access surgery - a review," *Mechatronics*, vol. 13, pp. 1163-1177, Dec 2003.

[30] T. Hoshi and H. Shinoda, "A sensitive skin based on touch-area-evaluating tactile elements", *Proceedings of the Symposium on Haptic Interfaces for Virtual Environment and Teleoperator Systems*, pp. 89–94, 2006.

[31] D.C Ruspini, K. Kolarov and O. Khatib, "The haptic display of complex graphical environments", *Proceedings of the 24th Annual Conference on Computer Graphics and Interactive Techniques*, pp. 345–52, 1997.

[32] D. J. Beebe, A. S. Hsieh, D. D. Denton, and R. G. Radwin, "A silicon force sensor for robotics and medicine," *Sensors and Actuators A-Physical*, vol. 50, pp. 55-65, Aug 1995.

[33] M. R. Wolffenbuttel and P. P. L. Regtien, " Polysilicon bridges for the realization of tactile sensors," *Sensors and Actuators A-Physical*, vol. 26, pp. 257-264, Mar 1991.

[34] Z. Chu, P. M. Sarro, and S. Middelhoek, "Silicon three-axial tactile sensor," *Sensors and Actuators A-Physical*, vol. 54, pp. 505-510, Jun 1996.

[35] B. L. Gray, R. S. Fearing, "A surface micromachined microtactile sensor array", *1996 Ieee International Conference on Robotics and Automation, Proceedings*, vol. 1-4, pp. 1-6, 1996.

[36] M. Leineweber, G. Pelz, M. Schmidt, H. Kappert, and G. Zimmer, "New tactile sensor chip with silicone rubber cover," *Sensors and Actuators A-Physical*, vol. 84, pp. 236-245, Sep 1 2000.

[37] P. Dario and D. de Rossi, "Tactile sensors and gripping challenge", *IEEE Spectr.* vol. 22 pp 46–52, 1985.

[38] E. S. Kolesar, C. S. Dyson, R. R. Reston, R. C. Fitch, D. G. Ford, and S. D. Nelms, "Tactile integrated circuit sensor realized with a piezoelectric polymer", *Proc. 8th IEEE Int. Conf. Innovative Syst. Silicon* pp 372–81, 1996.

[39] J.-I. Yuji, C. Sonoda "A PVDF tactile sensor for static contact force and contact temperature", *Proc. IEEE Sens.* vol. 1-3, pp 738–41, 2006.

[40] M. Shimojo, A. Namiki, M. Ishikawa, R. Makino, and K. Mabuchi, "A tactile sensor sheet using pressure conductive rubber with electrical-wires stitched method," *IEEE Sensors Journal*, vol. 4, pp. 589-596, Oct 2004.

[41] C.-S. Park, J. Park, and D.-W. Lee, "A piezoresistive tactile sensor based on carbon fibers and polymer substrates," *Microelectronic Engineering*, vol. 86, pp. 1250-1253, 2009

[42] K. Kim, K. R. Lee, W. H. Kim, K.-B. Park, T.-H. Kim, J.-S. Kim, and J. J. Pak, "Polymer-based flexible tactile sensor up to 32x32 arrays integrated with interconnection terminals," *Sensors and Actuators A: Physical*, vol. 156, pp. 284-291, 2009.

[43] X. Tao *Smart Fibres, Fabrics and Clothing*, Cambridge: England, Woodhead, 2001.

[44] S. L. P. Tang and G. K. Stylios, "An overview of smart technologies for clothing design and engineering," *International Journal of Clothing Science and Technology*, vol. 18, pp. 108-128, 2006.

[45] T. Dias, W. Hurley, R. Monaragala, and R. Wijeyesiriwardana, "Development of Electrically Active Textiles," in *Smart Textiles*. vol. 60, P. P. R. Vincenzini, Ed., ed, 2009, pp. 74-84.

[46] F. Carpi and D. De Rossi, "Electroactive polymer-based devices for e-textiles in biomedicine", *IEEE Transactions on Information Technology in Biomedicine*, vol. 9, pp. 574-574, Dec 2005.

[47] D. De Rossi, F. Carpi, F. Lorussi, A. Mazzoldi, E. P. Scilingo, and A. Tognetti, "Electroactive fabrics for distributed, conformable and interactive systems," in *Sensors, 2002. Proceedings of IEEE*, vol.2, pp. 1608-1613, 2002.

[48] V. L. Pushparaj, M. M. Shaijumon, A. Kumar, S. Murugesan, L. Ci, R. Vajtai, R. J. Linhardt, O. Nalamasu, and P. M. Ajayan, "Flexible energy storage devices based on nanocomposite paper," *Proceedings of the National Academy of Sciences of the United States of America*, vol. 104, pp. 13574-13577, Aug 21 2007.

[49] L. Hu, M. Pasta, F. La Mantia, L. Cui, S. Jeong, H. D. Deshazer, J. W. Choi, S. M. Han, and Y. Cui, "Stretchable, Porous, and Conductive Energy Textiles," *Nano Letters*, vol. 10, pp. 708-714, Feb 2010.

[50] T. Suga, H. Konishi, and H. Nishide, "Photocrosslinked nitroxide polymer cathode-active materials for application in an organic-based paper battery," *Chemical Communications*, pp. 1730-1732, 2007.

[51] R. Bhattacharya, M. M. de Kok, and J. Zhou, "Rechargeable electronic textile battery," *Applied Physics Letters*, vol. 95, Nov 30 2009.

[52] D.-H. Kim, J.-H. Ahn, W. M. Choi, H.-S. Kim, T.-H. Kim, J. Song, Y. Y. Huang, Z. Liu, C. Lu, and J. A. Rogers, "Stretchable and foldable silicon integrated circuits," *Science*, vol. 320, pp. 507-511, Apr 25 2008.

[53] B. Karaguzel, C. R. Merritt, T. Kang, J. M. Wilson, H. T. Nagle, E. Grant, and B. Pourdeyhimi, "Flexible, durable printed electrical circuits," *Journal of the Textile Institute*, vol. 100, pp. 1-9, 2009.

[54] L. F. Chen and Y. P. Hong, "Multifiber ceramic capacitor," *Journal of Materials Science-Materials in Electronics*, vol. 12, pp. 187-191, 2001.

[55] T. Suga, H. Konishi, and H. Nishide, "Photocrosslinked nitroxide polymer cathode-active materials for application in an organic-based paper battery," *Chemical Communications*, pp. 1730-1732, 2007.

[56] T. Suga, H. Ohshiro, S. Sugita, K. Oyaizu, and H. Nishide, "Emerging N-Type Redox-Active Radical Polymer for a Totally Organic Polymer-Based Rechargeable Battery," *Advanced Materials*, vol. 21, pp. 1627, Apr 27 2009.

[57] T. Suga, Y.-J. Pu, S. Kasatori, and H. Nishide, "Cathode- and anode-active poly(nitroxylstyrene)s for rechargeable batteries: p- and n-type redox switching via substituent effects," *Macromolecules*, vol. 40, pp. 3167-3173, May 1 2007.

[58] G. Nystrom, A. Razaq, M. Stromme, L. Nyholm, and A. Mihranyan, "Ultrafast All-Polymer Paper-Based Batteries," *Nano Letters*, vol. 9, pp. 3635-3639, Oct 2009.

[59] S. Tominaka, H. Nishizeko, J. Mizuno, and T. Osaka, "Bendable fuel cells: on-chip fuel cell on a flexible polymer substrate," *Energy & Environmental Science*, vol. 2, pp. 1074-1077, 2009.

[60] W. Cai, X. Gong, Y. Cao, "Polymer solar cells: Recent development and possible routes for improvement in the performance", *Solar Energy Materials & Solar Cells*, vol. 94, pp 114, 2010.

[61] C. Lungenschmied, G. Dennler, H. Neugebauer, S. N. Sariciftci, M. Glatthaar, T. Meyer, and A. Meyer, "Flexible, long-lived, large-area, organic solar cells," *Solar Energy Materials and Solar Cells*, vol. 91, pp. 379-384, Mar 6 2007.

[62] G. Dennler, S. Bereznev, D. Fichou, K. Holl, D. Ilic, R. Koeppe, M. Krebs, A. Labouret, C. Lungenschmied, A. Marchenko, D. Meissner, E. Mellikov, J. Meot, A. Meyer, T. Meyer, H. Neugebauer, A. Oepik, N. S. Sariciftci, S. Taillemite, and T. Woehrle, "A self-rechargeable and flexible polymer solar battery," *Solar Energy*, vol. 81, pp. 947-957, 2007.

[63] E. A. Olivetti, J. H. Kim, D. R. Sadoway, A. Asatekin, and A. M. Mayes, "Sol-gel synthesis of vanadium oxide within a block copolymer matrix," *Chemistry of Materials*, vol. 18, pp. 2828-2833, Jun 13 2006.

[64] S. H. Lee, P. Liu, C. E. Tracy, and D. K. Benson, "All-solid-state rocking chair lithium battery on a flexible Al substrate," *Electrochemical and Solid State Letters*, vol. 2, pp. 425-427, Sep 1999.

[65] J. W. Schultze and H. Karabulut, "Application potential of conducting polymers," *Electrochimical Acta.*, vol. 50, pp. 1739-1745, Feb 15 2005.

[66] J. Wheldon, W.-J. Lee, D.-H. Lim, A. B. Broste, M. Bollinger, W.H. Smyrl, "High-performance flexible miniature fuel cell", *Electrochemical and Solid-State Letters*, v 12, n 5, p B86-B89, 2009.

[67] T. Ito, K. Kimura, M. Kunimatsu, "Characteristics of micro DMFCs array fabricated on flexible polymeric substrate", *Electrochemistry Communications*, v 8, n 6, p 973-976, 2006.

[68] S.H. Park, A. Roy, S. Beaupre, S. Cho, N. Coates, J.S. Moon, D. Moses, M. Leclerc, K. Lee, A.J. Heeger, "Bulk heterojunction solar cells with internal quantum efficiency approaching 100%", *Nat. Photonics*, vol. 3, pp. 297–303, 2009.

[69] Y.Y. Liang, D.Q. Feng, Y. Wu, S.T. Tsai, G. Li, Gang, C. Ray, L.P. Yu, "Highly efficient solar cell polymers developed via fine-tuning of structural and electronic properties", *J. Am. Chem. Soc*, vol. 131, pp. 7792–7799, 2009.

[70] F.C. Krebs, H. Spanggaard, "Significant improvement of polymer solar cell stability", *Chem. Mater.* vol. 17, pp. 5235–5237, 2005.

[71] M. Jørgensen, K. Norrman, F.C. Krebs, "Stability/degradation of polymer solar cells", *Sol. Energy Mater. Sol. Cells*, vol. 92, pp. 686–714, 2008.

[72] Y. Gao, N. Guo, B. Gauvreau, M. Rajabian, O. Skorobogata, E. Pone, O. Zabeida, L. Martinu, C. Dubois, and M. Skorobogatiy, "Consecutive solvent evaporation and co-rolling techniques for polymer multilayer hollow fiber preform fabrication," Journal of Materials Research, vol. 21, pp. 2246-2254, Sep 2006.

[73] J. F. Gu, S. Gorgutsa, and M. Skorobogatiy, "Soft capacitor fibers using conductive polymers for electronic textiles," *Smart Materials & Structures*, vol. 19, Nov 2010.

[74] S. Nakamura, G. Sawa, "Percolation phenomena and electrical conduction mechanism of carbon black-polyethylene composites", *Proc. of Intl. Symp. on Electrical Insulating Materials*, pp. 333-336, 1998.

[75] J. Feng, C.-M. Chan, "Effects of strain and temperature on the electrical properties of carbon black-filled alternating copolymer of ethylene-tetrafluoroethylene composites", *Polym. Eng. Sci.*, vol. 43, pp. 1064-70, 2003.

[76] B. Schulte, W. Tischer, W. Waldenrath, H. Kaloff, “Stretched polycarbonate films filled with carbon black”, *US Patent* 4791016, 1988.

[77] H. Tang, X. G. Chen, and Y. X. Luo, "Studies on the PTC/NTC effect of carbon black filled low density polyethylene composites," *European Polymer Journal*, vol. 33, pp. 1383-1386, Aug 1997.

[78] G. Yu, M.Q. Zhang, H.M. Zeng, “Carbon-black-filled polyolefine as a positive temperature coefficient material: Effect of composition, processing, and filler treatment”, *J. Appl. Polym. Sci.*, vol. 70, pp. 559-66, 1998.

[79] W. Zhang, A.A. Dehghani-Sanij, R.S. Blackburn, “Carbon based conductive polymer composites”, *J. Mater. Sci.*, vol. 42, pp. 3408-18, 2007.

[80] G. Wu , S. Asai, C. Zhang, T. Miura and M. Sumita, “A delay of percolation time in carbon-black-filled conductive polymer composites”, *J. Appl. Phys*., vol. 88, pp. 1480-87, 2000.

[81] Q. Cao, Y. Song, Z. Liu and Q. Zheng, “Influence of annealing on rheological and conductive behaviors of high-density polyethylene/carbon black composites”, *J. Mater. Sci.*, vol. 44, pp. 4241-45, 2009.

[82] I. Alig, T. Skipa, D. Lellinger and P. Pötschke, “Destruction and formation of a carbon nanotube network in polymer melts: Rheology and conductivity spectroscopy”, *Polymer*., vol. 49, pp. 3524-32, 2008.

[83] A. Chenite and F. Brisse, " Structure and conformation of poly(ethylene oxide), PEO, in the trigonal form of the PEO-urea complex at 173 K ", *Macromolecules*, vol. 24, pp. 2221-2225, Apr 29 1991.

[84] Y. Liu, H. Antaya, and C. Pellerin, "Characterization of the stable and metastable poly(ethylene oxide)-urea complexes in electrospun fibers," *Journal of Polymer Science Part B-Polymer Physics*, vol. 46, pp. 1903-1913, Sep 15 2008.

ARTICLE 1 - A WOVEN 2D TOUCHPAD SENSOR AND A 1D SLIDE SENSOR USING SOFT CAPACITOR FIBERS

IOP PUBLISHING SMART MATERIALS AND STRUCTURES
Smart Mater. Struct. **21** (2012) 015010 (10pp) doi:10.1088/0964-1726/21/1/015010

A woven 2D touchpad sensor and a 1D slide sensor using soft capacitor fibers

Stephan Gorgutsa, Jian Feng Gu and Maksim Skorobogatiy

Genie Physique, Ecole Polytechnique de Montreal, Montreal, H3C 3A7, Canada

E-mail: maksim.skorobogatiy@polymtl.ca

Received 17 August 2011, in final form 16 November 2011
Published 19 December 2011
Online at stacks.iop.org/SMS/21/015010

Abstract
Recently reported soft conductive-polymer-based capacitor fibers are used to build a fully woven 2D touchpad sensor and a 1D slide sensor. An individual capacitor fiber features a swiss-roll like structure having two dielectric and two conductive polymer films rolled together in a classic multilayer capacitor configuration. The soft fibers of sub-1 mm outer diameter are fabricated using a fiber drawing procedure from a macroscopic polymeric preform. An individual capacitor fiber is then demonstrated to act as a distributed sensor that allows the touch position to be determined by measuring the fiber's AC response. In other words, a single fiber acts as a 1D slide sensor. Furthermore, we develop an electrical ladder network model to predict the distributed sensor properties of an individual fiber and show that this model describes the experimental measurements very well. Finally, a two-dimensional touchpad sensor is presented. The sensor is built by weaving a one-dimensional array of capacitor fibers in parallel to each other. The performance of the touchpad sensor is then characterized.

(Some figures may appear in colour only in the online journal)

1. Introduction

Touch sensing as a human interface device (HID) technology is becoming increasingly popular and ubiquitous finding its applications in smart phones, computers and responsive garments to name a few. Various touch sensing systems have been developed based on different physical principles including resistive, capacitive, infrared, surface acoustic wave, electromagnetic, near field imaging, etc. Resistive [1] and capacitive [2] methods have been widely used in conventional touch screens of commercial products such as mobile phones, PDAs, and consumer electronics devices. Resistive touch screens are composed of two material sheets that are coated with a resistive material, commonly indium tin oxide (ITO), and separated by an air gap or microdots. When a finger presses the screen, the two sheets are connected at the touch position which changes the current flow in the screen. A sensing circuit then detects changes and locates the touch position. A capacitive touch sensor is based on the capacitive coupling effect. A typical design involves coating the screen with a thin, transparent metallic layer, in order to form a collection of capacitors on the surface. When a user touches the surface, the disturbance caused by the finger changes the capacitance and current that flows on the display.

A significant limitation for most of these technologies is that they are only capable of detecting a single touch. Multi-touch techniques allow touch screens to recognize touches of multiple fingers or inputs of multiple persons simultaneously. Multi-touch detection mechanisms can be classified into three categories: sensor array, capacitive sensing, and vision and optical based ones. A sensor array touch surface consists of a grid of touch sensors that work independently. When a user exerts multiple touches on the surface, the system can identify activated sensors and determine these touch positions simultaneously. An example is the FMTSID (fast multiple-touch-sensitive input device) [3], one of the first multi-point touch sensor-based devices. The system consists of a sensor matrix panel, the ranks of select register, an A/D converter and a control CPU. The design of the sensor matrix is based on the technique of capacitance measurement between a fingertip and a metal plate. A capacitive touch method uses the capacitive coupling between two conductors to sense a touch. Typically, the touch surface contains a mesh of horizontal and vertical

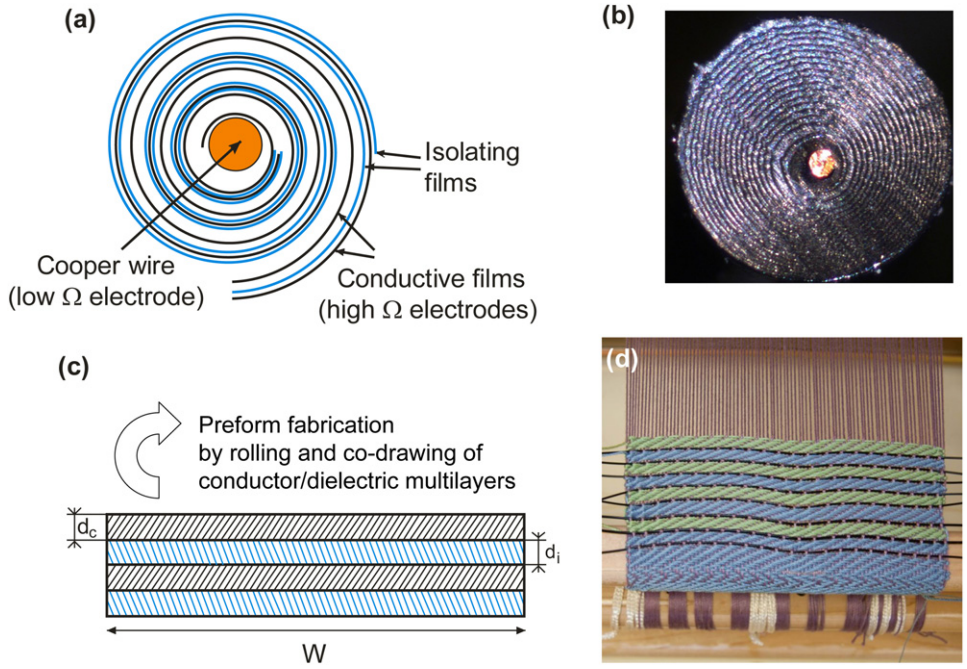

Figure 1. (a) Schematic of a capacitor fiber featuring a spiraling multilayer comprising two conductive and two isolating films. The black curves represent the two conductive films, while the blue curves represent the isolating films. (b) Photo of the cross section of a drawn capacitor fiber (900 μm in diameter) with a copper wire (100 μm in diameter) embedded in the center. A multilayer ($N \sim 30$) structure can be clearly seen. (c) The fiber preform is made by co-rolling four polymer layers (two conductive and two isolating) into a swiss-roll structure. The number of resultant layers in the spiral structure is proportional to the width of the unrolled multilayer. In the drawn fiber, the thicknesses of the conductive d_c and isolating d_i layers can be smaller than 10 μm, while the unwrapped width W of the layers fitting into a 1 mm diameter fiber can be in excess of 3 cm. (d) Weaving a two-dimensional touchpad sensor on a Dobby loom.

antennas which function as either transmitters or receivers of electric signals. Examples based on this technology include Rekimoto's SmartSkin [4], and DiamondTouch [5] developed by Dietz and Leigh.

In addition to touch screens, touch sensors with force sensing ability have been studied as tactile sensors for many years [6]. Such sensors have found their applications in artificial skin for robot applications [7], minimally invasive surgery [8], wearable computers [9], and mobile or desktop haptic devices [10]. To date tactile sensors have mainly focused on silicon-based sensors that use piezoresistive [11, 12] or capacitive sensing mechanisms [13–15]. Silicon tactile sensors have limitations of mechanical brittleness, and hence are not capable of sustaining large deformations. Polymer-based tactile sensing approaches that use piezoelectric polymer films [16–18], pressure-conductive rubber [19], carbon fiber based polymer composite [20] and conductive polymers [21], have been reported as well. These sensors provide good resolution but the applied force range is low due to the limited thickness of a membrane.

In this paper we demonstrate that the soft capacitor fibers recently developed in our laboratory [22] are well suited for integration into woven textile products, and that these electroactive fibers can be used as building blocks for textile-based slide sensors and touchpads. We start the paper with a description of the structure and fabrication technique of a capacitor fiber. We then continue with the study of the AC response of a single fiber and show that a single capacitor fiber can be used as a touch-based slide sensor. We, furthermore, introduce a theoretical model to describe the electrical response of a single capacitor fiber using an electrical ladder network model. Finally, we present the prototype of a woven touchpad sensor featuring a one-dimensional array of capacitor fibers, and then study the touchpad's performance.

2. Soft capacitor fibers as building blocks for textile touch sensors

Recently our group presented a novel, highly flexible fiber with high electric capacitance [22]. In its cross section the capacitor fiber features a swiss-roll structure where two conductive films (carbon-black-filled polyethylene (PE)) and two dielectric films (low density PE) are co-rolled to form a round multilayer capacitor (see figures 1(a) and (b)). The fiber is fabricated by drawing from a macroscopic preform. The fiber preform is made by periodically stacking four conductive and isolating layers (see figure 1(c)) and then rolling the multilayer into a swiss-roll configuration featuring a large central hole. The thus fabricated preform is a cylinder of a typical size of 30 cm in length and 2 cm in diameter. The all-polymer preform is then drawn at around 200 °C into a capacitor fiber. This fabrication technique is directly analogous to the one used in the manufacture of microstructured polymer optical fibers [23]. Additionally, a small-diameter (typically 50–150 μm) copper wire can be embedded into the fiber during the drawing process by passing it inside the fiber preform central hole

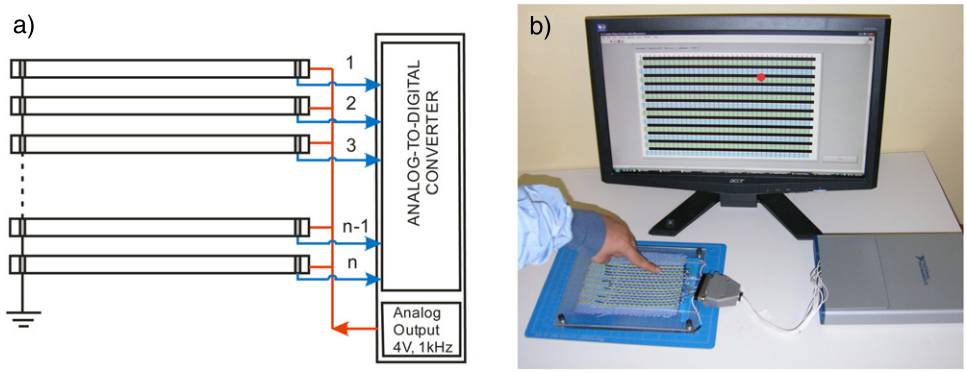

Figure 2. The woven touchpad sensor. (a) Schematic representation of the woven 2D touchpad sensor featuring a one-dimensional array of capacitor fibers. All the connections to and from the fibers are made using a 120 μm diameter copper wire (denoted by red lines). The fibers in the array have a common ground and a common source; however, they are interrogated individually. The analog output of the ADC board is used as a function generator that provides a sinusoidal signal at 1 kHz with an amplitude of 4 V. (b) Photograph of the woven touchpad connected to the ADC board, as well as the monitor image of a textile with an interpreted touch position.

and letting the preform collapse around the wire in the neckdown region. Introduction of a copper wire into the fiber drawing process actually improves the fiber drawability and eases connectorization of the resultant fibers in textile-based electrical circuits. In practical applications, the copper wire in the fiber center serves as a low resistivity electrode attached to one of the two high resistivity conductive plastic electrodes of a fiber capacitor. The other high resistivity conductive plastic electrode of a fiber is brought to the fiber surface to ease connectorization. Typical fibers fabricated using the above-mentioned fabrication procedure have a sub-millimeter diameter, contain at least 30 layers, and have a typical capacitance of 100 nF m^{-1}, which is almost three orders of magnitude higher than that of a standard coaxial cable of a comparable diameter.

At the same time, the soft, while highly elastic, mechanical nature of the fibers makes them easy to use in a conventional weaving process (figure 1(d)). In our laboratory we have used a table Dobby loom (Leclerc Voyager $15\frac{3}{4}''$ 4 s) to weave the fibers into a one-dimensional senor array integrated into a wool-based textile matrix (see figure 1(d)). The resulting 15 cm $\times$ 10 cm woven touchpad contained 15 capacitor fibers, each 12 cm long (see figure 2(b)).

The high resistivity of the conductive polymer electrodes together with their high capacitance endows the fiber with interesting electrical properties, which, as we will see in what follows, makes the fiber well suited for distributed sensing applications of touch. In a typical implementation of a touch sensor, we ground the outer fiber electrode (high Ω electrode) on one end, while applying the AC voltage to the copper wire (low Ω electrode) on the other end (see figure 2(a)). We then read out the voltage on the fiber outer electrode (high Ω electrode) at the same end where the copper wire is connectorized. In our experiments we find that the read out voltage is highly sensitive to the position of the touch along the fiber, which allows us to build a touchpad sensor that can localize in two dimensions the position of touch (figure 2(b)).

In our experimental setup the inner electrodes of all the fibers (copper wires) are connected to the analog voltage source integrated into the analog-to-digital converter (ADC) card providing a sinusoidal signal at 1 kHz with an amplitude of 4 V. The outer electrodes of the fibers are connected to the individual channels of the ADC card (National Instruments USB-6343 X-series DAQ) in order to measure the voltage at their endpoints. The connections are made using thin copper wires (0.120 μm diameter) and secured with a conductive epoxy. The ADC board is plugged into a PC and the touch position can then be monitored on the computer screen via LabVIEW software.

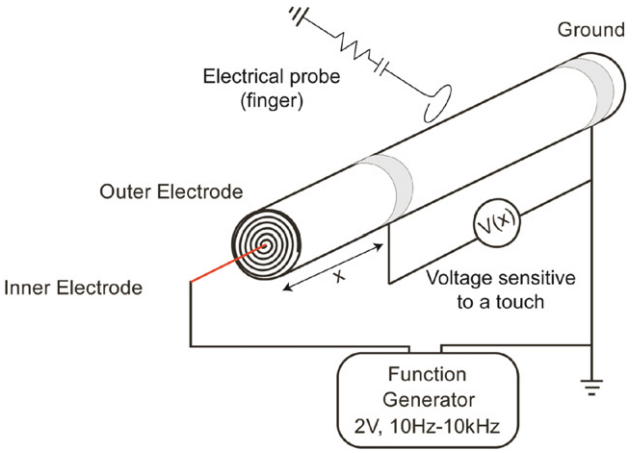

Figure 3. Schematic of a 1D slide sensor based on a single capacitor fiber.

2.1. Sensing of touch with a single fiber: a 1D slide sensor

In order to understand the sensing principle behind a touchpad we first consider the electrical response to touching of a single capacitor fiber. To characterize a single fiber we use the general electrical layout outlined earlier. In particular, a sinusoidal signal of voltage amplitude V_0 and constant frequency (10 Hz–10 kHz) is provided by an external function generator and is applied to the copper wire electrode of a fiber (see figure 3). The voltage response is acquired using a sliding contact on the outer electrode of the fiber (high Ω

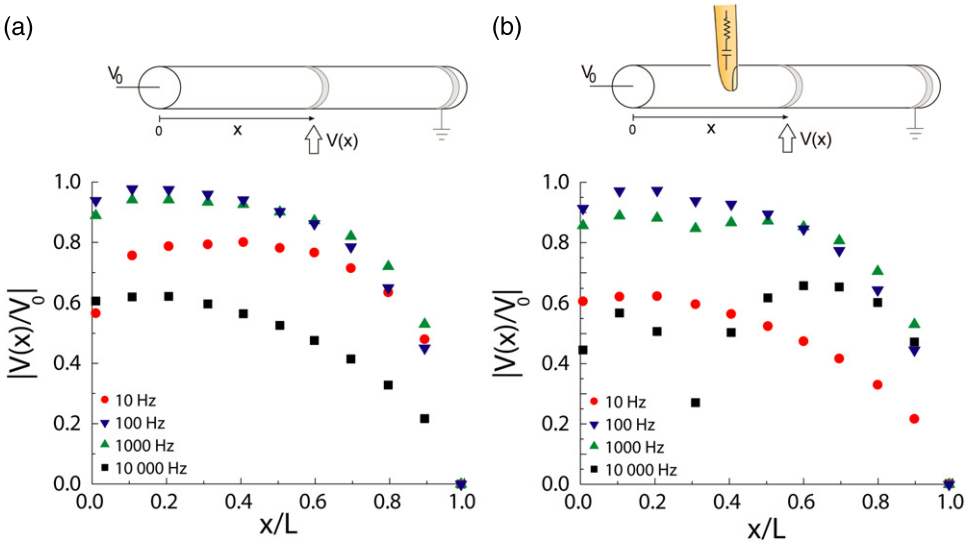

Figure 4. Voltage distribution along the outer fiber electrode for (a) an isolated fiber, (b) a fiber touched with an equivalent human probe. The four data sets correspond to the different driving frequencies of 10 Hz, 100 Hz, 1 kHz and 10 kHz. The voltage distribution along the fiber touched with a probe shows a dip in the vicinity of the touching position.

electrode). The sliding contact is connected to the oscilloscope (GDS-1022, Good Will Instrument Co., Ltd) through a 10× probe (GTP-060A-4, Good Will Instrument Co., Ltd). This arrangement allows measurement of the voltage distribution along the fiber length both when the fiber is touched and when it is not. As a human body is largely composed of conductive electrolytes covered with a layer of dielectric skin, the human body can be approximated by an equivalent electrical circuit comprising a resistor connected in series to a capacitor. Typical values of effective resistance and capacitance are 1.44 kΩ and 150 pF respectively. In our experimental studies of a single fiber's response to touching, we use an equivalent human probe with these effective electrical parameters to guarantee repeatability between measurements and to simplify the theoretical interpretation of the acquired data.

2.1.1. Experimental characterization of a single capacitor fiber and a 1D slide sensor. In figure 4 we present the voltage distribution along the fiber length for an isolated fiber (figure 4(a)), and for a fiber that is touched with an equivalent human probe (figure 4(b)). Here x/L represents the normalized position of the sliding contact along the fiber length. The fiber length used in our experiments was $L = 12.3$ cm. $|V(x)/V_0|$ represents the voltage measured by the sliding contact along the outer electrode of a capacitor fiber. When using the equivalent human probe (figure 4(b)), we fix it at the position $x/L = 0.3$. The different data sets in figure 4 correspond to the four different frequencies of the function generator used in our measurements (10 Hz, 100 Hz, 1 kHz, 10 kHz).

In the DC case (not shown in the figures), the voltage along the outer electrode of a capacitor is constant and zero as the capacitor fiber breaks the DC electrical circuit. For an isolated fiber (figure 4(a)) in the AC case, the voltage distribution along the fiber length shows the same trend at all frequencies. In particular, it saturates exponentially fast from zero at the grounded end to some maximal value at the other end of the fiber. The maximal voltage amplitude at the outer fiber electrode is strongly dependent on the operation frequency and it reaches its maximum at frequencies between 100 Hz and 1 kHz. When the fiber is touched with an equivalent human probe, the voltage distribution along the fiber's outer electrode shows high sensitivity to the operation frequency (figure 4(b)). Thus, at low driving frequencies (10, 100 Hz) the voltage distribution along the fiber's outer electrode is virtually unchanged by the touch. At higher frequencies (above 100 Hz) a dip appears in the voltage distribution in the vicinity of the point of contact with an equivalent human probe. Finally, at high frequencies (above 1 kHz) this dip becomes very pronounced and easy to detect. The overall frequency response of the capacitor fiber can be understood from basic electric circuit theory. Thus, the fiber used in these experiments had a capacitance per unit length of $C = 93$ nF m^{-1} and a transverse resistance of $R_t = 14.5$ kΩ m (bulk resistance of conductive layers 4.8 Ω m). The characteristic frequency associated with the corresponding RC circuit is $\nu = 1/(2\pi R_t C) = 120$ Hz. The electric response of a capacitor fiber is, in fact, that of a high pass filter. Namely, at frequencies well below 120 Hz the fiber operates in a quasi-DC regime where it simply breaks the electrical circuit. The fiber's response to touch is, therefore, minimal at low frequencies. At frequencies comparable to or higher than 120 Hz the capacitor fiber acts as a relatively low resistivity distributed complex impedance. At these higher frequencies touching the capacitor fiber can modify significantly the local current flows and voltage distributions, thus resulting in sensitivity of its various electrical parameters to touching.

From figure 4(b) it is clear that when operating at higher driving frequencies the touch position can be determined from the dip in the voltage distribution along the fiber's outer electrode. For practical implementation of a slide sensor it

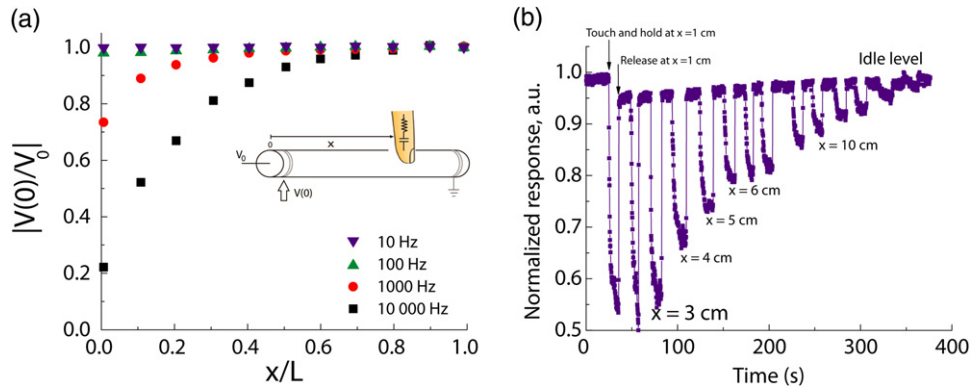

Figure 5. Detection of touch with a 1D slide sensor. (a) Voltage measured at the extremity of a capacitor fiber opposite to the fiber's grounded end. (b) Typical time resolved response of a slide sensor. The dips in the measured voltage correspond to the touch and release events.

is, however, inconvenient to require the knowledge of the voltage distribution across the whole fiber length. Therefore, the important question is whether the position of the touch can be determined by continuously measuring the voltage at a single fixed point on the fiber's outer electrode. To answer this question in figure 5(a) we present the value of voltage as measured at the fiber extremity ($x = 0$) as a function of the touch position along the fiber. As before, x/L represents the touch position of the equivalent human probe, while $|V(0)/V_0|$ represents the voltage measured at the fiber end opposite to the grounded end. We observe that for driving frequencies above 100 Hz, the voltage at the fiber extremity changes significantly depending on the position of the touch. In turn, this allows building of a 1D sliding sensor with a convenient acquisition procedure based on a single point measurement.

Finally, a 1D slide sensor was characterized in a realistic setting with a student touching the sensor consecutively at different positions along the fiber's length. This time the sensor was touched with an actual finger and not an equivalent probe. The driving frequency was 1 kHz and it was provided by the analog output of an ADC card. The same card was also employed as a signal acquisition unit with an acquisition rate of 20 kHz. Such high acquisition rates were only used for the purpose of resolving the time response of a sensor and in practice significantly slower acquisition rates (<10 Hz) could be used. To deduce the touch position we continuously measured the voltage at the endpoint of the fiber's outer electrode. Figure 5(b) presents an example of the measured voltage as a function of time. To operate the sensor we first record for several seconds the voltage level ('idle' level) without touching the fiber. We then touch the sensor at $x = 1$ cm from the fiber end. At the moment of touch the signal drops very rapidly (in a matter of 1 s) to almost its equilibrium value; this is followed by a much slower (∼10 s) relaxation to the actual equilibrium value. We believe that the fast time scale corresponds to a pure electrical response of the fiber, while the slow time scale corresponds to small pressure induced changes in the fiber's electrical parameter due to fiber deformation under touch. As soon as the finger is removed, the signal returns back to the 'idle' level in a matter of 0.2 s. Next, by touching, holding, and releasing the fiber at various positions along its length we can record a complete calibration curve. Then, the position of a touch can be determined from the voltage level at the bottom of a dip corresponding to a touching event. This is, of course, the simplest implementation of a touch sensor. To avoid person-dependent calibration of the sensor one can, for example, perform two voltage measurements from opposing sides of a fiber (by simultaneously flipping the ground from one side to the other), then use analytical models to extract the effective electrical parameters of a human finger and find the touch position.

2.1.2. Ladder network model and user-specific calibration procedure. To model the electrical response of the capacitor fibers we use an RC ladder network which is an extension of the method originally developed in [22].

First, we consider a stand-alone capacitor fiber without touching. We define the conductive polymer electrode transverse resistance as $R_t \approx r_t/L$, where the electrode resistivity is $r_t = \rho_v W/d_c$. We also use the following definitions: ρ_v is the volume resistivity of the conductive films, L is the length of the fiber, W and d_c denote respectively the width and thickness of the conductive electrodes wrapped in the fiber cross section (see figure 1(c)). To measure the transverse resistance one has to ensure that there are no longitudinal (along the fiber length) currents in the fiber. In practice, to deduce the transverse resistivity one covers the outer fiber electrode (high resistivity electrode) with a metallic foil, and then measures the fiber's AC response by applying the voltage between the inner copper electrode and the outer metallic foil.

Similarly, we define the conductive polymer electrode longitudinal resistance as $R_l \approx r_l L$, where the electrode's longitudinal resistivity is $r_l = \rho_v/(W d_c)$. To measure the longitudinal resistance one has to ensure that there are no transverse (perpendicular to the fiber length) currents in the fiber. In practice, it is difficult to measure the longitudinal resistivity directly. In principle, if the electrode length (fiber length) is much longer than the net width of a conductive electrode wrapped in the fiber cross section, the longitudinal resistivity can be deduced from the AC measurement where

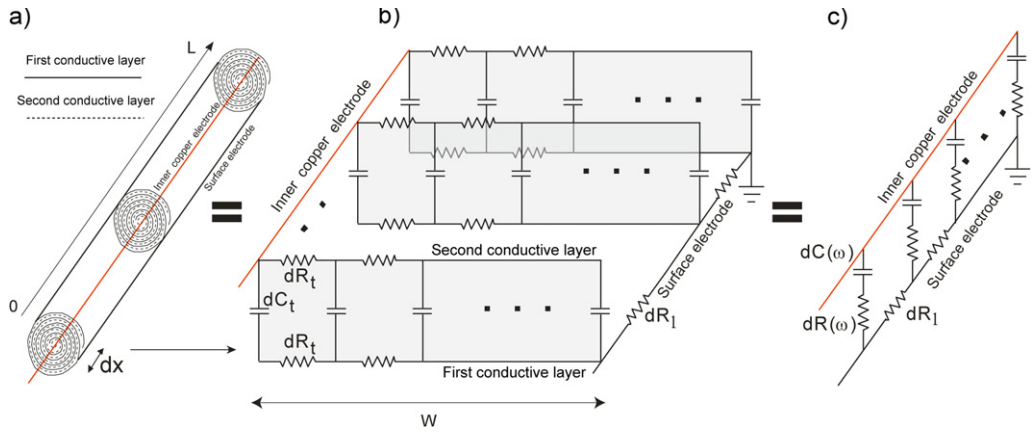

Figure 6. The ladder RC network model of a stand-alone capacitor fiber. (a) The fiber is modeled as a sequence of fiber dR_l (high resistivity outer cross sections of small length dx connected in series via longitudinal resistive electrode elements), while we assume that the inner copper electrode has a constant potential along its length. (b) The electrical response of an individual fiber cross section is modeled as an RC network where the transverse resistivity elements dR_t are connected via capacitance dC_t elements. (c) One can show that the equivalent circuit that describes the electrical response of an individual fiber cross section is given simply by the frequency dependent resistivity d$R(\omega)$ connected in series with the frequency dependent capacitance d$C(\omega)$. Finally, the electrical response of a fiber is modeled as another RC network with frequency dependent resistivity and capacitance.

the high resistivity outer electrode of a fiber is grounded on one end, while the inner high resistivity electrode of the fiber is connected to a voltage supply at the other end. Note that the low resistivity copper electrode has to be removed from the fiber for this measurement.

Finally, the total fiber capacitance is proportional to the fiber length, while the fiber capacitance per unit length is simply $C_\mathrm{t} \approx 2\varepsilon_0\varepsilon W/d_\mathrm{i}$, where d_i is the thickness of the isolating films in the fiber, ε is the dielectric constant of the isolating films, and ε_0 is the permeability of vacuum. We note that the relatively high capacitance of our fibers is due to the small thickness of the isolating films, and the large net width of the conductive layers. Thus, a typical fiber features conductive and isolating layers with thicknesses smaller than 10 μm, while the net width W of the layers wrapped into a 1 mm diameter fiber can be in excess of 3 cm.

To model the electrical response of a fiber we consider it as a sequence of thin cross sections of length dx (figure 6(a)) each having a longitudinal resistance d$R_\mathrm{l} = r_\mathrm{l}\,\mathrm{d}x$. We then consider the electrical response of an individual cross section, while assuming that along the fiber length the individual fiber sections are connected via longitudinal resistance elements dR_l (figure 6(b)). The electrical response of an individual fiber cross section is modeled as an RC network where transverse resistivity elements d$R_\mathrm{t} = r_\mathrm{t}/\mathrm{d}x$ are connected via capacitance d$C_\mathrm{t} = C_\mathrm{t}\,\mathrm{d}x$ elements. In [22] we show that the equivalent circuit that describes the electrical response of an individual fiber cross section of length dx is given by the frequency dependent resistivity d$R(\omega)$ connected in series with the frequency dependent capacitance d$C(\omega)$, where

$$\mathrm{d}C(\omega) = -\frac{\mathrm{d}x}{\omega r_\mathrm{t}\,\mathrm{Im}(f(B))}, \tag{1}$$

$$\mathrm{d}R(\omega) = \left(\frac{1}{2} + \mathrm{Re}(f(B))\right)\frac{r_\mathrm{t}}{\mathrm{d}x}, \tag{2}$$

and $f(B) = \frac{1+\cosh(B)}{B\sinh(B)}$; $B = \sqrt{2\mathrm{j}\omega r_\mathrm{t} C_\mathrm{t}}$.

The electrical response of a stand-alone fiber can, therefore, be modeled as another RC ladder with frequency dependent parameters d$R(\omega)$, d$C(\omega)$, and frequency independent parameters dR_l (see figure 6(c)).

Now that the model for a stand-alone capacitor fiber is defined, we modify it slightly in order to analyze a 1D slide sensor. In particular, the fiber is assumed to be touched at a position x_b with a finger having effective electric parameters $R_\mathrm{b} = 1.44$ kΩ, $C_\mathrm{b} = 150$ pF. Moreover, to simplify comparison with experiment we include in our model the effective circuit of an oscilloscope probe used in our measurements. The probe is attached at a position x_p on the fiber surface (see figure 7), and the effective circuit parameters of the probe and oscilloscope are $R_p = 10$ MΩ, $C_p = 200$ pF. The necessity to include the effective circuit of a probe into the model comes from the realization that the resistance of the standard 10× probe (10 MΩ) used in our experiments has the same order of magnitude as the transverse resistance of the short fiber segments used in our studies. For example, the transverse resistance of the 10 cm-long fiber pieces typically ranges from 0.1 to 1 MΩ. Moreover, one can show that at frequencies lower than $\nu \approx 1/(2\pi R_p C_\mathrm{b}) \approx 100$ Hz or higher than $\nu \approx 1/(2\pi R_\mathrm{b} C_p) \approx 55$ kHz, the effective impedance of a probe becomes smaller than that of a finger; therefore the probe's effective circuit has to be included into the model to accurately explain the experimental measurements.

In figure 7 we distinguish three parts of an RC latter network. The first part is located to the left of the probe, where $i''(x)$ denotes the longitudinal current flowing in the polymer conductive film, while d$i''(x)$ denotes the transverse current flowing in the thin section of length dx. To the right of the probe, while still before the finger touch position the longitudinal and transverse currents in the polymer electrode are denoted as $i(x)$ and d$i(x)$. Finally, to the right of the touch position the corresponding currents are $i'(x)$ and d$i'(x)$. V_0 is the voltage difference between the inner copper electrode and

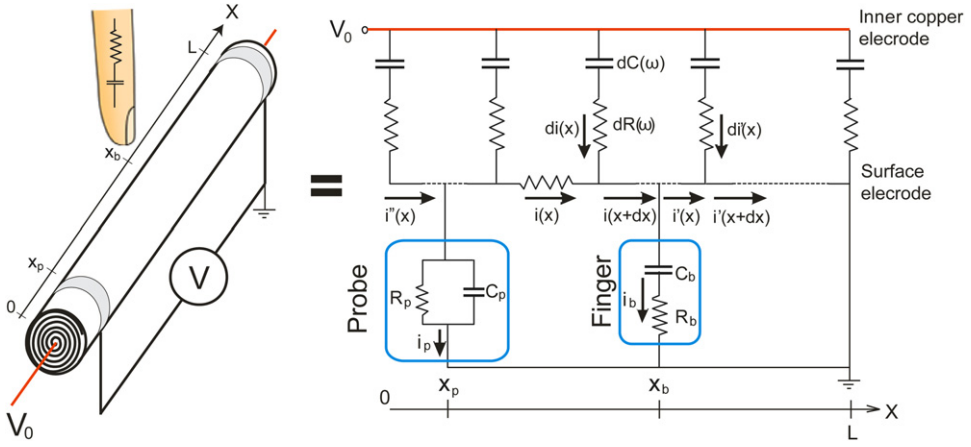

Figure 7. The ladder network model of a 1D slide sensor. The fiber is assumed to be touched at a position x_b with a finger having effective electric parameters R_b, C_b. Moreover, to simplify the comparison with experiment we include in our model the effective circuit (with parameters R_p, C_p) of an oscilloscope probe used in our measurements; the probe is attached at a position x_p.

the outer electrode at $x = L$. We also assume that the fiber material parameters are position and frequency independent. Furthermore, we consider that the probe is attached to the left of the touch position, $x_p < x_b$. We now apply Kirchhoff's voltage law and the current conservation law to the ladder circuit to arrive at the following equations for any position x along the fiber. Thus, using Kirchhoff's voltage law we get

$$\begin{aligned}
&0 < x < x_p;\\
&\quad \mathrm{d}i''(x)\left(\frac{1}{\mathrm{j}\omega\,\mathrm{d}C(\omega)} + \mathrm{d}R(\omega)\right)\\
&\qquad + \int_x^{x_p} r_l i''(l)\,\mathrm{d}l = V_0 - V(x_p)\\
&x = x_p; \qquad i_p \frac{R_p}{1 + \mathrm{j}\omega\, C_p R_p} = V(x_p)\\
&x_p < x < x_b;\\
&\quad \mathrm{d}i(x)\left(\frac{1}{\mathrm{j}\omega\,\mathrm{d}C(\omega)} + \mathrm{d}R(\omega)\right)\\
&\qquad + \int_x^{x_b} r_l i(l)\,\mathrm{d}l = V_0 - V(x_b)\\
&x = x_b; \qquad i_b\left(\frac{1}{\mathrm{j}\omega\, C_b} + R_b\right) = V(x_b)\\
&x_b < x < L;\\
&\quad \mathrm{d}i'(x)\left(\frac{1}{\mathrm{j}\omega\,\mathrm{d}C(\omega)} + \mathrm{d}R(\omega)\right) + \int_x^{L} r_l i'(l)\,\mathrm{d}l = V_0.
\end{aligned} \tag{3}$$

Using the current conservation law we get

$$\begin{aligned}
&0 < x < x_p; && i''(x) + \mathrm{d}i''(x) = i''(x + \mathrm{d}x)\\
&x = x_p; && i''(x_p) = \mathrm{i}(x_p) + i_p\\
&x_p < x < x_b; && i(x) + \mathrm{d}i(x) = i(x + \mathrm{d}x)\\
&x = x_b; && i(x_b) = i'(x_b) + i_b\\
&x_p < x < L; && i'(x) + \mathrm{d}i'(x) = i'(x + \mathrm{d}x).
\end{aligned} \tag{4}$$

Finally, the boundary conditions are

$$i''(0) = 0. \tag{5}$$

To solve these equations, we can first differentiate equations (3) with respect to x to obtain three similar second order differential equations with respect to i, i' or i'' of the following form:

$$\frac{\mathrm{d}^2 i(x)}{\mathrm{d}x^2}\left(\frac{1}{\mathrm{j}\omega\,\mathrm{d}C(\omega)/\mathrm{d}x} + \mathrm{d}x\,\mathrm{d}R(\omega)\right) - r_l i(x) = 0. \tag{6}$$

Then, in each of the three sections of the fiber, we can write solution for the currents as

$$\begin{aligned}
i = C_1 \mathrm{e}^{\tilde{B}x} + C_2 \mathrm{e}^{-\tilde{B}x}, \qquad i' = C_3 \mathrm{e}^{\tilde{B}x} + C_4 \mathrm{e}^{-\tilde{B}x},\\
i'' = C_5 \mathrm{e}^{\tilde{B}x} + C_6 \mathrm{e}^{-\tilde{B}x},
\end{aligned} \tag{7}$$

where

$$\tilde{B} = \sqrt{\frac{r_l}{\left(\frac{1}{\mathrm{j}\omega\,\mathrm{d}C(\omega)/\mathrm{d}x} + \mathrm{d}x\mathrm{d}R(\omega)\right)}} = \sqrt{\frac{r_l}{r_t\left(\frac{1}{2} + f(B)\right)}}, \tag{8}$$

and B, $f(B)$ are defined in (1) and (2). Insertion of expressions (7) into the remaining equations (3)–(5) results in a set of linear equations from which the constants $C_1 - C_6$ can be determined. Finally, from the known current distributions the voltage distribution in each section can be easily found as

$$V(x) = V_0 - \frac{\mathrm{d}^2 i(x)}{\mathrm{d}x^2}\left(\frac{1}{\mathrm{j}\omega\,\mathrm{d}C(\omega)/\mathrm{d}x} + \mathrm{d}x\,\mathrm{d}R(\omega)\right). \tag{9}$$

2.1.3. Comparison of the experimental data with the predictions of a theoretical model. In figure 8 we present the experimental data and theoretical RC ladder model (3)–(9) predictions for the dependence of voltage measured at $x_p = 0$ as a function of the equivalent human probe touch position x_b. In each graph, different sets of curves correspond to distinct fibers which are different from each other in a single parameter. Thus, in figure 8(a) we present measurements of three fibers which were drawn using preforms containing different numbers of conductive layers, and, as a consequence, have different capacitances. The preforms were drawn using the same temperature profile and drawing speed so as to guarantee similar values of the bulk resistivities of the polymer electrodes. Then, the fiber geometrical parameters such as layer thicknesses,

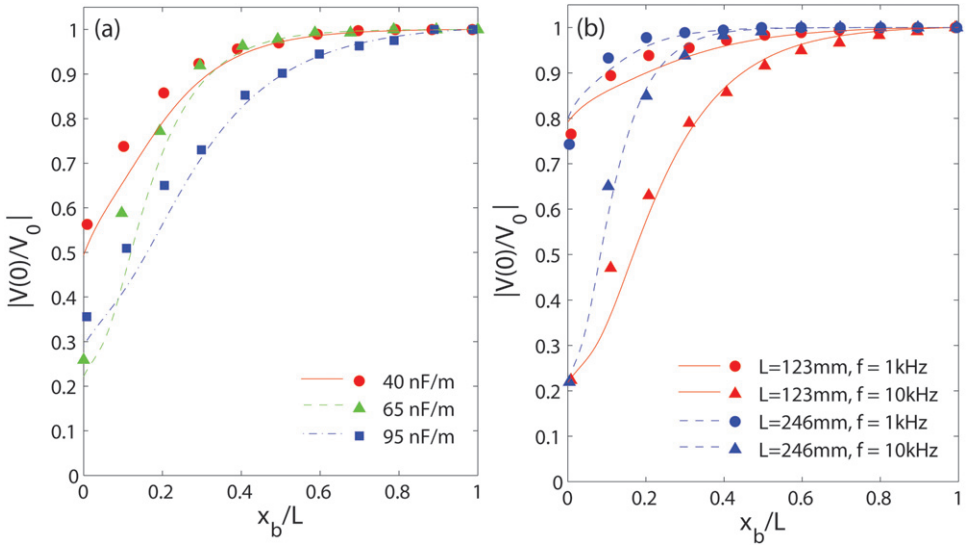

Figure 8. Fiber response to the touch of the equivalent human probe—comparison between predictions of the RC ladder model and experimental data. (a) Response at 10 kHz of three distinct fibers of the same length and different capacitances $C_t = 40, 65, 95$ nF m^{-1}. The rest of the geometrical and electrical parameters of the fibers are similar to each other. (b) Response at 1 kHz and 10 kHz of two distinct fibers of the different lengths. The rest of the geometrical and electrical parameters of the fibers are identical to each other as the shorter fiber was obtained by cutting a longer fiber in half.

electrode width and fiber length were measured using the optical microscope. The parameters of the oscilloscope effective circuit were measured independently. Finally, the bulk resistivity of the conductive layers in a fiber was measured as in [22] by wrapping the fiber's outer electrode into a foil and then extracting the transverse resistivity and, consequently, the bulk resistivity of the conductive layers from the fiber's AC response. In this arrangement the currents are purely transverse and the RC ladder model was shown [22] to give precise fits for the bulk resistivity parameter. We then use all these model parameters found in the independent measurements to predict the response of the fiber to the touch. From figure 8(a) we see that at the operating frequency of 10 kHz the experimental curves are very well described by the RC ladder model which does not use any fitting parameter.

Similarly, in figure 8(b) we present the fiber response to touch for two identical fibers of different lengths. In these experiments we first use a fiber of 24.6 cm in length and then cut it in half to 12.3 cm and repeat the measurement. The rest of the input parameters necessary for the use of a theoretical model were measured as described above. From the figure we see that the fiber response is very well described by the RC ladder model both at 1 and 10 kHz operating frequencies. Moreover, we see that this particular fiber becomes insensitive to touch if the touch point x_b is further than 10 cm from the measuring point x_p.

The measurement of fiber response as a function of fiber length presented in figure 8(b) brings about an important question about the maximal length of a 1D slide sensor, and about the optimal frequency of operation. We note that the functional form of the currents (7) flowing between the probe and the measurement point is exponential with the characteristic length

$$\tilde{L} = \frac{1}{\mathrm{Re}(\tilde{B})} = \frac{W}{\sqrt{2}} \frac{1}{\mathrm{Re}((1+2f(B))^{-\frac{1}{2}})}, \tag{10}$$

where we used $\sqrt{r_t/r_l} = W$. We now use asymptotic expansions of the function $f(B)$:

$$f(B) = \frac{1+\cosh(B)}{B\sinh(B)} \underset{B=\sqrt{2j\omega r_t C_t}}{=} \begin{cases} \dfrac{1}{B}, & \omega \gg \dfrac{1}{r_t C_t}, \\ \dfrac{2}{B^2}, & \omega \ll \dfrac{1}{r_t C_t}, \end{cases} \tag{11}$$

to get the following limiting values for the characteristic length of the current decay:

$$\tilde{L} = \frac{W}{\sqrt{2}} \begin{cases} 1, & \omega \gg \dfrac{1}{r_t C_t}, \\ \dfrac{1}{\sqrt{\omega r_t C_t}}, & \omega \ll \dfrac{1}{r_t C_t}. \end{cases} \tag{12}$$

Note that for the slide sensor of length L to be sensitive along its whole length we have to require that $L \sim \tilde{L}$. From expressions (12) this means that at high frequencies $\omega \gg 1/(r_t C_t)$ the maximal sensor length is limited by the net width of the polymer electrode wrapped into the fiber cross section. Note that for most of our fibers the region of high frequency is in the vicinity of or above 1 kHz. Furthermore, in a typical fiber of $D = 1$ mm diameter, we can currently fit $N \sim 10$–50 turns of the conductive electrode, which results in a net width of a conductive electrode in the fiber of $W \sim \pi DN \sim 3$–15 cm. Therefore, for operation frequencies in the vicinity of or above 1 kHz, the maximal length of the capacitor fiber-based slide sensor is currently limited to several tens of centimeters.

In principle, operation at lower frequencies allows matching of the fiber length and the characteristic current decay length $L \sim \tilde{L}$ for any desired length of fiber. This,

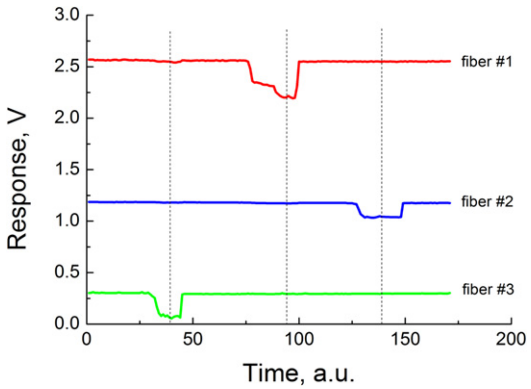

Figure 9. Recorded voltage response as a function of time for three neighboring fibers in the woven touchpad. No detectable cross-talk between the fibers was observed. The dips on the graphs correspond to the individual touch events that take place at different moments in time.

however, demands very low operation frequencies, $\omega \sim (W/L)^2/(r_t C_t)$, that even for a relatively short 1 m-long fiber can be as low as 1–10 Hz. Operation at low frequencies, however, is prone to strong electrical interference and noise. Moreover, at low frequencies ~1 Hz the finger has a very large impedance ≫1 MΩ, which is mismatched with that of our fiber. This makes the sensor of very low sensitivity at low frequencies.

2.2. Crosstalk between fibers in a 1D fiber array (2D touchpad sensor)

Finally, we address the question of crosstalk between the fibers in the woven 2D touchpad sensor. As discussed earlier, the sensor comprises a 1D fiber array separated by 1 cm of textile and is presented in figures 1 and 2. In principle, false responses in our system could be induced by cross-talk between individual fibers that may lead to interference effects between measured signals. In this case the electrical signal at one channel may induce a signal at another channel which might be detected as a false touch. In figure 9 we show an example of a typical recorded voltage response as a function of time for three neighboring fibers in the touchpad. No detectable cross-talk between the fibers was observed during recording. The dips on the graphs correspond to the individual touch events that take place at different moments in time. As can be seen in figure 9, after each touch and release, all the sensor channels successfully return back to the idle state. Despite the fact that in the simplest interrogation configuration each individual fiber incorporated into the textile is not multi-touch sensitive (only the touch closest to the outer electrode will be detected), the absence of inter-channel cross-talk enables simultaneous interrogation of the individual slide sensors. In this sense a 2D touchpad has a partial multi-touch functionality.

3. Conclusion

In conclusion, we have demonstrated that conductive-polymer-based capacitor fibers can be used to build a fully woven 2D touchpad sensor and a 1D slide sensor. An individual capacitor fiber was demonstrated to act as a distributed sensor that allows determination of the touch position along its length by measuring the fiber's AC response. In other words, a single fiber acts as a 1D slide sensor. A theoretical RC ladder model was developed and shown to describe successfully the experimental sensor performance. Then, a fully woven two-dimensional touchpad sensor was presented. The sensor was built by weaving a one-dimensional array of capacitor fibers in parallel to each other. The performance of the touchpad sensor was then characterized and the absence of inter-channel crosstalk was confirmed. It was concluded that the 2D touchpad has partial multi-touch functionality.

References

[1] Cok R S, Bourdelais R R and Kaminsky C J 2004 Flexible resistive touch screen *US Patent Specification* 0212599 A1
[2] Kalendra P W and Piazza W J 1994 Automatic calibration of a capacitive touch screen used with a fixed element flat screen display panel *US Patent Specification* 5283559
[3] Lee S, Buxton W and Smith K C 1985 A multi-touch three-dimensional touch-sensitive tablet *Proc. SIGCHI Conf. on Human Factors in Computing Systems* pp 21–5
[4] Rekimoto J 2002 SmartSkin: an infrastructure for freehand manipulation on interactive surfaces *Proc. SIGCHI Conf. on Human Factors in Computing Systems* pp 113–20
[5] Dietz P and Leigh D 2001 DiamondTouch: a multiuser touch technology *Proc. UIST, 14th Annu. ACM Symp. on User Interface Software and Technology* pp 219–26
[6] Dahiya R S, Metta G, Valle M and Sandini G 2010 Tactile sensing—from humans to humanoids *IEEE Trans. Robot.* **26** 1–20
[7] Engel J, Chen J and Liu C 2003 Development of polyimide flexible tactile sensor skin *J. Micromech. Microeng.* **13** 359–66
[8] Eltaib M E H and Hewit J R 2003 Tactile sensing technology for minimal access surgery—a review *Mechatronics* **13** 1163–77
[9] Hoshi T and Shinoda H 2006 A sensitive skin based on touch-area-evaluating tactile elements *Proc. Symp. on Haptic Interfaces for Virtual Environment and Teleoperator Systems* pp 89–94
[10] Ruspini D C, Kolarov K and Khatib O 1997 The haptic display of complex graphical environments *Proc. 24th Annu. Conf. on Computer Graphics and Interactive Techniques* pp 345–52
[11] Beebe D J, Hsieh A S, Denton D D and Radwin R G 1995 A silicon force sensor for robotics and medicine *Sensors Actuators* A **50** 55–65
[12] Wolffenbuttel M R and Regtien P P L 1991 Polysilicon bridges for the realization of tactile sensors *Sensors Actuators* A **26** 257–64
[13] Chu Z, Sarro P M and Middelhoek S 1995 *Transducers* **1** 656
[14] Gray B L and Fearing R S 1996 *Proc. IEEE Int. Conf. on Robotics and Automation* p 1
[15] Leineweber M, Pelz G, Schmidt M, Kappert H and Zimmer G 2000 *Sensors Actuators* A **84** 236
[16] Dario P and de Rossi D 1985 Tactile sensors and gripping challenge *IEEE Spectr.* **22** 46–52
[17] Kolesar E S, Dyson C S, Reston R R, Fitch R C, Ford D G and Nelms S D 1996 Tactile integrated circuit sensor realized

with a piezoelectric polymer *Proc. 8th IEEE Int. Conf. Innovative Syst. Silicon* pp 372–81

[18] Yuji J and Sonoda C 2006 A PVDF tactile sensor for static contact force and contact temperature *Proc. IEEE Sens.* pp 738–41

[19] Shimojo M, Namiki A, Ishikawa M and Makino R 2004 A tactile sensor sheet using pressure conductive rubber with electrical-wires stitched method *IEEE Sensors. J.* **4** 589–95

[20] Park C-S, Park J and Lee D-W 2009 A piezoresistive tactile sensor based on carbon fibers and polymer substrates *Microelectron. Eng.* **86** 1250–3

[21] Kim K, Lee K R, Kim W H, Park K-B, Kim T-H, Kim J-S and Pak J J 2009 Polymer-based flexible tactile sensor up to 32 × 32 arrays integrated with interconnection terminals *Sensors Actuators* A **156** 284–91

[22] Gu J F, Gorgutsa S and Skorobogatiy M 2010 Soft capacitor fibers using conductive polymers for electronic textiles *Smart Mater. Struct.* **19** 115006

[23] Gao Y, Guo N, Gauvreau B, Rajabian M, Skorobogata O, Pone E, Zabeida O, Martinu L, Dubois C and Skorobogatiy M 2006 Consecutive solvent evaporation and co-rolling techniques for polymer multilayer hollow fiber preform fabrication *J. Mater. Res.* **21** 2246–54